2013-09-27

A Novel Autophagy Regulatory Mechanism that Functions During Programmed Cell Death: A Dissertation

Tsun-Kai Chang
University of Massachusetts Medical School

A NOVEL AUTOPHAGY REGULATORY MECHANISM THAT FUNCTIONS DURING PROGRAMMED CELL DEATH

A Dissertation Presented

By

Tsun-Kai Chang

Submitted to the Faculty of the

University of Massachusetts Graduate School of Biomedical Sciences, Worcester

in partial fulfillment of the requirements for the degree of

DOCTOR OF PHILOSOPHY

September 27th, 2013

Program in Cancer Biology

A NOVEL AUTOPHAGY REGULATORY MECHANISM THAT FUNCTIONS DURING PROGRAMMED CELL DEATH

A Dissertation Presented

By

Tsun-Kai Chang

The signatures of the Dissertation Defense Committee signify completion and approval as to style and content of the Dissertation

Eric H. Baehrecke, Ph.D., Thesis Advisor

Marc R. Freeman, Ph.D., Member of Committee

Y. Tony Ip, Ph.D., Member of Committee

Michael Overholtzer, Ph.D., Member of Committee

Neal Silverman, Ph.D., Member of Committee

The signature of the Chair of the Committee signifies that the written dissertation meets the requirements of the Dissertation Committee

Andreas Bergmann, Ph.D., Chair of Committee

The signature of the Dean of the Graduate School of Biomedical Sciences signifies that the student has met all graduation requirements of the school

Anthony Carruthers, Ph.D.,
Dean of the Graduate School of Biomedical Sciences
Program in Cancer Biology
September 27th, 2013

Dedication

This work is dedicated to my family, for their indefinite love and support though all these years.

Acknowledgement

I would like to thank my wonderful mentor Eric for all your guidance and encouragement in the past five years. You have been the greatest inspiration when I was stuck for ideas and my greatest cheerleader during paper submission. You have been so thoughtful and supportive to me, and I wish someday I can be as good as you are. I also want to thank my TRAC/thesis committee members: Marc, Neal, Andreas, Tony, and Mike for your knowledge, caring, and mentoring, and in addition as well, thanks to my collaborators Wade, Sharad, and Craig for their scientific input.

I wish to thank all the Baehrecke lab members, past and present for your support and all the fun times we have shared. You guys are like my second family here. Especially to Bhupendra for being my “guru” in the lab. You taught me how to perform genetic experiments and how to become a better scientist. To Charles, for all the scientific input, your hilarious “that’s what she said” jokes, and the Chuck Norris facts. To Tina, for your delicious chocolate cakes (another piece, please!) and being such a nice, warm, and thoughtful person. To Lin, for you are a sweetheart and the sunshine of the lab.

It is also my great pleasure to have had the support from fellow Taiwanese friends. Thanks to my best friend Yu-Jie and Li-Ching for your support and friendship. Thanks to Chien-Ling and Yen-Tsung for everything you have done to make our life joyful. You guys are our role models. Thanks to Tsai-Yi for broadening my views. My gratitude to Tse-Chun and Chih-Fei for helping us settle in this foreign country. Thanks

to JJ, Te-Chen, Mike, and Lisa for sharing all the information about the balance between work and life. Thanks to Ting-Hao, Kuan-Hung, Ming-Hung, Jay, and Stanley for all the good times playing softball and watching football. Thanks to Josephine, Becky, Nick and everyone in the Boston Taiwanese Christians Church.

I couldn't have achieved this moment without my beloved family. Dad, thank you for your support and I wish I have made you proud. Mom, thank you for the million things you have done for us, and always concerning about our well-being. Also I would like to thank my in-laws, my aunts and my extended family members back in Taiwan. Thanks to my son, Ashton (Shane-Shane), for bringing me all the joy and teaching me to cherish every moment of this beautiful life. Finally, to Iris, my lovely better half, you complete me and make me a better person than I alone could ever be. Thank you for all your support and sacrifice so that we can move forward together to fulfill our master plan.

Last, I would like to thank the Lord for his blessing and bringing inner peace to me, reminding me always to be humble and open-minded. There is so much yet to learn!

Abstract

Autophagy is a cellular process that delivers cytoplasmic materials for degradation by the lysosomes. Autophagy-related (*Atg*) genes were identified in yeast genetic screens for vehicle formation under stress conditions, and *Atg* genes are conserved from yeast to human. When cells or animals are under stress, autophagy is induced and Atg8 (LC3 in mammal) is activated by E1 activating enzyme Atg7. Atg8-containing membranes form and surround cargos, close and mature to become the autophagosomes. Autophagosomes fuse with lysosomes, and cargos are degraded by lysosomal enzymes to sustain cell viability. Therefore, autophagy is most frequently considered to function in cell survival. Whether the *Atg* gene regulatory pathway that was defined in yeast is utilized for all autophagy in animals, as well as if autophagy could function in a cell death scenario, are less understood.

The *Drosophila* larval digestive tissues, such as the midgut of the intestine and the salivary gland, are no longer required for the adult animal and are degraded during the pupal stage of development. Cells stop growing at the end of larval development, and proper cell growth arrest is required for midgut degradation. Ectopic activation of the PI3K/Akt signaling induces cell growth and inhibits autophagy and midgut degradation. Down regulating PI3K/Akt pathway by *Pten* mis-expression activates autophagy. In addition, mis-expression of autophagy initiator *Atg1* inhibits cell growth and knocking down autophagy restore PI3K/Akt activity. Together, these results indicate that autophagy and growth signaling mutually inhibit each other.

Midgut destruction relies on the autophagy gene *Atg18*, but not caspase activation. The intestine length shortens and the cells undergo programmed cell size reduction, a phenomenon that also requires *Atg18*, before cell death occurs during midgut destruction. To further investigate whether cell size reduction is cell autonomous and requires other *Atg* genes, we reduced the function of *Atg* genes in cell clones using either gene mutations or RNAi knockdowns. Indeed, many *Atg* genes, including *Atg8*, are required for autophagy and cell size reduction in a cell autonomous manner. Surprisingly, *Atg7* is not required for midgut cell size reduction and autophagy even though this gene is essential for stress-induced autophagy. Therefore, we screened for known E1 enzymes that may function in the midgut, and discovered that *Uba1* is required for autophagy, size reduction and clearance of mitochondria. Uba1 does not enzymatically substitute for Atg7, and Ubiquitin phenocopies Uba1, suggesting Uba1 functions through ubiquitination of unidentified molecule(s) to regulate autophagy.

In conclusion, this thesis describes: First, autophagy participates in midgut degradation and cell death. Second it reveals a previously un-defined role of *Uba1* in autophagy regulation. Third it shows that the *Atg* genes are not functionally conserved and the requirement of some *Atg* genes can be context dependent.

Table of Contents

List of Figures

List of Third Party Copyrighted Material

The following figures were reproduced from journals: No permission required

Figure Number	Publisher
All Chapter II Figures	Nature Publishing Group
All Chapter III Figures	Nature Publishing Group

Author's Footnotes

All work was performed at University of Massachusetts Medical School in the laboratory of Eric Baehrecke. Chapter II and III were published in

D Denton*, **T-K Chang***, S Nicolson, BV Shravage, RT Simin, EH Baehrecke and S Kumar (*: equal contribution, 2012). Relationship between growth arrest and autophagy in midgut programmed cell death in *Drosophila*. *Cell Death and Differentiation*. 19:1299-307

and

T-K Chang, BV Shravage, SD Hayes, CM Powers, RT Simin, JW Harper and EH Baehrecke (2013). Uba1 functions in Atg7- and Atg3-independent autophagy. *Nature Cell Biology*. (doi:10.1038/ncb2804)

Chapter II was a collaboration with Drs. Donna Denton and Sharad Kumar from the Centre of Cancer Biology, University of Adelaide, Australia. Chapter III was a collaboration with Drs. Sebastian Hayes and J. Wade Harper from Harvard Medical School, U.S.A. Please see author contribution section for in the end of chapter II and III for details.

CHAPTER I

Introduction

Programmed cell death

Cell growth and death are a yin and yang of life and it is critical to reach the balance. Uncontrolled cell growth leads to diseases such as cancer. Cancer cell grows without regulation of proper upstream signaling and eventually affects the function of normal cells. Excess amounts of cell death can result in diseases such as neurodegeneration, a rising health and social problem to the aged population. Therefore, it is important to understand how to reach the balance between cell growth and cell death and what the mechanisms regulating these processes are.

Programmed cell death (PCD) is critical for elimination of cells during animal development. For example, PCD is required for degrading interdigital region in the handplates and foodplates to form digits. PCD is also necessary for an amphibian tadpole to lose its tail while transforming into a frog, and for a larva to degrade salivary glands and the midgut of the intestine during insect metamorphosis [1].

In 1973, Schweichel and Merker characterized different types of cell death based on electron microscopic morphology [2]. They observed three types of cell death in toxin-

treated rodent embryos and fetuses, and categorized them by their use of lysosomes. Lysosome-dependent cell death can be separated by the source of the lysosome: either lysosome from other cells [type I, heterophagy (hetero: other, phagy: eat)] or from the dying cell itself [type II, autophagy (auto: self)]. Type I death, also called apoptosis [3] can be regulated by both extrinsic (by ligand-receptor interaction) or intrinsic (by mitochondria) pathways, and possesses characteristics such as DNA fragmentation, chromosome condensation, and cell membrane blebbing [4]. Cysteine-dependent aspartate-specific proteases (caspases) play significant roles in regulating apoptosis. Later dying cells break apart and form apoptotic bodies, which will be engulfed and degraded by phagocytes.

Type II cell death involves autophagy, but not phagocytes. The cells use their own lysosomes for degradation (see below). Type III cell death, later coined as necrosis, is less known. It involves RIP1 and RIP3 kinases but not caspases [5], and appears to be an acute death first with cell swollenness then cell breakdown. Because of this, necrosis is associated with inflammation. Necrosis does not require lysosomes.

Autophagy, cell survival and cell death

Two major catabolic processes that are used by cells are the ubiquitin (ub) proteasome system (UPS) and the lysosome machinery. Proteins are delivered to the proteasome in an ub-dependent manner that involves an E1 activating enzyme, an E2 conjugating enzymes and an E3 ligase. Two major types of ubiquitination have been identified, based on which Lysine (K) residue (K-48 or K-63) of the ub is covalently

bound to the glycine residues on its target proteins. Proteins with K-48 ubiquitination are sent to the 26S proteasome for degradation. Differently, K-63 is linked to signal transduction. UPS is thought to be target specific and the specificity is conveyed from different E3 ligases. There are total two E1s (Uba1 and Uba6), dozens of E2s and hundreds of E3s in the mammalian genome and each E3 binds to a particular set of targets.

By contrast, autophagy is a balk catabolic process that delivers cytoplasmic materials, including proteins and organelles, to lysosomes. Some types of autophagy also have target specificity and some don't (see below). Autophagy can be categorized into three forms based on how materials are delivered to lysosomes: microautophagy chaperone-mediated autophagy (CMA), and macroautophagy. The mechanism of microautophagy is poorly understood, and is believed to occur by lysosome–mediated pinocytosis of cytoplasmic material[6]. In CMA, protein chaperones recognize cytoplasmic proteins and send them directly to lysosomes via a LAMP2–dependent mechanism [7]. Of the three forms of autophagy, macroautophagy is best studied and will henceforth be referred to as autophagy.

During macroautophagy, double-layered isolation membranes are formed from preautophagosomal structures near the cargos. Endoplasmic reticulum (ER) and mitochondria are the membrane sources [8-10], and Ravikumar et al. also reported that plasma membrane could also contribute [11]. With the help from autophagy-related (*Atg*) genes (see below), the isolation membrane closes to form the autophagosome. Then

lysosomes fuse with the outer membrane of the autophagosome and the cargos are degraded by acidic lysozymes.

Beside the non-selective form of autophagy which has no cargo specificity, selective autophagy, which involves cargo recognition by ubiquitination, has been observed. The specificity comes from different E2 and E3 enzymes. Ubiquitinated cargos are recognized by autophagy cargo receptors such as p62/Sequestosome1, NDP52, NBR1, Optineurin/OPTN, and so on. These receptors all have a microtubule-associated protein 1 light chain 3 (LC3, mammalian homolog of yeast Atg8 [12])-interacting region that binds to LC3 and recruit the cargos to forming autophagosomes. For example, clearance of mitochondria, also called mitophagy, requires the E3 ligase activity of Parkin. During mitophagy, Parkin ubiquitinates proteins on the outer mitochondria membrane [13] and recruits p62 for autophagic destruction.

Autophagy has been best studied in the context of promoting cell survival during cell stress. When animals and cells are well fed, insulin signaling activates phosphatidylinositol 3-kinase (PI3K) and its downstream kinase Akt, and then subsequently activates the mammalian target of rapamycin (mTOR). mTOR directly binds to and inhibits a key autophagy regulator ULK1 (*Atg1* in the fruit fly *Drosophila melanogaster*) by phosphorylating Serine (S) residue 757 [14]. Akt can also phosphorylate and inhibit the autophagy regulator Beclin1 (mammalian homolog of yeast Atg6) [15]. While nutrient levels are low, mTOR activity is low, allowing ULK1 to actively induce autophagy. Furthermore, lower nutrient levels exhibit lower adenosine tri-phosphate

(ATP) and higher adenosine mono-phosphate (AMP). High amounts of AMP activate AMP Kinase which activates ULK1 by S777 and S317 phosphorylation [16]. It is still unclear, but an identified phosphatase is speculated to be able to dephosphorylate S757 on ULK1 under nutrient deprivation. It is known that ULK1/Atg1 is sufficient to induce autophagy [17] to degrade organelles such as mitochondria or ribosome-endoplasmic reticulum (ER) to provide energy to sustain cell survival. This function of autophagy in cell survival is conserved from yeast to humans, and has led to the assumption that autophagy always promotes cell survival. However, autophagy has also been observed in dying cells of diverse organisms, and recent genetic studies indicate that autophagy can promote cell death under specific cell contexts.

Autophagic cell death has been best studied during the development of the fruit fly *Drosophila melanogaster*. A larva and an adult fly are morphologically and behaviorally different. A larval possesses very strong digestive tissues that allow the larva to grow hundreds of times in size in three to four days. By contrast, an adult fly does not increase in size, and has strong reproductive tissues to produce lots of progenies efficiently. Therefore, the larval tissues are eliminated and the adult tissues are formed during the transitional pupal stage, also known as the metamorphosis. During metamorphosis, most larval cells and tissues are destroyed by PCD, and many of these dying cells possess high levels of autophagy. Larval salivary glands and the midgut of the larval intestine are two organs that are degraded during metamorphosis and possess extensive autophagy. Gland degradation requires both autophagy genes and caspases: autophagy and caspase activation synergistically facilitate gland

degradation [18]. In contrast to apoptosis, caspase activation is required but no phagocytosis is involved in salivary gland cell death. Loss of either autophagy or caspase activity leads to incomplete gland degradation during the pupal stage. By contrast, the degradation of midgut is less complex. Caspases activity is not required for midgut destruction which proceeds normally even when caspases are mutated or covalently inhibited by p35 mis-expression [19]. However, autophagy is essential for midgut destruction. Loss of autophagy leads to persisting gastric ceca and proventriculus [19], two larval midgut structures that are destroyed during metamorphosis.

Regulation of autophagy

Atg genes were first identified in genetic screens in yeast for altered vesicle formation inside vacuoles after nutrient deprivation [20]. Thirty-one *Atg* genes have been identified since then, with 15 of them functioning as “core” regulators: those required for starvation-induced autophagy, the cytoplasm to vacuole targeting [21] (Cvt, delivery of the hydrolase aminopeptidase I to the yeast vacuole of lysosome) pathway and pexophagy [22] (autophagic degradation of peroxisomes). The core *Atg* genes are conserved from yeast to humans and are all thought to be required for autophagy. The core *Atg* genes can be broadly divided into the Atg1 complex, the Vps34 complex, the Atg9/2/18 complex and two ubiquitin-like conjugating systems (Fig. 1). Here, I will use the names that are most commonly used for these factors in *Drosophila*.

1. Atg1 complex

The *Drosophila* Atg1 complex includes Atg1 (ULK1/2 in mammals or unc-51 in *C. elegans*), Atg13, FIP200/CG1347 (RB1CC1 in mammals), and Atg101/CG7053 (C12orf44 in mammals). Atg1's Serine/ Threonine (Ser/Thr) kinase activity is critical for initiating autophagy [23, 24]. Mis-expression of *Atg1* induces autophagy in multiple *Drosophila* tissues [17, 18] (and see Chapter II) and is sufficient to induce caspase-dependent cell death in the larval fat body [17], while in the salivary gland, Atg1 induces caspase-independent cell death [18]. In the midgut of fly intestine, mis-expression of *Atg1* inhibits PI3K/Akt pathway and negatively influences cell growth (see Chapter II). Atg13 interacts with Atg1 and serves as a nutrient sensor. When nutrients are abundant, the TOR Complex 1 phosphorylates Atg13. After starvation, Atg13 is de-phosphorylated and activates Atg1 [23, 25]. FIP200 is important for autophagy in mammalian cells under starvation conditions [26] as well as in *Drosophila* [27]. Atg17 is only essential for starvation-induced autophagy, but not in the Cvt pathway, therefore it is still debatable whether Atg17 and FIP200 are related. However, Atg101 is metazoan specific. The function of Atg101 is unclear, but it is required for autophagy under nutrient deprivation [28] (also see Appendix 1).

2. Vps34 complex

The Vps34 complex consists of Vps34 (class III PI3K), Atg6 (Beclin1 in mammals and, Vps30 in yeast), Vps15 (also called p150 or Ird1 in *Drosophila*), and metazoan-specific components UV irradiation resistance-associated gene (Uvrag), CG11877 (Atg14 in yeast, and Barkor in mammal) and endophilin B/EndoB (Bif 1 in mammal). Many of the components of the Vps34 complex were identified and shown to have

important functions in vacuolar protein sorting (hence Vps), suggesting a close relationship between autophagy and other forms of vesicle trafficking. Vps34 phosphorylates phosphatidylinositol (PtdIns) to PtdIns3P (PI3P) whose function is required in both autophagy and protein sorting [29, 30]. PI3P then recruits FYVE domain or PX domain-containing proteins and initiates vesicle nucleation. Atg6 has a BH3-like domain and interacts with Bcl-2 [31]. Atg6 is a haploinsufficient tumor suppressor (see below) and is required for autophagy, endocytosis, protein secretion and hematopoiesis in *Drosophila* [32]. Vps15 is also a Ser/Thr kinase and is required for the function of the Vps34 complex and starvation-induced autophagy [33, 34]. Uvrag is a coiled-coil protein that enhances Atg6 binding to Vps34 [35]. Atg14 and EndoB are two Beclin1 binding proteins that are required for autophagy [36, 37].

3. Atg9/2/18 complex

Atg9 is, among the core *Atg* encoding genes, the only protein that has an integral membrane domain. After initiation of autophagy, Atg9 containing vesicles translocate and form the pre-autophagosomal structures (PAS) [38] and *Atg9* is thought to be important for isolation membrane recruitment. Atg2 and Atg18 form a complex and are responsible for either retrograde movement of Atg9, or recycling Atg9-containing vesicular membrane [39, 40]**.** Atg18 also has a WD40 domain that binds to PI3P (generated by the Vps34 complex) and PI(3,5)P [41].

4. Two ubiquitin-like conjugating systems

Atg8 (GABARAP or LC3 in mammals) and Atg12 are two ubiquitin-like molecules [42-44]. The cysteine protease Atg4 cleaves and reveals the carboxyl (C)-terminal glycine (Gly) residue of Atg8 [45]. Atg12 has a free Gly residue on the C-terminus. The Gly residue from cleaved Atg8 and Atg12 are conjugated separately to the lysine residue on the E1 activating enzyme Atg7, and the E2 conjugating enzymes Atg3 (for Atg8) and Atg10 (for Atg12) [46-50]. Atg12 is transferred to Atg5 which then forms a complex with Atg16. Although it is not clear whether an E3 ligase is required for Atg12-5 conjugation, the Atg12-5/16 complex could serve as the E3 for Atg8 conjugation to lipid phosphatidylenthanolamine (PE) [51]. Lipidated Atg8 (Atg8-PE) is allowed to locate to the PAS and on both the inner and the outer membrane of the isolation membrane. Atg12-5/16 also covers the outer membrane by Atg5-membrane association [52], and together with Atg8-PE, facilitates closing of the isolation membrane to form an autophagosome. Additionally, Atg4 can also cleave the PE group from Atg8 so that Atg8 can be recycled after autophagosomes fuse with lysosomes [45].

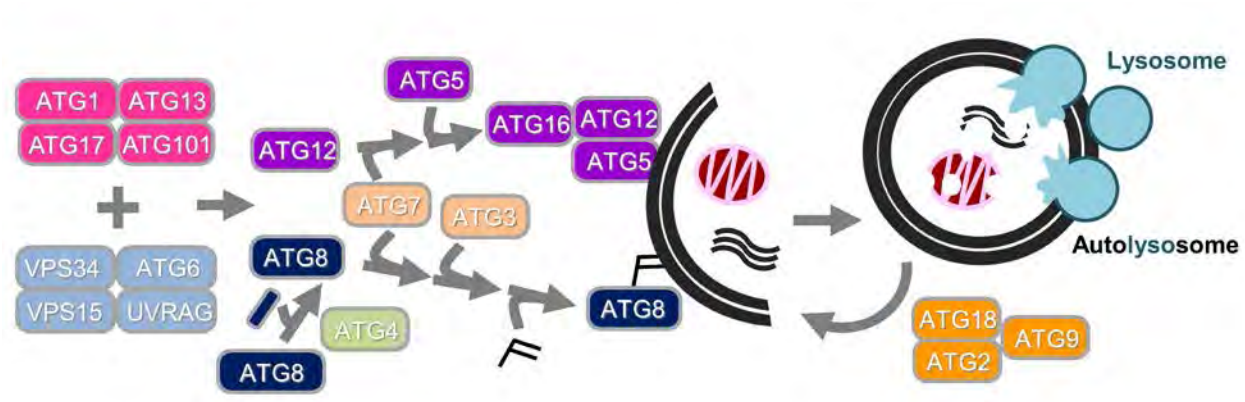

Figure 1-1: Schematic of autophagy.

Alternative forms of autophagy

It has been assumed that most, if not all, forms of autophagy require the entire core *Atg* genes [40, 53]. However, it should be noted that the majority of studies of this process have focused on nutrient deprivation-triggered autophagy, and that alternative autophagy that does not involve some *Atg* genes has been reported [54]. Nishida et al. discovered that double-membraned, autophagosome-like structures were observed either following cytotoxin etoposide, a DNA damaging agent which causes DNA break, treatment or under starvation conditions in Atg5$^{-/-}$ mouse embryonic fibroblast (MEF) cells [55]. The formation of these structures requires the function of components of the Atg1 and Vps34 complexes, but not the activation of ubiquitin-like molecule LC3 (Atg8) to form lipidated LC3-PE. Since LC3 conjugation is not essential, it is not surprising that this form of autophagy does not require the E1 Atg7. This *Atg5*/*7*-independent autophagy raises an important question: how is LC3 recruited to the PAS membrane without PE?

Atg6-independent forms of autophagy have also been reported in various *Atg6* knocked down cell lines following stimulations by cytotoxins and hydrogen peroxide [56-58]. These alternative forms of autophagy all require Atg1 as well as components of the ubiquitin-like conjugation pathway, such as Atg7 and Atg8. The discovery of these alternative forms of autophagy and the concept of this pathway as a therapeutic target indicates the importance of studying autophagy and the need to better understanding the underlying mechanisms.

Autophagy and diseases

Autophagy degrades protein aggregates and damaged organelles, and defects in autophagy have been linked to various human disorders, such as cancer, neurodegeneration and infectious disease. Cancer is the second leading cause for human mortality in the United States. Infectious diseases kill more than 20% of people worldwide every year. The numbers of neurodegerative disease cases are growing and are a major concern for the quality of life in the aged population. Therefore, it is critical to understand the mechanisms that regulate autophagy to potentially modulate this process for therapeutic benefit when treating diseases.

1. Cancer

The role of autophagy in cancer has been debated, and the current consensus is that autophagy can be both tumor suppressive and tumorigenic [59, 60]. Reactive oxygen species (ROS) is a by-product from oxidative phosphorylation, the process of making ATP in the mitochondria, and can be carcinogenic. Because of this, mitochondria accumulate mutations and become damaged with age. Damaged mitochondria create excess ROS, causing gene mutations through DNA damage. One way to prevent ROS from accumulating is to clear mitochondria by autophagy, a process called mitophagy. Moreover, autophagy has been reported to suppress cell grow by inhibiting the PI3K pathway [17] (and also see Chapter II), a signaling pathway that is frequent activated in cancers and induces cell proliferation. This suggests another active role for autophagy as a tumor suppressive mechanism. Furthermore, Atg6 (Beclin1) is a haploinsufficient tumor suppressor; one allele of Beclin1 is frequently deleted in breast, ovarian and

prostate cancers and tumor cell lines [61]. Consistent with these data, allelic loss of Beclin1 can result in an increased number of lymphomas and solid tumors in mice compared to age-matched litter mates [62].

By contrast, loss of *Atg5* can result in adenomas in the liver where cells experience significant stress, but no evidence of tumor initiation was found in any other tissues [63]. Furthermore, progression to cancer was not observed in the liver, suggesting that autophagy may be required for tumor progression. In addition, Kenzelmann Broz et al. found that under oncogene stimulation using a mouse model of activated Ras-triggered lung cancer, that loss of *Atg5* promoted tumor transformation [64]. They also showed that autophagy is required for p53-induced apoptosis under oncogenic E1A or H-Ras stimulation, indicating that autophagy can act as a component of the core p53 tumor suppression response.

When a tumor has developed, cells proliferate at a high rate and may deplete the nutrients and oxygen before blood vessels can be formed to replenish nutrients. This hypoxic and low energy environment inhibits the progression of cellular processes such as DNA and protein synthesis, and these effects may be disadvantageous for tumor growth. In this state, autophagy can degrade unneeded organelles to provide energy for tumor cell survival. Thus, autophagy can promote tumorigenesis. This suggests autophagy as a therapeutic target and can be modulated as antitumor drugs.

2. Neurodegeneration

Classical neurodegerative diseases include Huntington's disease (HD), Parkinson's disease (PD), Alzheimer's disease (AD), prion-associated diseases, and amyotrophic lateral sclerosis (ALS). Common features of these diseases are protein aggregation and accumulation of autophagic structures [65]. These proteins include huntingtin in HD, α-synuclein in PD, β amyloid peptide in AD, and TDP-43 or FUS in ALS. These proteins have prion-like domains, are aggregation-prone and can be toxic for cells and organisms.

The accumulation of autophagic structures suggests a defect in autophagic flux that autophagosomes and autolysosomes, together with cargo proteins, are not efficiently degraded and therefore accumulate inside of the cells. Indeed, loss of autophagy regulator functions in the mice leads to neurodegeneration [66, 67]. Excitingly, histone deacetylase 6 (HDAC6) rescues degeneration in a fly model of the spinobulbar muscular atrophy in an autophagy-dependent manner [68]. Ectopic activation of autophagy by mTOR inhibitor rapamycin reduces toxicity from aggregated polyglutamine [69]. Together, these reports suggest a potential therapeutic value of autophagy to treat neurodegenerative diseases.

3. Infectious disease

Pathogens invade cells via phagocytosis and autophagy is the first initiated anti-pathogen response after infection. Autophagy recognizes pathogens which are later degraded by the host lysosomes. Thus it is critical for pathogens to disguise themselves and escape from host autophagy surveillance. For example, *Listeria monocytogenes*

uses ActA proteins to form aggregates which cannot be ubiquitinated and be recognized by p62 proteins and selective autophagy [70]. *Legionella pneumophila* uses RavZ to modify Atg8 (LC3) to inhibit autophagy after infection [71]. Similarly, deletion of Atg5 results in defective autophagy, defective pathogen clearance, enhanced bacterial growth, and decreased host survival in mice, flies, and plants [72]. Conversely, rapamycin suppresses lung inflammation and *Burkholderia cenocepacia* infection by activating autophagy-associated bacteria clearance [73]. These findings suggest that autophagy can be targeted as a therapy against infectious diseases.

Biology of *Drosophila* midgut

The *Drosophila* intestine consists of the foregut (fly equivalent of the esophagus), the midgut (fly stomach and small intestine), and the hindgut (fly equivalent of the large intestine). My work focuses on the midgut at the larval and pre-pupal stages of development. The fly midgut is functionally and cytologically very similar to mammalian intestine. Polytenic enterocytes (ECs) are the working units—they have microvilli and are responsible for nutrient uptake. The enteroendocrine (EE) cells are secretory cells. The adult midgut progenitor (AMP) islands have two different diploid cell types: the AMP and the peripheral cell (PC, see Fig. 2). The PC is derived from an AMP and serves as a niche to keep the AMP from differentiating. During metamorphosis, PCs are “lysed” and AMPs are free to differentiate into adult intestinal stem cells, enteroblasts (EBs), EEs, and ECs [74].One of the differences between fly and mammalian intestine is that fly EBs are not proliferating; the EBs are transitional cells and will become either ECs or EEs.

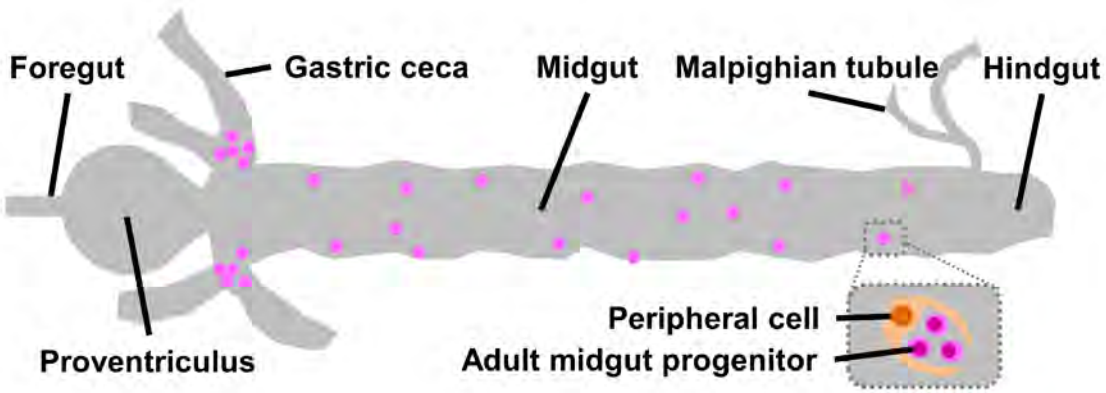

Figure 1-2: The larval intestine of *Drosophila*.

Steroid signaling, metamorphosis, and the destruction of the larval midgut and salivary glands

The larval midgut and salivary glands are not needed for adult animals, and are degraded by PCD during metamorphosis. The steroid hormone 20-hydroxyecdysone (hereafter ecdysone) controls development and tissue PCD. Two ecdysone pulses are critical for metamorphosis. The first pulse at late third instar larval stage initiates puparium formation (this is set as time point zero), and leads to the degradation of the larval midgut. The second ecdysone pulse happens 12 hours after puparium formation, triggering head eversion and also the degradation of salivary glands. Ecdysone initiates cell death by regulating gene expression through binding to the ecdysone receptor, which complexes with its partner Ultraspiracle [75]. This hormone receptor complex then functions as a transcription regulator that facilitates expression of the early transcription factor genes E93, E74, and Broad Complex [76]. EcR is required for midgut degradation but the requirement of the early genes is unclear [77] (also Chang and Baehrecke unpublished). E93, activated by the second ecdysone pulse, is critical for salivary gland

degradation [78]. In the dying salivary gland, E93 is required for the proper expression of pro-apoptotic and *Atg* genes [79, 80].

Ecdysone induces PCD in the midgut at the onset of puparium formation [81]. Midgut size decreases at the late larval to early pre-pupal stage and accompanies the formation of the adult midgut epithelium [77]. During the early pre-pupal stage, features such as the shortening of the midgut, disappearance of the proventriculus and gastric ceca, and proliferation/differentiation of the AMPs can be observed (Fig. 1-3). The decrease in midgut size is partly inhibited by mutations in ecdysone-regulated early response genes [77]. At the subcellular level, cells become TUNEL-positive, and possess autophagosomes based on transmission electron microscopy and Atg8 reporter analyses [19, 77]. The midgut condenses to form the meconium (also known as the yellow body) during pupation, and this structure persists in newly eclosed adults at which time it is expelled by defecation.

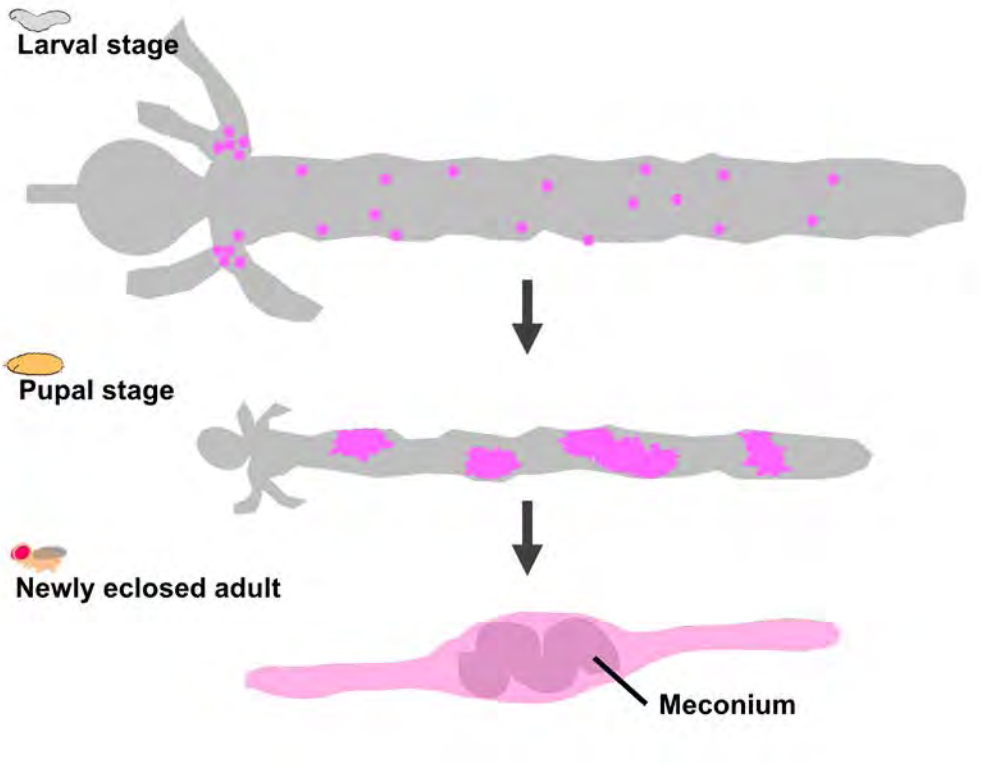

Figure 1-3: Diagram showing the general morphological changes that occur during metamorphosis.

Surprisingly, unlike the salivary gland, midgut destruction does not require the activation of caspases for degradation. Neither disruption of either initiator or effector caspases nor inhibition of effector caspases by mis-expression of the baculoviral protein p35 block midgut destruction [19]. Nevertheless, autophagy is essential for midgut destruction: loss of core *Atg* genes inhibit midgut size reduction and also tissue destruction[19]. Prior to my work, however, it was unclear how autophagy contributed to the death and clearance of midgut cells, and it was critical to understand how autophagy was regulated in the dying midgut.

Outstanding remaining questions

Autophagy is regulated by *Atg* genes, functions in cell death, and is associated with many human disorders. Research in mammalian cells usually uses various cell stressors to induce autophagy, such as nutrient deprivation (starvation) and cytotoxins. These studies focus only on how cells deal with stress and could be superficial. Starved cells use autophagy to degrade nonessential proteins and organelles to sustain viability; however, cell stress responses are non-physiological. Therefore, studying autophagy only in cell stress settings could be too narrow and would not reveal if autophagy is involved in other cellular processes. In *Drosophila*, autophagy is primarily used not only to cope with cell stress, but also to degrade tissues during metamorphosis. It is not known whether *Atg* gene functions are conserved in these two types of autophagy and whether all cell types in a given animal use the same regulatory mechanism. Moreover, different cell types may possess distinct autophagic features, such as different autophagosomal membrane sources, and may involve additional regulatory molecules.

The length of the midgut shortens during the late larval stage, and the gastric caeca (GC) of the midgut disappear in the pre-pupal stage. It is still unclear how these two physiological phenomena are accomplished and whether they share similar mechanisms. The midgut cells possess signatures of cell death, such as DNA breaks even when the functions of many caspases are reduced. This raises a couple of questions. First, can cytoplasmic autophagy induce nuclear DNA break in a trans-regulatory fashion; if so, what are the cellular mechanisms for achieving this. Second, can autophagy execute cell death without the involvement of caspases?

In this thesis, I describe, first, that autophagy and cell growth signaling antagonize each other (Chapter II), second, an *Atg7*- and *Atg3*-independent autophagy that requires *Uba1* (Chapter III), and touch upon many previously unsolved issues. My research suggests an animal may use different autophagic regulatory pathways in a tissue-specific manner. This tissue-specificity should be carefully considered when designing future experiments to study the therapeutic value of autophagy against human diseases.

CHAPTER II

Relationship between growth arrest and autophagy in midgut programmed cell death in *Drosophila*

Abstract

Autophagy has been implicated in both cell survival and programmed cell death (PCD), and this may explain the apparently complex role of this catabolic process in tumorigenesis. Our previous studies have shown that caspases have little influence on *Drosophila* larval midgut PCD, whereas inhibition of autophagy severely delays midgut removal. To assess upstream signals that regulate autophagy and larval midgut degradation, we have examined the requirement of growth signaling pathways. Inhibition of the class I phosphoinositide-3-kinase (PI3K) pathway prevents midgut growth, whereas ectopic PI3K and Ras signaling results in larger cells with decreased autophagy and delayed midgut degradation. Furthermore, premature induction of autophagy is sufficient to induce early midgut degradation. These data indicate that autophagy and the growth regulatory pathways have an important relationship during midgut PCD. Despite the roles of autophagy in both survival and death, our findings suggest that autophagy induction occurs in response to similar signals in both scenarios.

Introduction

Programmed cell death (PCD) is essential for removing excess and unwanted cells to maintain tissue homeostasis, deleting cells damaged by pathogens or genotoxic stress, and has been implicated in diseases, including cancer and neurodegeneration. The canonical caspase-dependent apoptotic pathways are important mediators of developmental PCD. However, recent studies in many model systems suggest that some physiological cell deaths require alternative pathways, including programmed necrosis and autophagy [82, 83]. One of the unique forms of cell death requiring autophagy is evident in the removal of the *Drosophila* larval midgut [19, 77, 84].

Macroautophagy (autophagy) has roles in normal development, stress response, neurodegeneration, cell growth, PCD and cancer, and is known to promote cell survival under nutrient deprivation and stress conditions [60, 85]. Under cell growth promoting conditions, autophagy occurs at basal levels and is induced to high levels under growth limiting conditions, such as contact inhibition, metabolic stress, and nutrient limitation. Studies using transformed cells with oncogenic Ras expression have shown that a complex relationship exists between autophagy, cell growth and cell death. Activated Ras expression can promote cell growth accompanied by increased autophagy, or can result in cell death that also is accompanied by increased autophagy [86, 87]. The highly conserved insulin receptor/class I phosphoinositide-3-kinase (InR/PI3K) pathway regulates cell and tissue growth whereby under growth conditions it promotes the activation of target of rapamycin (TOR) kinase resulting in inhibition of autophagy [88].

The down-regulation of PI3K activity by several tumour suppressor genes, including PTEN, TSC1 and TSC2, promotes autophagy induction [24, 89].

The association between growth signalling and autophagy, where autophagy is increased in growth inhibited cells, suggests that autophagy may be contributing to limiting cell growth. Indeed, induction of autophagy in the *Drosophila* fat body leads to a reduction in cell size and inhibition of autophagy results in larger cells under starvation conditions [17, 25]. However, the signalling pathways that regulate autophagy have additional roles; for example, TOR affects metabolism by regulating ribosome biogenesis and protein synthesis affecting metabolism [90]. Therefore, the relationship between autophagy and cell growth has been difficult to evaluate. Furthermore, the relationship between growth signalling and autophagy in cell death is poorly understood.

Although the subject of some debate, supportive evidence for the role of autophagy in developmental cell death is emerging. For example, autophagy is required for PCD in various *Drosophila* tissues during development [18, 19, 91-93]. During *Drosophila* development a rise in steroid hormone triggers PCD of the obsolete larval tissues, including the midgut and salivary glands [78, 81]. The steroid receptor complex regulates the transcription of several cell death genes as well as genes involved in autophagy in both salivary gland and midgut prior to their removal by PCD [80, 94]. The removal of the salivary glands requires both the canonical apoptosis machinery [81, 95-97] and autophagy [18, 98]. Indeed when inhibition of both caspases and autophagy are combined, a greater block in salivary gland degradation occurs compared to inhibition of either pathway

alone which suggests they function as independent degradation pathways [18]. Furthermore, maintenance of growth in the salivary glands was able to block autophagy and delay degradation indicating that growth arrest is required prior to the removal of the salivary gland [18].

Our previous studies have shown that loss of the canonical caspase activation pathway has no effect on midgut PCD whereas genetic inhibition of autophagy severely delays midgut removal [19]. Surprisingly, inhibition of autophagy suppressed midgut PCD without affecting caspase activation or activity, suggesting that caspases alone fail to execute cell death and autophagy plays an active and necessary role in midgut degradation [19, 99]. However, the precise role of autophagy and the cross-talk between cell growth regulatory pathways during this novel form of PCD remain unclear. Here we have examined the requirement of growth signalling in midgut degradation. We report that inhibition of the class I PI3K growth pathway prevents midgut growth. Conversely, ectopic PI3K and Ras signalling resulted in cell overgrowth with reduced autophagy and delayed midgut destruction. Furthermore, premature induction of autophagy by expression of *Atg1* resulted in premature midgut degradation. Surprisingly, unlike in salivary glands, where the Hippo pathway is required for cell growth arrest, autophagy and degradation [100], this pathway was not involved in regulating midgut PCD.

Result

Premature autophagy induction leads to midgut PCD

The removal of the obsolete *Drosophila* larval midgut requires autophagy and does not depend on the canonical caspase activation pathway [19]. Given that autophagy inhibition severely delayed midgut removal, we examined if early autophagy induction, as assessed by Atg8a puncta, alone was sufficient to induce premature midgut removal. The degradation of the larval midgut initiates at the end of the larval stage when the gastric caeca, present at the onset of puparium formation, begin to contract and are removed by +4h relative to puparium formation (RPF), while the remaining gut continues to condense (Fig. 2-1a). Induction of autophagy by expression of *Atg1* in the midgut resulted in more contracted gastric caeca, at an earlier time point as compared to the control (Fig. 2-1a, b). Quantification of the length of gastric caeca showed a significant reduction when *Atg1* was expressed compared to the control (Fig. 2-1c). However, at later time points (+12h RPF) once the normal induction of autophagy has initiated midgut removal appeared to occur normally (Fig. 2-1a, b). Mosaic clones of cells overexpressing *Atg1* in the midgut of feeding larvae revealed that, compared to the surrounding wild-type cells, there is a high level of autophagy induction, as shown by Atg8a puncta, and smaller cell size (Fig. 2-1d). This indicates that *Atg1* expression is sufficient to induce autophagy which results in smaller cell size.

Growth arrest is required for midgut PCD

Previous studies provide evidence for an association between growth signalling and autophagy in both cell survival and during removal of the salivary glands [18, 24]. To

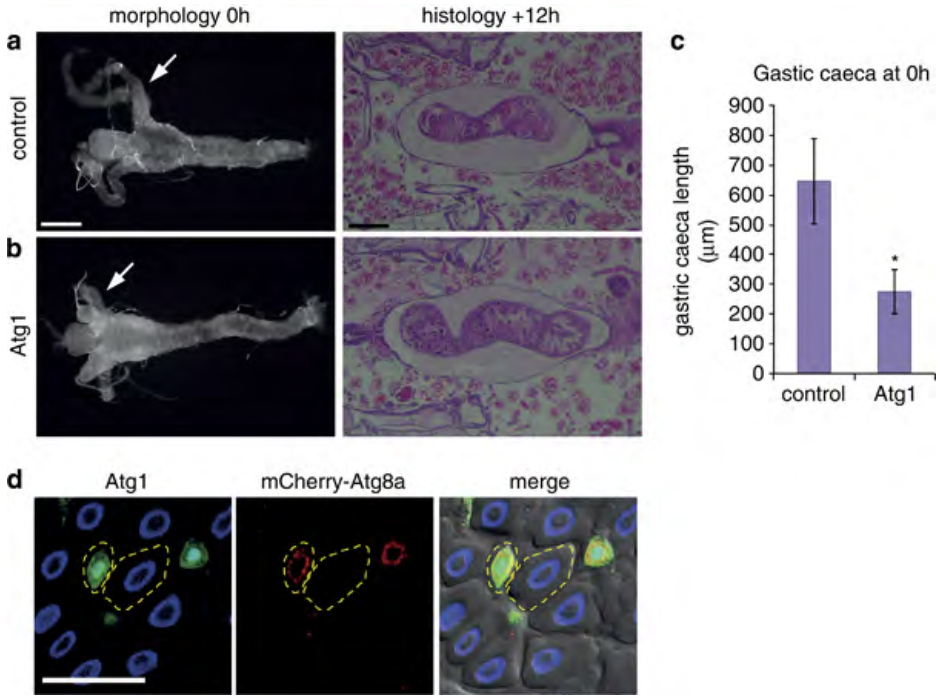

Figure 2-1: Premature induction of autophagy induces midgut PCD

Morphology of midguts at 0h RPF (left) showing (a) control (*NP1-GAL4/+*) compared to (b) *Atg1* overexpression (*NP1-GAL4/+; UAS-Atg1^{6B}/+*) with premature contraction of gastric caeca (arrows). Histological analysis of paraffin sections at +12h RPF (right) shows that at the later time point midgut contraction is similar in (a) control (*NP1-GAL4/+*) and (b) *Atg1* overexpression (*NP1-GAL4/+; UAS-Atg1^{6B}/+*). Scale bars in (a) represent 200 µm. (c) Quantification of the length of the gastric caeca at 0h RPF measured with Zeiss automeasure software from control (*NP1-GAL4/+*) and *Atg1* overexpression (*NP1-GAL4/+; UAS-Atg1^{6B}/+*) (N = 4 and 9, respectively). Quantification is average length (µm) ± standard deviation. * $p<0.001$ (compared to the control). (d) Mosaic clones from feeding larvae expressing *Atg1* marked by GFP (green) and DNA (blue) (*hsFLP; mcherry-Atg8a/+; Act>CD2>GAL4, UAS-nlsGFP/UAS-Atg1^{6B}*) have increased mCherry-Atg8a puncta (red) compared to the neighboring cells and smaller cell size. Atg1 clone and neighbouring cell outlined. Scale bars in (d) represent 50 µm.

determine if this is a more widespread occurrence and in particular the importance of cell growth on PCD, we examined the relationship between growth signalling and

autophagy during midgut removal. The PI3K growth signalling pathway leads to formation of phosphatidylinositol-3, 4, 5-P3 (PIP3) on the plasma membrane and this can be assessed using the *t*GPH reporter (*tubulin*-GFP-Pleckstrin Homology) [101]. During active PI3K signalling *t*GPH is recruited to the cell cortex and following growth arrest this localisation is lost. Under conditions of larval growth *t*GPH was localised to the cortex of gastric caeca cells and this localisation was lost at +2h RPF (Fig. 2-2a). This indicates that growth arrest occurs in the midgut coinciding with the timing of midgut PCD.

To investigate the relationship between growth and autophagy we examined the effect of autophagy inhibition on growth signalling during midgut death. Important regulators of autophagy, including *Atg1*, *Atg2* and *Atg18*, have previously been shown to be required for autophagy [19]. Interestingly, the inhibition of autophagy, using *Atg2* mutants or knockdown of *Atg1* by RNAi, resulted in persistent cortical localisation of *t*GPH in the midgut at +2h RPF (Fig. 2-2a, b). This implies that class I PI3K pathway signalling is no longer down-regulated following puparium formation as seen in the control midgut. Another marker of PI3K activity is the localisation of phosphorylated Akt to the cell cortex, due to its interaction with PIP3, and its subsequent phosphorylation that is required for downstream signal transduction. To further investigate if autophagy inhibition by knockdown of *Atg1* or *Atg18* results in persistent growth signalling in the midgut we examined the localisation of phosphorylated Akt, compared to the cell cortex marker Fasciclin III. In control midguts during late larval stages (-4h RPF) phosphorylated Akt was detected at the cell cortex, and following puparium formation

(+2h RPF) this cortical localisation was reduced (Fig. 2-2c). However, in *Atg1* and *Atg18* RNAi midguts a significant amount of phosphorylated Akt remained at the cortex at this later stage (+2h RPF) (Fig. 2-2c). Prior to the onset of autophagy in dying midguts, the localisation of phosphorylated Akt was similar in control and either $Atg1^{IR}$ or $Atg18^{IR}$ midguts from feeding larvae (Fig. 2-3). We also examined the effect of autophagy induction on the localisation of phosphorylated Akt. In midguts expressing *Atg1* there was a reduction in cortically localised phosphorylated Akt (-4h RPF) compared to the control (-4h RPF) (Fig. 2-2c). These data suggest that autophagy is required for down-regulation of class I PI3K signalling and that there is a feedback regulation between autophagy and growth signalling pathways.

Maintaining growth signalling prevents autophagy and delays midgut cell death

The observation that inhibition of autophagy results in persistent class I PI3K signalling in midguts during the pre-pupal stage led us to investigate the requirement of upstream growth signalling on midgut degradation. Activation of the PI3K pathway in response to insulin leads to phosphorylation of the insulin receptor and its substrate, Chico, activating the catalytic subunit Dp110 [102]. Active Dp110 converts PIP2 to PIP3 on the plasma membrane enabling interaction with Akt and activation of the downstream effectors leading to phosphorylation of TOR kinase that stimulates cell growth and negatively regulates autophagy [102].

Cell growth was maintained by expression of the positive regulators of class I PI3K, including the active subunit of PI3K Dp110 and activated Ras^{V12} in mosaic clones

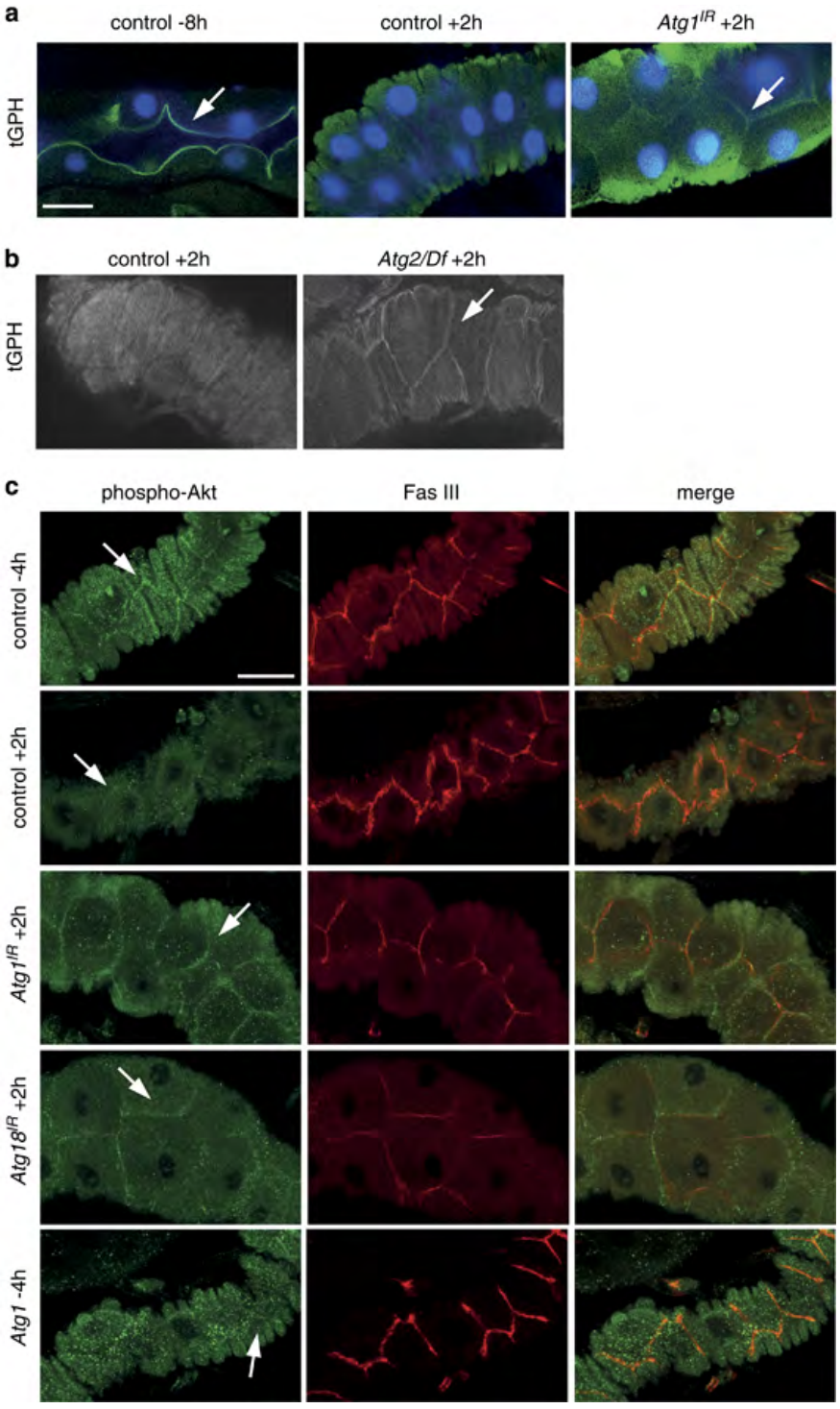

Figure 2-2: Association of growth arrest with autophagy and midgut degradation

The localisation of class I PI3K activity reporters, *t*GPH (a, b) and phospho-Akt (c), in midguts. (a) Cortical localisation of *t*GPH (green) and DNA (blue) in midgut from feeding larvae at -8h RPF (left, arrow) and following puparium formation +2h RPF (middle) *t*GPH is no longer

localised at the cortex. Inhibition of autophagy by (a) *Atg1*^{IR} knockdown (*NP1-GAL4/+; UAS-Atg1-IR/+*) and (b) in *Atg2* mutant (*Atg2/Df*) display cortical localisation of *t*GPH at +2h RPF (arrow) compared to controls. Scale bar in (a) represents 25 μm in all panels in (a) and (b). (c) Cortical localisation of phospho-Akt (green, arrow) adjacent to Fasciclin III (red), a cell surface marker, in control midgut from late larvae (-4h RPF). Following puparium formation (+2h RPF) phospho-Akt is redistributed from the cell cortex. Inhibition of autophagy by knockdown of *Atg1*^{IR} (*NP1-GAL4/+; UAS-Atg1*^{IR}*/+*) or *Atg18*^{IR} (*NP1-GAL4/+; UAS-Atg18*^{IR}*/+*) shows persistence of cortically localised phospho-Akt at +2h RPF (arrow). Induction of autophagy by expression of *Atg1* (*NP1-GAL4/+; UAS-Atg1*^{6B}*/+*) shows decreased cortically localised phospho-Akt (arrow). Scale bar is 30 μm in all panels in c.

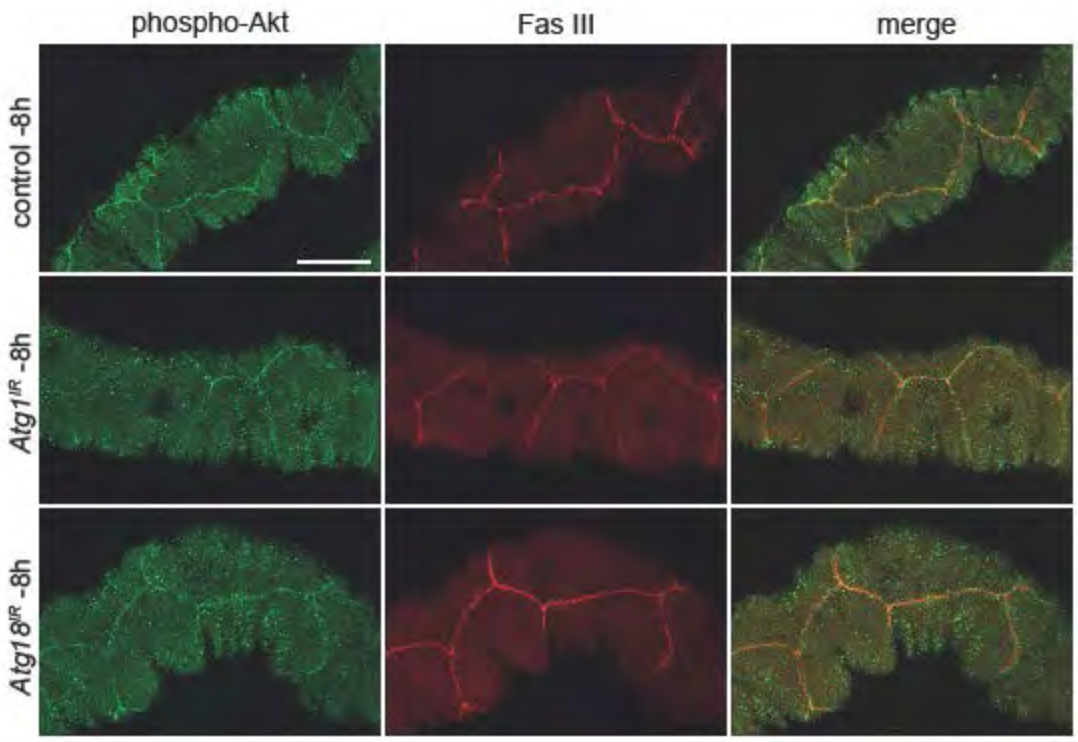

Figure 2-3: Cell size and growth signalling in feeding larvae

Midguts from feeding larvae (-8h RPF) have **c**ortically localised of phospho-Akt (green) adjacent to Fasciclin III, a cell surface marker (red). Inhibition of autophagy by knockdown of *Atg1*^{IR} (*NP1-*

GAL4/+; UAS-Atg1^{IR}/+) or *Atg18^{IR}* (*NP1-GAL4/+; UAS-Atg18^{IR}/+*) shows cortically localised phospho-Akt and cell size similar to the control. Scale bar is 30 μm.

of cells in gastric caeca of the midgut. This revealed that maintenance of growth signalling resulted in enlarged cells compared to the neighbouring control cells with reduced Atg8a puncta (Fig. 2-4a, b). The expression of Ras^{V12} in the entire midgut resulted in a large midgut with delayed degradation, as gastric caeca still persisted at +4h RPF and less condensed midgut was observed at +12h RPF compared to the control (Fig. 2-4c, d). Quantification of the size of gastric caeca showed a significant increase when Ras^{V12} was expressed compared to the control (Fig. 2-4e). These data show that maintaining growth results in suppression of autophagy and supports a role for growth arrest in midgut PCD.

We have previously shown that the caspase Decay is responsible for most of the caspase activity in the midgut and knockdown of *decay* or inhibition of caspase activity does not affect midgut degradation [19]. To determine if caspase activity is affected by growth signalling the levels of caspase-3-like activity in late third instar larvae was measured by cleavage of DEVD-AMC. Compared to the reduction in caspase activity when p35 is expressed in the midgut there was an increase in caspase activity when Ras^{V12} was expressed (Fig. 2-4f). This suggests that caspases remain active in the midgut in the presence of growth signals. There are several examples of nonapoptotic functions of caspases in *Drosophila* including border cell migration, sperm individualization, aristae shaping, dendrite pruning, sensory organ precursor

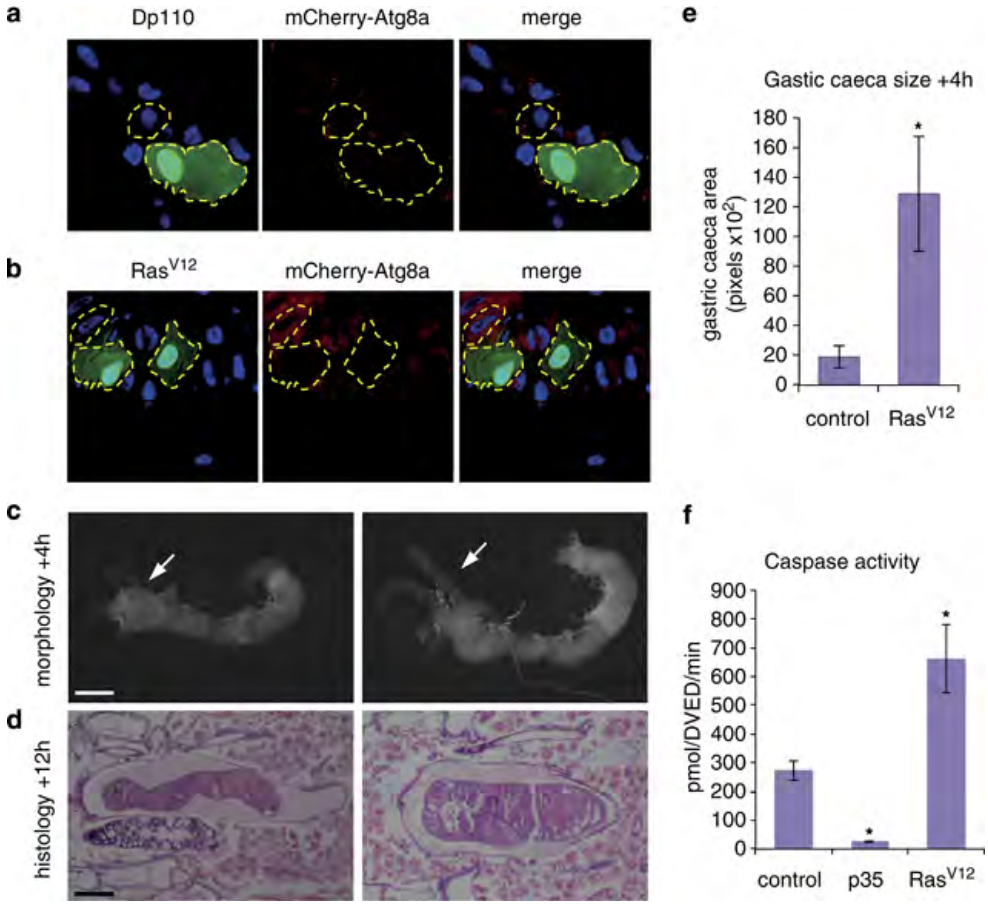

Figure 2-4: Maintenance of growth delays midgut removal

Mosaic clones of (a) *Dp110* (*hsFLP; mcherry-Atg8a/UAS-Dp110; Act>CD2>GAL4, UAS-nlsGFP*) and (b) *Ras^{V12}* (*hsFLP; mcherry-Atg8a/+; Act>CD2>GAL4, UAS-nlsGFP/UAS-Ras^{V12}*) from 0h RPF gastric caeca marked by GFP (green) have decreased levels of mCherry-Atg8a puncta (red) compared to the neighbouring cells and larger cell size. A Dp110 or Ras^{V12} clone and neighbouring cells are outlined. Scale bar in (a) represents 50 μm in all panels in (a) and (b). (c) Morphology of midguts at +4h RPF showing control (left, *NP1-GAL4/+*) compared to *Ras^{V12}* (right, *NP1-GAL4/+; UAS-Ras^{V12}/+*) showing persistent gastric caeca (arrow) compared to the absent gastric caeca in the control (arrow). (d) Histological analysis of paraffin sections at +12h RPF of control (left, *NP1-GAL4/+*) and *Ras^{V12}* (right, *NP1-GAL4 /+; UAS-Ras^{V12}/+*) shows less condensed midgut compared to control. Scale bars in (c, d) represent 200 μm. (e) Quantification of gastric caeca size (average pixels ± SD) at +4h RPF from control (*NP1-GAL4/+*) and *Ras^{V12}* overexpression (*NP1-GAL4/+; UAS- Ras^{V12}/+* (N = 8 and 7, respectively). * p<0.001 (compared

to the control). (f) Caspase activity was measured from -4h RPF larval lysates on DEVD-AMC, represented as pmol DEVD/min. The expression of p35 in the midgut inhibits the majority of caspase activity present in larvae. Data are mean from three independent experiments, with error bars representing SEM. * $p<0.05$ (compared to the control).

differentiation, and in the innate immune response [103]. The high level of caspase activity in the midgut raises the possibility of non-apoptotic functions of caspases in this tissue.

Inhibition of growth results in smaller midguts, which is suppressed by autophagy inhibition

As maintenance of growth is sufficient to delay midgut removal, we examined the effect of inhibiting the class I PI3K pathway by expression of the negative regulators, PTEN and TSC1/TSC2. The expression of either PTEN or TSC1/TSC2 resulted in smaller midguts at late 0h RPF compared with controls (Fig. 2-5a-c). While the larval midguts were smaller, they appeared to undergo rapid degradation and were particularly fragile to dissect at +4h RPF (Fig. 2-5a-c). Mosaic clone expressing PTEN in the midgut of feeding larvae resulted in autophagy induction, as shown by Atg8a puncta, and a smaller cell size compared to the surrounding wild-type cells (Fig. 2-5g). Quantification of the size of gastric caeca showed a significant decrease when PTEN or TSC1/TSC2 was expressed compared to the control at 0h RPF (Fig. 2-5h). Caspase activity levels were similar to controls when either PTEN or TSC1/TSC2 were expressed in the midgut of late third instar larvae (Fig. 2-5j).

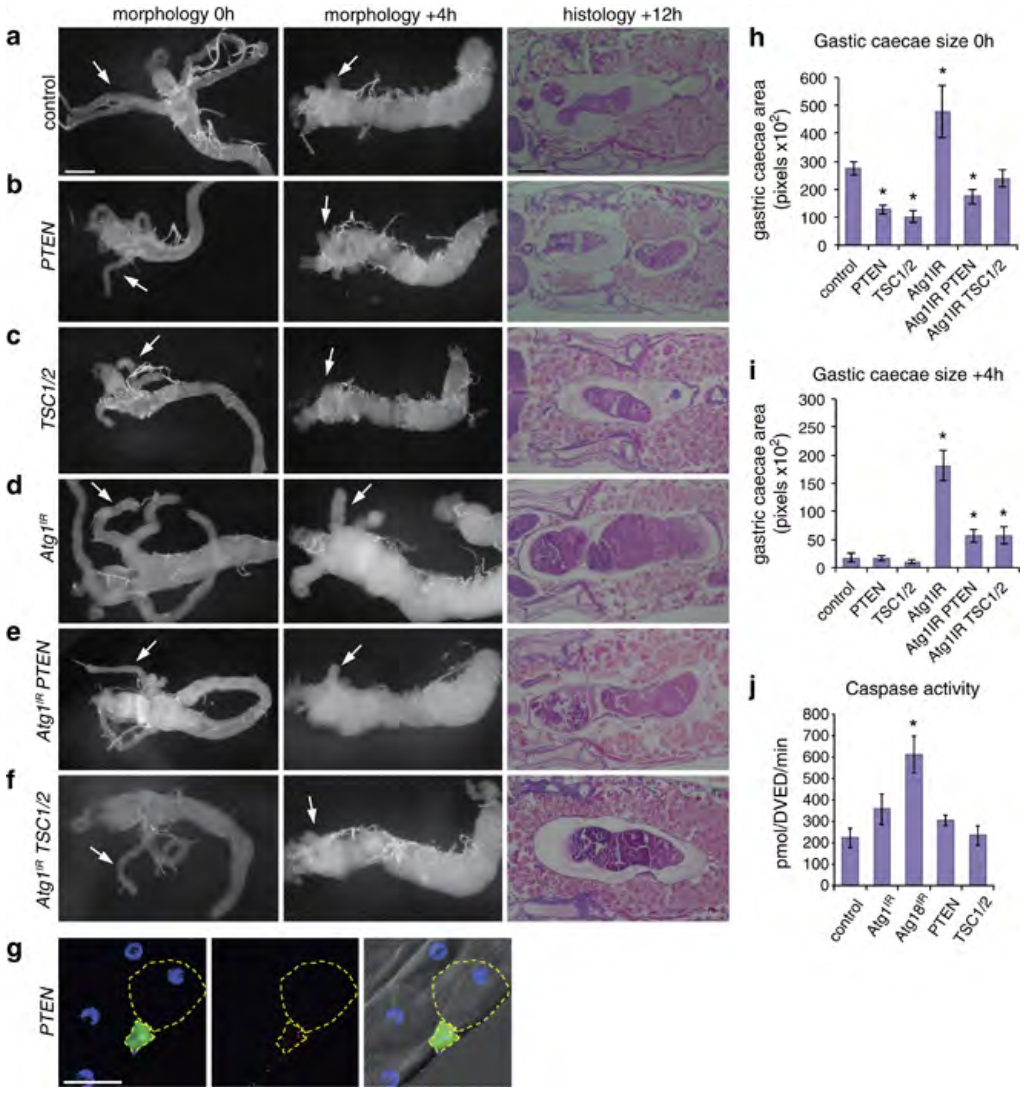

Figure 2-5: Autophagy inhibition delays midgut removal that is suppressed by inhibition of PI3K pathway

Morphology of midguts at 0h RPF (left) and +4h RPF (middle) showing (a) control (*NP1-GAL4/+*) compared to (b) *PTEN* expression (*NP1-GAL4/+; UAS-PTEN/+*) and (c) *TSC1*/2 expression (*NP1-GAL4/+; UAS-TSC1, UAS-TSC2/+*) showing decreased size with contracted gastric caeca at 0h RPF and smaller midgut at +4h RPF. Histological analysis of paraffin sections at +12h RPF (right) shows significant midgut contraction in (b) *PTEN* expression and (c) *TSC1*/2 expression compared to control (a) (*NP1-GAL4/+*). (d) Inhibition of autophagy severely delays midgut degradation. Morphology of midguts at 0h RPF (left) and +4h RPF (middle) show a significant delay in midgut histolysis in (d) $Atg1^{IR}$ (*NP1-GAL4/+; UAS-*$Atg1^{IR}$*/+*) compared to (a) control as

seen by the presence of less contracted gastric caeca at +4h RPF (arrows). Histological analysis of paraffin sections at +12h RPF (right) shows an enlarged midgut in (d) *Atg1^{IR}* compared to (a) control. The combined expression of (e) *Atg1^{IR} PTEN* and (f) *Atg1^{IR} TSC1/2* suppressed the delay in midgut histolysis with greater contraction of gastric caeca at +4h RPF (arrows) compared to (d) *Atg1^{IR}* alone. The delayed midgut histolysis in (d) *Atg1^{IR}* is reduced by co-expression of (e) *PTEN* or (f) *TSC1/2* at +12h RPF. Scale bars in (a) represent 200 μm in all panels. (g) Mosaic clones of *PTEN* (*hsFLP; mCherry-Atg8a/+; Act>CD2>GAL4, UAS-nlsGFP/UAS-PTEN*) marked by GFP (green) and DNA (blue) have smaller cell size with increased autophagy compared to the neighbouring cells. Scale bar in (g) is 50 μm. (h) Quantification of gastric caeca size (average pixels ± SD) at 0h RPF from control, *PTEN, TSC1/2*, *Atg1^{IR}*, *Atg1^{IR} PTEN* and *Atg1^{IR} TSC1*/2 (N=10, 12, 9, 8, 5 and 12, respectively). * $p<0.001$ (compared to the control). (i) Quantification of gastric caeca size (average pixels ± SD) at +4h RPF measured from control, *PTEN*, *TSC1*/2, *Atg1^{IR}*, *Atg1^{IR} PTEN* and *Atg1^{IR} TSC1*/2 (N=8, 8, 9, 9, 10 and 9, respectively). * $p<0.001$ (compared to the control). (j) Caspase activity was measured from -4 h RPF larval lysates on DEVD-AMC, represented as pmol DEVD/min. Data are mean from three independent experiments, with error bars representing SEM.

To determine if down-regulation of growth signalling was required for the induction of autophagy during midgut removal, we examined the interaction between the knockdown of autophagy genes *Atg1* and *Atg18* combined with expression of either PTEN or TSC1/TSC2. The inhibition of autophagy by knockdown of *Atg1* or *Atg18* severely delayed midgut removal, consistent with previous studies (Fig. 2-5d; 2-6a) [19]. When *Atg1* knockdown was combined with either PTEN or TSC1/TSC2 expression the midgut size was more similar to the control at 0h RPF compared to PTEN and TSC1/TSC2 expression or *Atg1* knockdown alone (Fig. 2-5e, f, h). Similarly, when *Atg18* knockdown was combined with either PTEN or TSC1/TSC2 expression the

growth retardation seen at 0h RPF of PTEN and TSC1/TSC2 expression alone were suppressed (Fig. 2-6b, c, d). Furthermore, the combined *Atg1* knockdown and PTEN or TSC1/TSC2 resulted in an increase in contraction of gastric caeca at +4h RPF and more condensed midgut at +12h RPF compared to *Atg1* knockdown alone (Fig. 2-5e, f, i). Again, similar results were observed with *Atg18* knockdown combined with PTEN or TSC1/TSC2 expression showing an increase in contraction of gastric caeca at +4h RPF and more condensed midgut at +12h RPF compared to *Atg18* knockdown alone (Fig. 2-6b, c, e). This suggests that whilst the degradation of growth-arrested midguts requires autophagy, there is a feedback between autophagy and down-regulation of growth signalling. An alternative model is that autophagy and growth signalling act in parallel pathways during midgut removal. This also raises the possibility that autophagy may have different influences on cell survival before and after growth arrest.

Salvador-Warts-Hippo pathway is not involved in regulating midgut cell death

The highly conserved Salvador-Warts-Hippo pathway is a negative regulator of cell and tissue growth, and central to the pathway are the Hippo (Hpo) and Warts (Wts) kinases that act to inhibit the Yorkie transcription factor [104]. The Salvador-Warts-Hippo pathway has been shown to be required for correct removal of salivary glands [100]. The salivary glands of *wts* mutants do not growth arrest, have decreased autophagy and persist beyond the normal time of degradation. Furthermore, the *wts* mutant salivary glands have altered PI3K signalling and the delayed degradation could be rescued by TOR inhibition. Given this, together with the role of PI3K pathway and autophagy in

midgut cell death, we examined the role of the *wts* in the degradation of the midgut to determine if this is a common requirement for PCD.

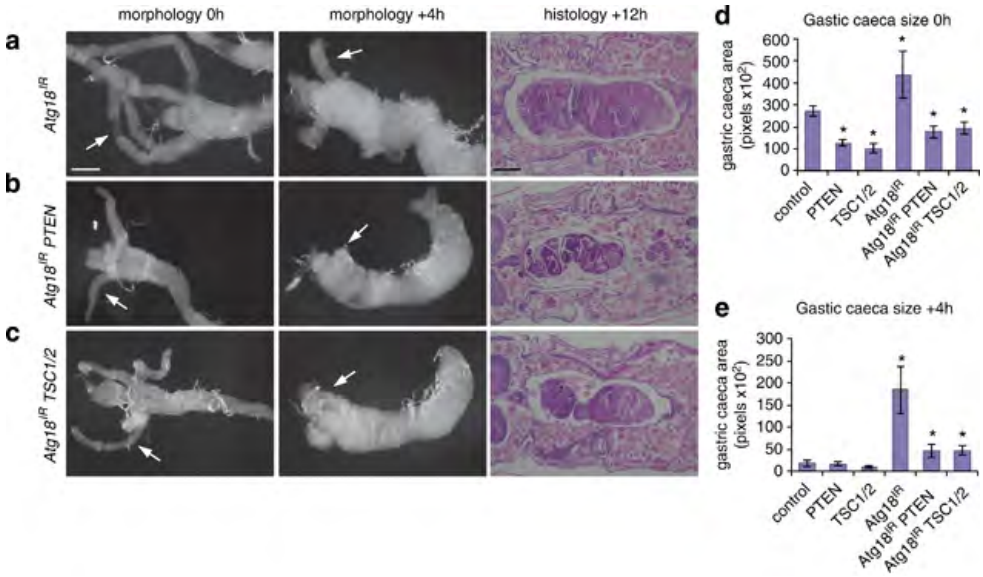

Figure 2-6: Autophagy inhibition by Atg18 knockdown delays midgut removal that is suppressed by inhibition of PI3K pathway

Morphology of midguts at 0h RPF (left) and +4h RPF (middle) show a significant delay in midgut histolysis in (a) *Atg18^{IR}* as seen by the presence of less contracted gastric caeca at +4h RPF (arrows). Histological analysis of paraffin sections at +12h RPF (right) shows an enlarged midgut in (a) *Atg18^{IR}*. The combined expression of (b) *Atg18^{IR} PTEN* and (c) *Atg18^{IR} TSC1/2* suppressed the delay in midgut histolysis with greater contraction of gastric caeca at +4 h RPF (arrows) compared to (a) *Atg18^{IR}* alone. The delayed midgut histolysis in (a) *Atg18^{IR}* is reduced by co-expression of (b) *PTEN* or (c) *TSC1/2* at +12h RPF. Scale bars represent 200 μm. (d) Quantification of gastric caeca size (average pixels ± SD) at 0h RPF from control, PTEN, TSC1/2, *Atg18^{IR}*, *Atg18^{IR} PTEN* and *Atg18^{IR} TSC1/2* (N=10, 12, 9, 7, 6 and 10, respectively). * $p<0.001$ (compared to the control). (e) Quantification of gastric caeca size (average pixels ± SD) at +4h RPF from control, PTEN, TSC1/2, *Atg18^{IR}*, *Atg18^{IR} PTEN* and *Atg18^{IR} TSC1/2* (N=8, 8, 9, 9, 5 and 6, respectively). * $p<0.001$ (compared to the control).

The knockdown of *wts* in the midgut did not alter the morphology or timing of midgut degradation (Fig. 2-7a,b,e). The gastric caeca were contracted at +4h RPF similar to the control and the midgut condensed at +12h RPF (Fig. 2-7a, b, e). In addition the midgut appeared to undergo normal degradation in wts^{lacZ} mutants (Fig. 2-7c, e). Mosaic clonal analysis also showed that expression of *yorkie* does not alter cell growth (Fig. S 2-7d). Thus, unlike in the salivary gland where *wts* is required for growth arrest and PCD, Hpo/Wts-dependent growth arrest pathway is dispensable for midgut degradation. This highlights the tissue specific requirements for different signalling pathways and the importance of understanding how these act to regulate autophagy not only in cell survival but also in cell death.

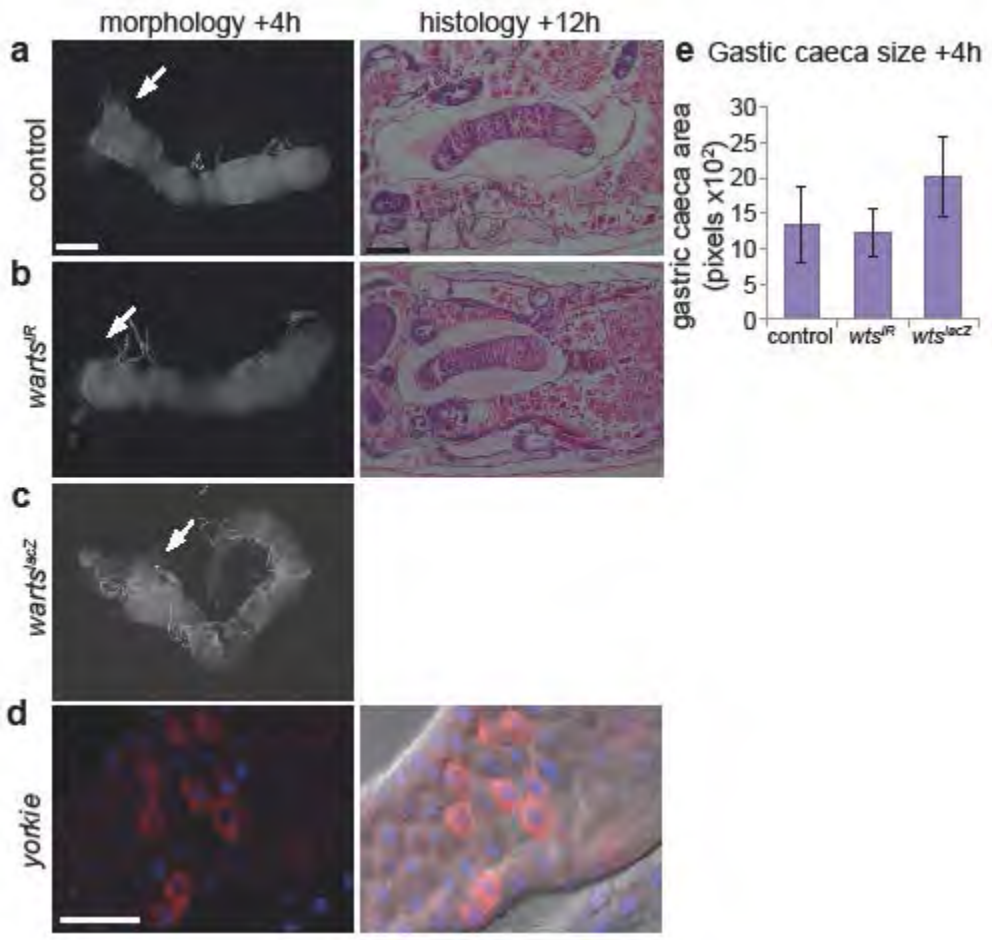

Figure 2-7: Salvador-Warts-Hippo pathway is not required for midgut programmed cell death

Morphology of midguts at +4h RPF (left) showing (a) control (*NP1-GAL4/+*) compared to (b) *warts*^{IR} knockdown (*NP1-GAL4/UAS-wts*^{IR}) and (c) *warts*^{lacZ} mutant showing contraction of the gastric caeca similar to control (arrows). Histological analysis of paraffin sections at +12h RPF (right) shows midgut contraction is similar in (a) control (*NP1-GAL4/+*), (b) *warts*^{IR} knockdown. *warts*^{lacZ} mutant animals die prior to +12h RPF. Therefore histological analysis of these animals was not feasible. Scale bars in (a-c) represent 200 µm. Mosaic clones of (d) *yorkie* overexpression (*hsFLP; +; Act>CD2>GAL4, UAS-DsRed/UAS-yorkie*) marked by DsRed (red) are a similar cell size compared to the neighbouring cells. (e) Quantification of gastric caeca size (average pixels ± SD) at +4h RPF from control, *warts*^{IR} and *warts*^{lacZ} (N=3). * p<0.001 (compared to the control).

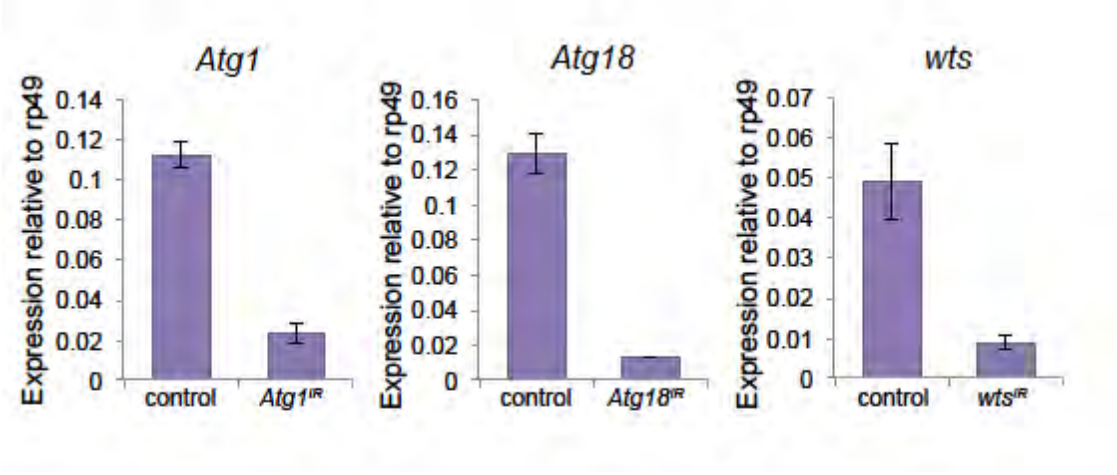

Figure 2-8: Quantitation of the level of gene knockdown in RNAi lines

Verification of the knockdown of *Atg1*, *Atg18,* and *wts* in the midguts of late third instar larvae (-4h RPF) by qPCR. Transcript levels were normalised against the internal control gene *rp49* and represented as relative expression. Error bars represent SD.

Discussion

Our work provides critical evidence that the autophagic cell death in *Drosophila* larval midgut is dependent upon growth inhibition. The developmental PCD of salivary glands that requires autophagy is dependent on down-regulation of PI3K [18]. The developmental induction of autophagy in the fat body that occurs in response to ecdysone also appears to be mediated by down-regulation of PI3K signalling [105]. We now demonstrate that this down-regulation of PI3K signalling is required for autophagic removal of obsolete larval midgut tissue.

We also found that despite apparent similarity in the requirement of autophagy for the destruction of the larval midgut and salivary glands, there are distinct differences between these tissues. While the removal of the larval salivary glands requires both

caspase activation and autophagy acting in parallel pathways, midgut removal that is dependent on autophagy and does not require the Salvador-Warts-Hippo growth inhibitory pathway. This study further reveals a relationship between autophagy and cell growth, as inhibition of autophagy maintained growth signalling and suggests that while they may be coordinately regulated there appears to be feedback signalling with autophagy required for down-regulation of class I PI3K signalling. This is a surprising finding and we propose the following possibilities for the mechanism/s of this novel feedback regulation: (i) autophagy has a role in the down regulation of growth signalling, potentially at the level of the cell surface receptor or PIP3 degradation/recruitment to autophagosome, (ii) autophagy indirectly degrades a negative regulator/inhibitor of the PI3K signalling, and (iii) autophagy is involved in a parallel pathway [11, 106].

In most circumstances starvation-induced autophagy has a role in cell survival rather than cell death. While the induction of autophagy during cell death appears to require the down-regulation of growth signalling, these same pathways can result in the induction of autophagy as a survival response in other situations. However, autophagic cell death may overcome feedback with growth signals resulting in maintained levels of autophagy that ultimately result in cell destruction. This may correlate with the levels of *Atg1* gene expression induced during metamorphosis, which is not seen under starvation conditions. In response to starvation, *Atg8* in yeast and *Atg8a* in *Drosophila* fat body are transcriptionally upregulated, while other *Atg* genes are not [107-109]. This is in contrast to the increase in expression of *Atg1* and many of the *Atg* genes during salivary gland and midgut cell death, where only a slight increase in *Atg8a* is observed [19, 80, 94,

[101]. Whilst autophagy induction in both survival and death may occur in response to similar growth signals, distinct components of the autophagy pathway may be rate limiting.

Studies in *Drosophila* suggest that most of the autophagic cell death occurs when nutrients are limiting such as the non-feeding stage of metamorphosis, depletion of extra-embryonic tissue, and in oogenesis during nutrient limitation [83, 85]. Thus in such context autophagy may be induced in response to reduced growth signals under nutrient limiting conditions to remove obsolete cells/tissues. These observations may provide a conceptual basis for the dual role of autophagy in cell growth and cell death in tumour cells [86]. Several important questions arise from this study. For example how does autophagy influence cell growth and mediate cell death? Does autophagy result in the specific degradation of either survival or death-inhibiting factors, or by general degradation of the cell mass [110]? Future work will address these critical issues.

Acknowledgements

This work was supported by the National Health and Medical Research Council of Australia Project Grant (626923) and a Senior Principal Research Fellowship (1002863) to SK, and NIH grant GM079431 to EHB. We thank Dr Kieran Harvey, the Australian *Drosophila* Research Support Facility, Vienna *Drosophila* RNAi Center, and Bloomington *Drosophila* Stock Center for *Drosophila* stocks, Developmental Studies Hybridoma Bank (University of Iowa) for antibodies, Earanee Niedzwiecki and Tina Fortier for maintaining stocks, and Amanda Rogers for tissue processing.

Author contributions

Fig. 2-1c,d, 2-2b, 2-3a,b, 2-4g were performed by T-K.C. Other experiments were performed by D.D. and S.N. B.S. and R.S. generated the pmCherry-Atg8a line. E.H.B. and S.K. supervised the experiments. D.D. and S.K. wrote the paper and all authors commented on it.

Materials and methods

Fly stocks

RNAi line *UAS-Atg18^{IR}* was obtained from the Vienna *Drosophila* RNAi Center (Vienna, Austria). The following stocks were from the Bloomington stock center (Bloomington, IN, USA): *UAS-Atg1^{IR}* (*y^{1} sc* v^{1}; P[TRiP.GL00047]attP2/TM3, Sb^{1}*), *UAS-Ras^{v12}*, *UAS-Dp110*, *hsflp UAS-nlsGFP, Act>CD2>GAL4*. The midgut driver, *NP1-GAL4*, was obtained from the *Drosophila* genetic resource center (Kyoto, Japan). Other stocks were obtained from: *UAS-Atg1* from T. Neufeld; *UAS-PTEN, UAS-TSC1,UAS-TSC2, UAS-wts^{IR}, UAS-hpo^{IR}* and *warts^{lacZ}* from K. Harvey. All flies were maintained and crosses performed at 25^{o}C. Larvae were grown on food containing 0.05% bromophenol blue as described [111], and staged by collection of wandering larvae onto damp Whatmann paper in a petri dish.

Promoter-mCherry-ATG8a reporter for autophagy detection

Autophagy was assessed by mCherry-ATG8a puncta formation. A region 2kb upstream of *Atg8a (CG32672)* was inserted upstream of mCherry-Atg8a in the pCaSpeR4 *Drosophila* transformation vector, as was previously described for a similar GFP-Atg8a reporter line.[3] The resulting plasmid pCaSpeR4-promoter-mCherry-Atg8a was used to generate transgenic *Drosophila* lines using standard procedures. Due to a lack of suitable reagents for monitoring autophagy flux, Atg8a puncta is commonly used for detecting autophagy in vivo in *Drosophila*.

Histology

For hematoxylin and eosin staining of whole pupal sections, +12h RPF pupae were fixed in FAAG (85% ethanol, 4% formaldehyde, 5% acetic acid and 1% glutaraldehyde), then paraffin embedded prior to sectioning and staining as previously described.[18,23] The controls were *w*^{1118} *Drosophila* crossed to either *NP1-GAL4*, or the experimental *UAS*-transgene line being analyzed. For each genotype a minimum of 10 pupae were examined using a stereozoom microscope (Olympus, Tokyo, Japan).

Immunohistochemistry

Midguts of the required genotype were dissected from appropriately staged animals in PBS then fixed with 4% paraformaldehyde in PBS for 20 min at room temperature. Primary antibodies used were rabbit anti-phospho-Drosophila-Akt (1:200) (Cell Signaling, Danvers, MA, USA) and mouse anti-Fasciclin III (1:100) (7G10, Developmental Studies Hybridoma Bank, Iowa, IA, USA). Secondary antibodies used were anti-rabbit Alexa-FLUOR 488 (Molecular Probes, Eugene, CA, USA), anti-mouse Alexa-FLUOR 566 (Molecular Probes). Hoechst 33342 (Sigma-Aldrich, St. Louis, MO, USA) was used to detect DNA. The samples were imaged with a Biorad confocal microscope (Bio-Rad Microscience, UK; at Detmold Imaging Core Facility, Hanson Institute, Adelaide, SA, Australia).

Live GFP and mCherry imaging

To assay for GFP-Atg8a and *t*GPH, the reporters were in *NP1-GAL4* background and crossed with appropriate control or experimental flies. Midguts from pupae staged +2h RPF were dissected in PBS, stained with Hoechst 33342 (Sigma-Aldrich) and imaged

immediately without fixation using a Biorad confocal microscope. To assay for mCherry-Atg8a, midguts were dissected in PBS, briefly fixed with 4% formaldehyde and stained with either Hoechst 33342 (Sigma-Aldrich) or DAPI (Roche, Indianapolis, IN, USA) to detect DNA.

Light microscopy

Pupae were staged 0 or +4h RPF and midguts were dissected in PBS, fixed in 4% formaldehyde/PBS and examined using a stereozoom microscope (Olympus). Measurements of gastric caeca size were done using either Zeiss automeasure software as in Fig. 1, or Photoshop (Adobe, San Jose, CA, USA) magnetic lasso tool. The histogram function was used to determine pixel area.

Imaging

Confocal images were obtained using a BioRad Radiance 2100 confocal microscope with Argon ion 488 nm (14 mw) and Green HeNe 543 nm (1.5 mw) lasers and an Olympus IX70 inverted microscope with a 40x UPLAPO (NA=1.2 water) objective. The dual labeled samples were imaged with two separate channels (PMT tubes) in a sequential setting. Green fluorescence was excited with an Ar 488 nm laser line and the emission viewed through a HQ515/30 nm narrow band barrier filter in PMT1. Red fluorescence was excited with a HeNe 543 nm laser line and the emission viewed through a long pass barrier filter (E570LP) in PMT2. Automatically all signals from PMTs 1 and 2 were merged. Image were captured using Confocal Assistant software for

Microsoft Windows (Todd Clark Brelje, Bethesda, MD, USA) and compiled using Photoshop CS5 (Adobe).

Caspase assays

The caspase activity assays were performed as previously described [41] using 30µg of late larval protein lysate with 100µM of DEVD-AMC (MP Biomedicals, Solon, OH, USA) made up to a final volume of 100µl in caspase assay buffer (50mM HEPES, pH 7.5, 100mM NaCl, 1mM EDTA, 0.1% CHAPS, 10% sucrose, 5mM DTT, 0.5% TritonX-100, 4% glycerol with protease inhibitor mix (Roche, Indianapolis, IN, USA)). The fluorescence was measured over a 3h time course at 30 min intervals using a FluoStar spectrophotometer (BD Biosciences, Franklin Lakes, NJ, USA) (excitation, 385 nm; emission, 460 nm) and the activity calculated as previously described [112].

Quantitative Real-Time PCR

Quantitation of the level of RNAi knockdown of various lines was done by qPCR (Fig. 2-8). Total RNA was isolated from *Drosophila* midguts using TRIzol reagent (Invitrogen, Carlsbad, CA, USA). cDNA was synthesized using High Capacity cDNA Reverse Transcription Kit (Applied Biosciences, Foster City, CA, USA) and oligo dT primer, with 1µg of total RNA. Real-Time PCR was performed on a Rotor-Gene 3000 (Corbett Research, Mortlake, NSW, Australia) using RT^2 Real-Time SYBR Green/ROX PCR MasterMix (Qiagen, Valencia, CA, USA) as per the manufacturer's instructions. Reactions were performed in triplicate and the mRNA expression levels normalized against the internal control gene *rp49* using the ΔΔCT method. Primer sets used are:

rp49 F 5’-CCAGTCGGATCGATATGCTAA; R 5'-ACGTTGTGCACCAGGAACTT

Atg1 F 5’-ACGGCGGACAAGATTCTCTA; R 5’ GCTGCTGCAATATGCTCAAA

Atg18 F 5’-AGGTGACCGACGTGTTTAGC; R 5’-ACGGTGGGAATGGAATACAC

wts F 5’-GAGGTGCTGGAGAGAAGTGG; R 5’-CAGGGTTTTCTCCCAGTTGA

Statistical analysis of data

Student’s t-test was used for all statistical analysis unless otherwise stated. Data are expressed as mean ± SD or mean ± SEM, as appropriate. $P<0.05$ was considered significant.

CHAPTER III

Uba1 Functions in Atg7- and Atg3-Independent Autophagy

Abstract

Autophagy is a conserved process that delivers components of the cytoplasm to lysosomes for degradation. The E1 and E2 enzymes encoded by *Atg7* and *Atg3* are thought to be essential for autophagy involving the ubiquitin-like protein Atg8. Here, we describe an Atg7- and Atg3-independent autophagy pathway that facilitates programmed reduction of cell size during intestine cell death. Although multiple components of the core autophagy pathways, including Atg8, are required for autophagy and cells to shrink in the midgut of the intestine, loss of either Atg7 or Atg3 function does not influence these cellular processes. Rather, Uba1, the E1 used in ubiquitination, is required for autophagy and reduction of cell size. Our data reveal that distinct autophagy programs are used by different cells within an animal, and disclose an unappreciated role for ubiquitin activation in autophagy.

Introduction

Macroautophagy (autophagy) is a system that is used to transfer cytoplasmic material, including proteins and organelles, to lysosomes by all eukaryotic cells [113]. Autophagy is augmented during cell stress to reduce damage to enable cell survival, and is also associated with the death of animal cells [114, 115]. Although most studies of this process have focused on stress-induced autophagy, such as nutrient deprivation, autophagy is also a normal aspect of animal development where it is required for proper death and removal of cells and tissues [18, 91, 110]. Defects in autophagy lead to accumulation of protein aggregates and damaged organelles, as well as human disorders [60, 113]. Most of our knowledge about the genes controlling autophagy is based on pioneering studies in the yeast *Saccharomyces cerevisiae* [20-22, 116], and it is not clear if cells that exist in extremely different contexts within multi-cellular organisms could use alternative factors to regulate this catabolic process.

Atg genes that are conserved from yeast to humans are required for autophagy, and include the Atg1 and Vps34 regulatory complexes, as well as two ubiquitin-like conjugation pathways [113]. The two ubiquitin-like molecules, named Atg8 (LC3/GABARAP in mammals) and Atg12, become associated with the isolation membranes that form autophagosomes through the activity of the E1 enzyme Atg7. Atg3 functions as the E2 conjugating enzyme for Atg8, while Atg10 functions as the E2 for Atg12 [117]. Atg12 associates with Atg5 and Atg16 during the formation of the autophagosome, and Atg8 is conjugated to the lipid phosphatidyl-ethanolamine enabling this protein to associate with the isolation membrane and autophagosome.

Lipidated Atg8 remains associated with autophagosomes until fusion with lysosomes to form autolysosomes where cargos are degraded by lysosomal enzymes.

Degradation of the midgut of the *Drosophila* intestine involves a large change in midgut length, has elevated autophagy and markers of caspases associated with it, requires autophagy, and appears to be caspase-independent [19, 84, 118]. Here, we show that autophagy is required for programmed reduction in cell size at the onset of intestine cell death in *Drosophila*. *Atg* genes encoding components of the Atg1 and Vps34 complexes are required for midgut cell autophagy and reduction in size. Surprisingly, although Atg8a is required for autophagy and programmed cell size reduction, the evolutionarily conserved E1 activating enzyme Atg7 and E2 conjugating enzyme Atg3 are not required for these cellular events. We screened the E1 activating enzymes encoded by the fly genome and identified *Uba1* as being required for autophagy and reduction of cell size during midgut cell death. Although the genes that control autophagy are conserved throughout eukaryotes, our data provide evidence indicating that the core autophagy machinery may not be identical in all cells within an organism.

Results

Autophagy is required for programmed cell size reduction during cell death

The dying *Drosophila* larval intestine undergoes a dramatic reduction in midgut length at the onset of puparium formation [84, 118], and this change in structure requires autophagy and appears to be caspase-independent [19]. We investigated the morphology of midgut cells in order to gain insight into how autophagy may contribute to the

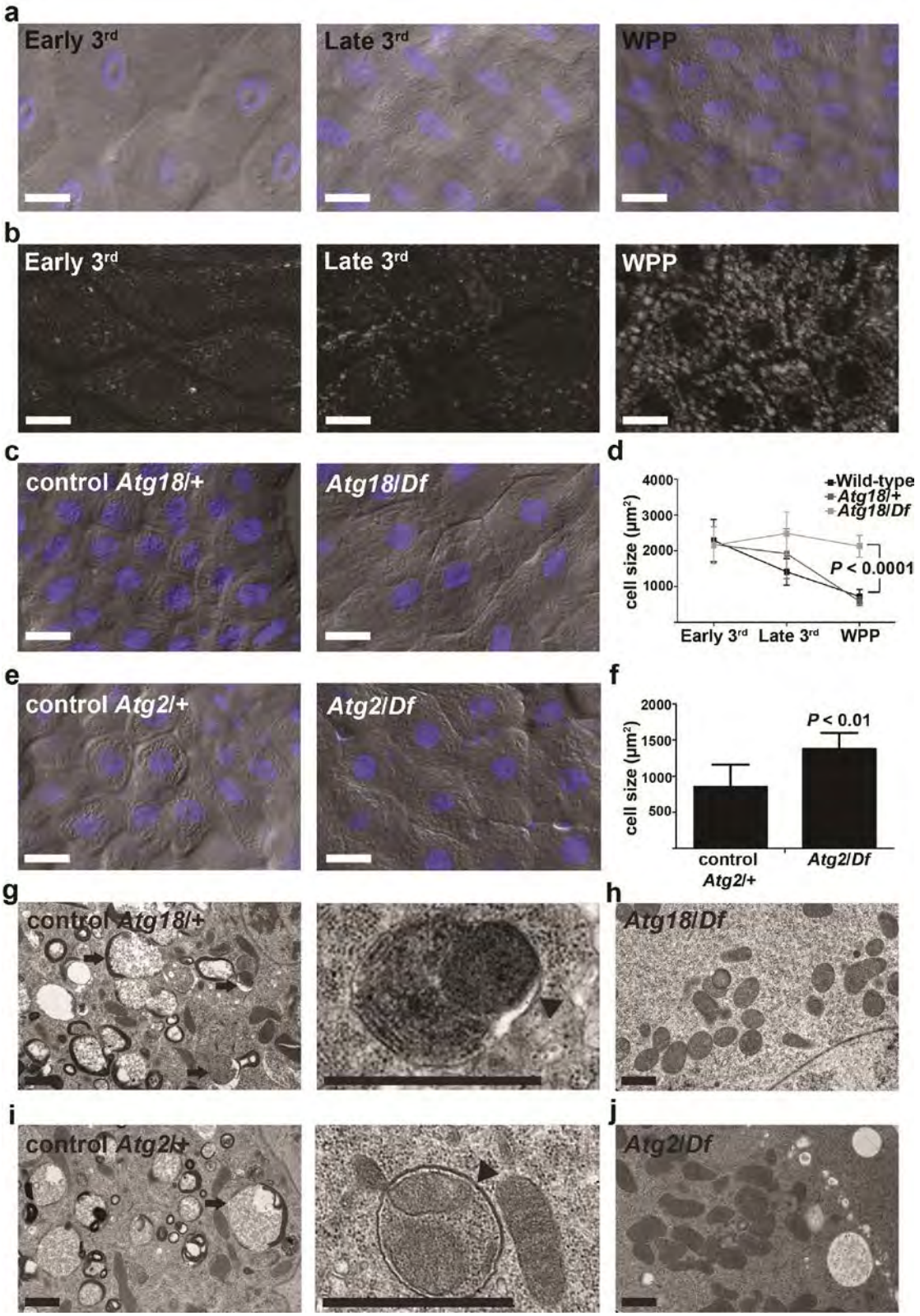
a
Early 3rd
Late 3rd
WPP
b
Early 3rd
Late 3rd
WPP
c
control Atg18/+
Atg18/Df
d
Wild-type
Atg18/+
Atg18/Df
cell size (μm²)
4000
3000
2000
1000
P < 0.0001
Early 3rd
Late 3rd
WPP
e
control Atg2/+
Atg2/Df
f
cell size (μm²)
2000
1500
1000
500
P < 0.01
control
Atg2/+
Atg2/Df
g
control Atg18/+
h
Atg18/Df
i
control Atg2/+
j
Atg2/Df

Figure 3-1 *Atg18* and *Atg2* are required for programmed cell size reduction in the *Drosophila* midgut. (**a**) Representative differential interference contrast (DIC) microscopy images of midgut cells from wild-type animals at the early third instar larval (Early 3rd), late third instar larval (Late 3rd) and at puparium formation (white prepupal, WPP) stages. (**b**) Autophagy detected by formation of mCherry-Atg8a punctate spots in midgut cells from wild-type animals at indicated stages. Representative images are shown. (**c**) Midguts from control *Atg18*^{KG03090}/wild-type (*Atg18*/+), *n* =14, and *Atg18*^{KG03090}/*Df(3L)*^{6112} mutant (*Atg18*/*Df*), *n* = 11, animals at puparium formation analyzed by DIC microscopy. Representative images are shown. (**d**) Wild-type, control (*Atg18*^{KG03090}/+) and *Atg18* mutant (*Atg18*/*Df*) midgut cell size quantification (μm^2) at indicated stages, *n* = 10 animal intestines/genotype with 5 cells measured/intestine/stage. (**e**) DIC images of midgut cells from *Atg2*^{EP3697}/wild-type control (*Atg2*/+) and *Atg2*^{EP3697}/*Df(3L)*^{6091} mutant (*Atg2*/*Df*) animals at puparium formation. Representative images are shown. (**f**) Cell size quantification (μm^2) from **e**, *n* = 12 (*Atg2*/+) and *n* = 7 (*Atg2*/*Df*) animal intestines/genotype with 5 cells measured/intestine. (**g-j**) Representative TEM images of intestine cells 2 hours after puparium formation. (**g**,**i**) Control *Atg18*^{KG03090}/wild-type (*Atg18*/+, **g**) and *Atg2*^{EP3697}/wild-type control (*Atg2*/+, **i**) cells with an enlarged image showing a double membrane structure (arrowhead) that surrounds a mitochondrion and endoplasmic reticulum. Arrows indicate autolysosomes. (**h**,**j**) *Atg18*^{KG03090}/*Df(3L)*^{6112} mutant (*Atg18*/*Df*, **h**) cell and *Atg2*^{EP3697}/*Df* (*Atg2*/*Df*, **j**) mutant cells lacking autophagic structures. Quantification is shown as mean ± standard deviation (s.d.). Scale bars represent 20 μm (**a-c** and **e**) and 1 μm (**g-j**).

dramatic change in larval intestine structure. We noticed that wild-type, as well as *Atg18*/wild-type and *Atg2*/wild-type heterozygous control, midgut cells undergo a dramatic reduction in size following the induction of autophagy from the third instar larval stage to pre-pupal stage (Fig. 3-1a-f). By contrast, *Atg18*/*Df* and *Atg2*/*Df* mutant animals lacked autophagy in the midgut based on transmission electron microscopy (TEM) (Fig. 3-1g-j) and GFP-Atg8a reporter analyses [19]. Moreover, we observed double

membrane autophagosomes containing either mitochondria or ribosomes in control midgut cells (enlarged images in Fig. 3-1g,i). Significantly, either *Atg18*/*Df* or *Atg2*/*Df* mutant midguts showed a remarkable inhibition of the decrease in cell size (Fig. 3-1c-f). Thus, the striking reduction in midgut cell size involves a programmed process requiring autophagy.

We tested if the requirement of *Atg* genes for cell size reduction is cell autonomous by expression of a double-stranded inverse-repeat (IR) construct designed to target and knockdown *Atg18* (*Atg18*^{IR}) in clones of cells. Indeed, cells expressing *Atg18*^{IR} were significantly larger than neighboring cells (Fig. 3-2a,b). Furthermore, cells that expressed *Atg18*^{IR} exhibited attenuated autophagy; compared to smaller neighboring cells, they possessed far fewer autophagosomes based on the detection of mCherry-Atg8a puncta (Fig. 3-2c). In addition, either a loss-of-function mutation in *Atg1* or knockdown of *Atg1* prevented cells from shrinking (Fig. 3-2d-f). Importantly, knockdown of *Atg1* in clones of cells also attenuated the formation of mCherry-Atg8a puncta compared to the smaller neighboring control cells (Fig. 3- 2f). Moreover, reduced *Atg1* function does not influence midgut cell size in third instar larvae (Fig. 3-3a,b), further indicating that loss of autophagy does not influence cell growth during early development and that autophagy is required for cells to decrease in volume at the end of larval development. We investigated if analyses of cell size reflect a similar change in midgut cell volume (Fig. 3-2g-k), and determined that 2-dimensional measurements of cell size accurately represent the changes observed in shrinking midgut cells. These data indicate that autophagy is required in a cell autonomous manner for the

programmed reduction of midgut cell size at the end of larval development.

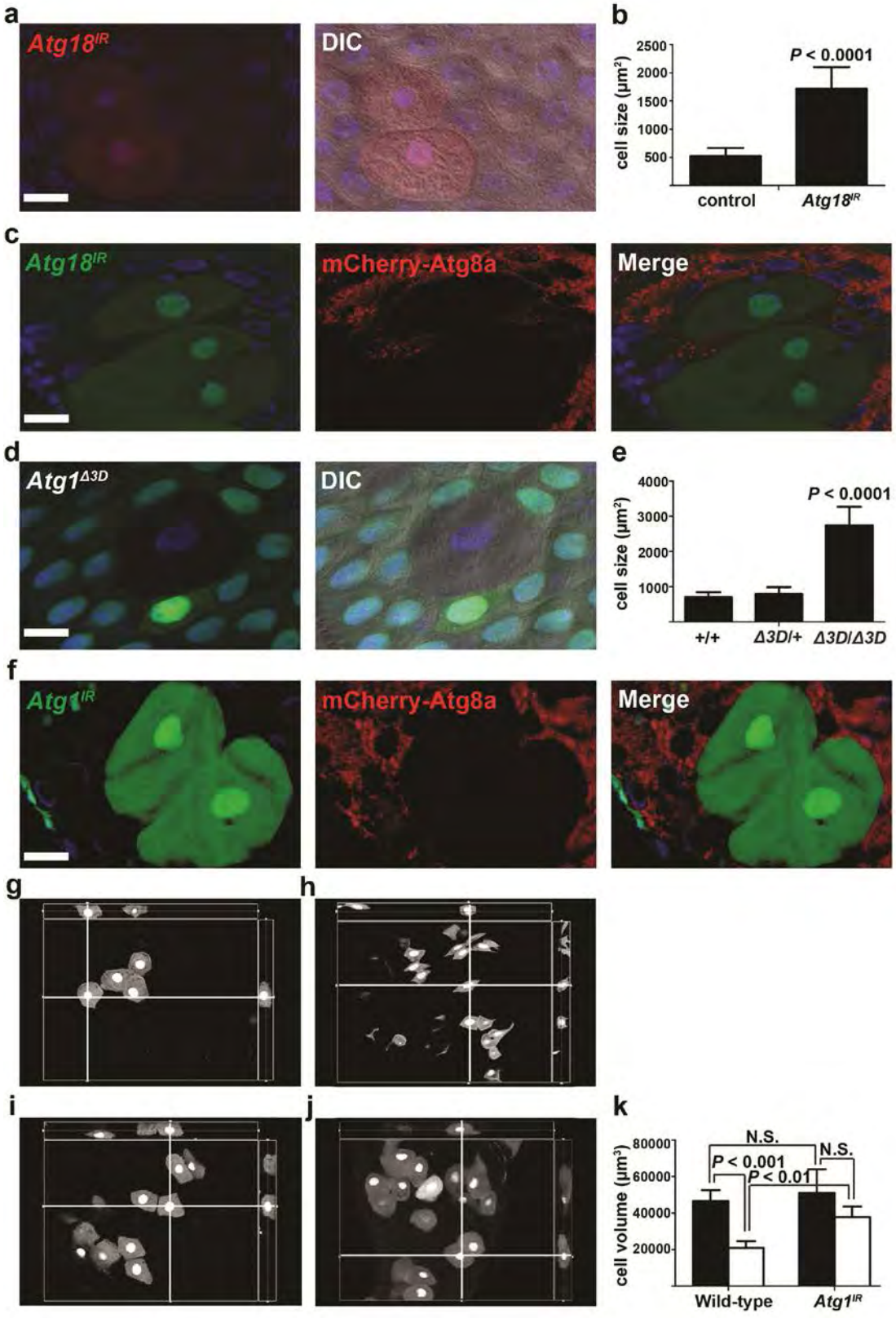

Figure 3-2 Programmed size reduction is cell autonomous and requires *Atg18* and *Atg1*. (**a**) Midguts dissected from animals expressing $Atg18^{IR}$ specifically in DsRed-marked clones of cells at puparium formation and analyzed by fluorescence and DIC microscopy. Representative images are shown. (**b**) Quantification (μm^2) from **a**, *n* = 12 animal intestines/genotype with 1-5 cells measured/intestine. (**c**) Midguts expressing mCherry-Atg8a in all cells, and expressing $Atg18^{IR}$ specifically in GFP-marked cell clones dissected from animals at 2 h after puparium formation. Representative images are shown. (**d**) Midguts dissected from animals at puparium formation that contain an $Atg1^{\Delta 3D}$ loss-of-function mutant cell clone (lacking GFP) and analyzed by fluorescence and DIC microscopy. Wild-type (+/+) control cell possesses stronger GFP and heterozygous $Atg1^{\Delta 3D}$/wild-type (*Δ3D*/+) cells have weaker GFP. Representative images are shown. (**e**) Quantification (μm^2) from **d**, *n* = 7 (+/+), *n* = 8 (*Δ3D*/+), and *n* = 8 (*Δ3D*/*Δ3D*) animal intestines/genotype with 1-5 cells measured/intestine. (**f**) Midguts dissected from animals expressing mCherry-Atg8a in all cells, and expressing $Atg1^{IR}$ specifically in GFP-marked clones of cells at 2 h after puparium formation. Representative images are shown. (**g-j**) Representative cut views from 3D reconstitution images from wild-type (**g**,**h**) and *Atg1* knockdown (**i**,**j**) cells at early 3rd instar larval stage (**g**,**i**) and at puparium formation (**h**,**j**). (**k**) Quantification of cell volume (μm^3) from **g-j**, *n* = 5 animal intestines/genotype with 1-5 cells measured/intestine/stage. Black columns: early 3rd instar larval stage. White columns: puparium formation stage. Quantification is shown as mean ± s.d.. N.S.: no significance. Scale bars represent 20 μm.

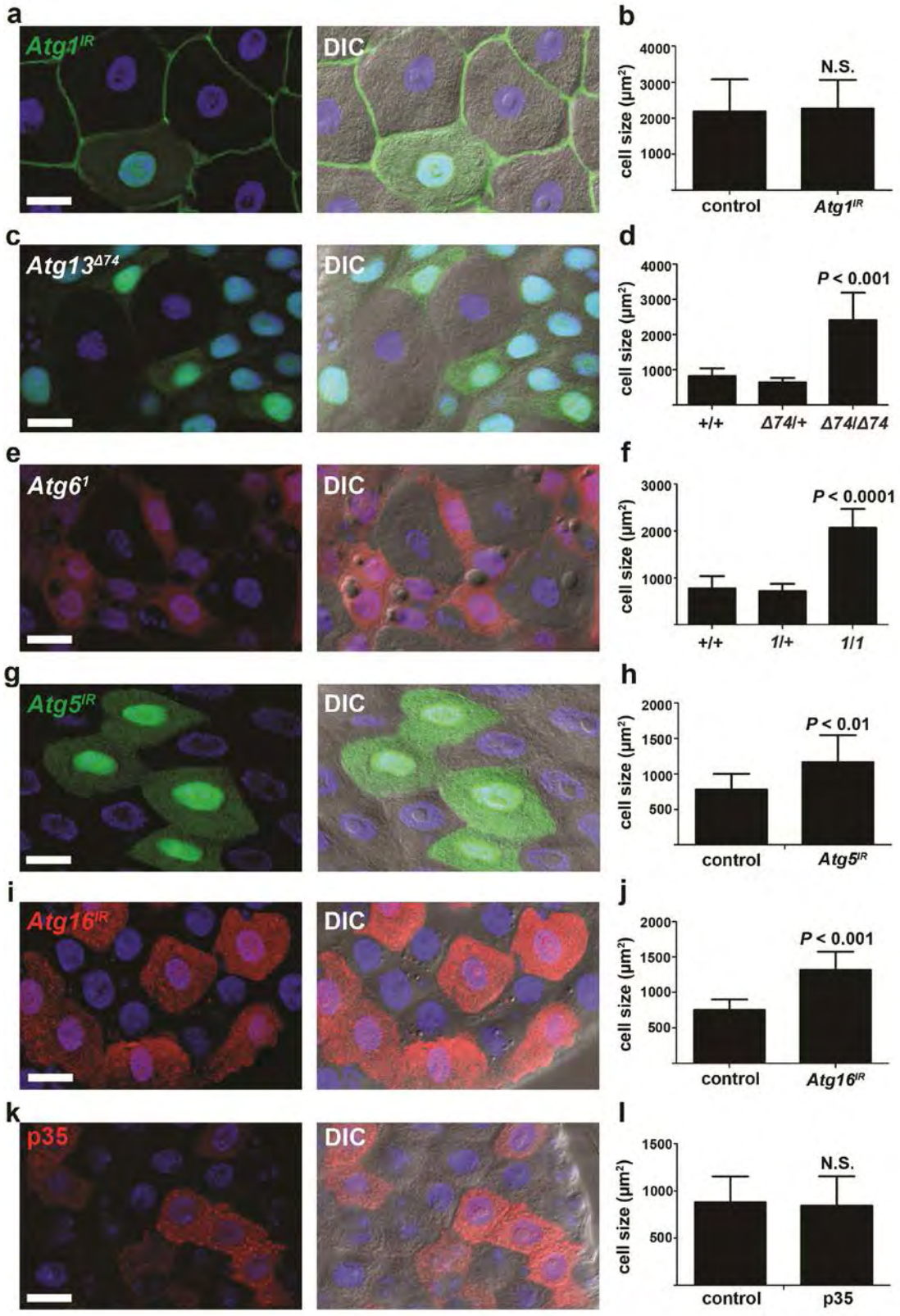
a
Atg1IR
DIC
b
cell size (μm²)
4000
3000
2000
1000
N.S.
control
Atg1IR
c
Atg13Δ74
DIC
d
cell size (μm²)
4000
3000
2000
1000
P < 0.001
+/+
Δ74/+
Δ74/Δ74
e
Atg6¹
DIC
f
cell size (μm²)
3000
2000
1000
P < 0.0001
+/+
1/+
1/1
g
Atg5IR
DIC
h
cell size (μm²)
2000
1500
1000
500
P < 0.01
control
Atg5IR
i
Atg16IR
DIC
j
cell size (μm²)
2000
1500
1000
500
P < 0.001
control
Atg16IR
k
p35
DIC
l
cell size (μm²)
1500
1000
500
N.S.
control
p35

Figure 3-3 Knockdown of *Atg1* does not alter cell growth, and *Atg13*, *Atg6*, *Atg5*, and *Atg16* (*CG31033*), but not caspases, are required for midgut cell size reduction in *Drosophila*. (**a**) Midguts dissected from early third instar larvae that mis-express $Atg1^{IR}$ (GFP in nucleus and cytoplasm) and are stained to detect Discs large (green) on the cortex of all cells. Representative images are shown. (**b**) Cell size quantification (μm^2) from **a**, *n* = 10 animal intestines/genotype with 1-5 cells measured/intestine. (**c**) Midguts dissected from animals at puparium formation that contain $Atg13^{\Delta 74}$ loss-of-function mutant cell clones (lacking GFP) and analyzed by fluorescence and DIC microscopy. Wild-type (+/+) control cells possess stronger GFP and heterozygous $Atg13^{\Delta 74}$/wild-type (*Δ74*/+) cells have weaker GFP. Representative images are shown. (**d**) Cell size quantification (μm^2) from **c**, *n* = 6 animal intestines/genotype with 1-5 cells measured/intestine. (**e**) Midguts dissected from animals at puparium formation that contain $Atg6^{1}$ loss-of-function mutant cell clones (lacking RFP) and analyzed by fluorescence and DIC microscopy. Wild-type (+/+) control cells possess stronger RFP and heterozygous $Atg6^{1}$/wild-type (*1*/+) cells have weaker RFP. Representative images are shown. (**f**) Cell size quantification (μm^2) from **e**, *n* = 8 animal intestines/genotype with 1-5 cells measured/intestine. (**g**) Midguts dissected from animals expressing $Atg5^{IR}$ specifically in GFP-marked clones of cells at puparium formation and analyzed by fluorescence and DIC microscopy. Representative images are shown. (**h**) Cell size quantification (μm^2) from **g**, *n* = 16 animal intestines/genotype with 1-5 cells measured/intestine. (**i**) Midguts dissected from animals expressing $Atg16^{IR}$ specifically in DsRed-marked clones of cells at puparium formation and analyzed by fluorescence and DIC microscopy. Representative images are shown. (**j**) Cell size quantification (μm^2) from **i**, *n* = 7 animal intestines/genotype with 1-5 cells measured/intestine. (**k**) Midguts dissected from animals expressing p35 in DsRed-marked clones of cells at puparium formation and analyzed by fluorescence and DIC microscopy. Representative images are shown. (**l**) Cell size quantification (μm^2) from **k**, *n* = 13 animal intestines/genotype with 1-5 cells measured/intestine. Quantification is shown as mean ± s.d.. N.S.: no significance. Scale bars represent 20 μm.

To test whether other autophagy genes are required for midgut cells to shrink, we altered the function of multiple *Atg* genes in clones of midgut cells. *Vps34*, *Atg8a*, *Atg12*, *Atg13*, *Atg6*, *Atg5*, and *Atg16* (*CG31033*) were each required for programmed size reduction of midgut cells (Fig. 3-3c-j and Fig. 3-4a-f). By contrast, expression of the caspase inhibitor p35 in clones of midgut cells did not influence cell size (Fig. 3-3k,l). These data indicate that autophagy, but not caspase activation, is required for *Drosophila* midgut degradation during animal development.

Mis-expression of Atg1 is sufficient to induce autophagy in multiple *Drosophila* cell types [17, 18]. Similarly, Atg1 mis-expression in clones of early third instar larval midgut cells was sufficient to induce premature autophagy and decreased the size of these cells (Fig. 3-4g,g'). Importantly, knockdown of *Atg8a* suppressed Atg1-induced cells from shrinking (Fig. 4h), indicating that the sufficiency for Atg1 to induce premature cell shrinking depends on core autophagy gene function. Surprisingly, however, knockdown of *Atg7* failed to suppress the Atg1-induced autophagy and reduction in cell size phenotypes (Fig. 3-4i,i') even though the same *Atg7* knockdown strain suppresses starvation-induced autophagy in the fat body (Fig. 3-5a). Our results indicate that many of the core autophagy genes that are conserved between yeast and humans are required for autophagy and cell size reduction during larval midgut cell death and this process appears to be independent of *Atg7*.

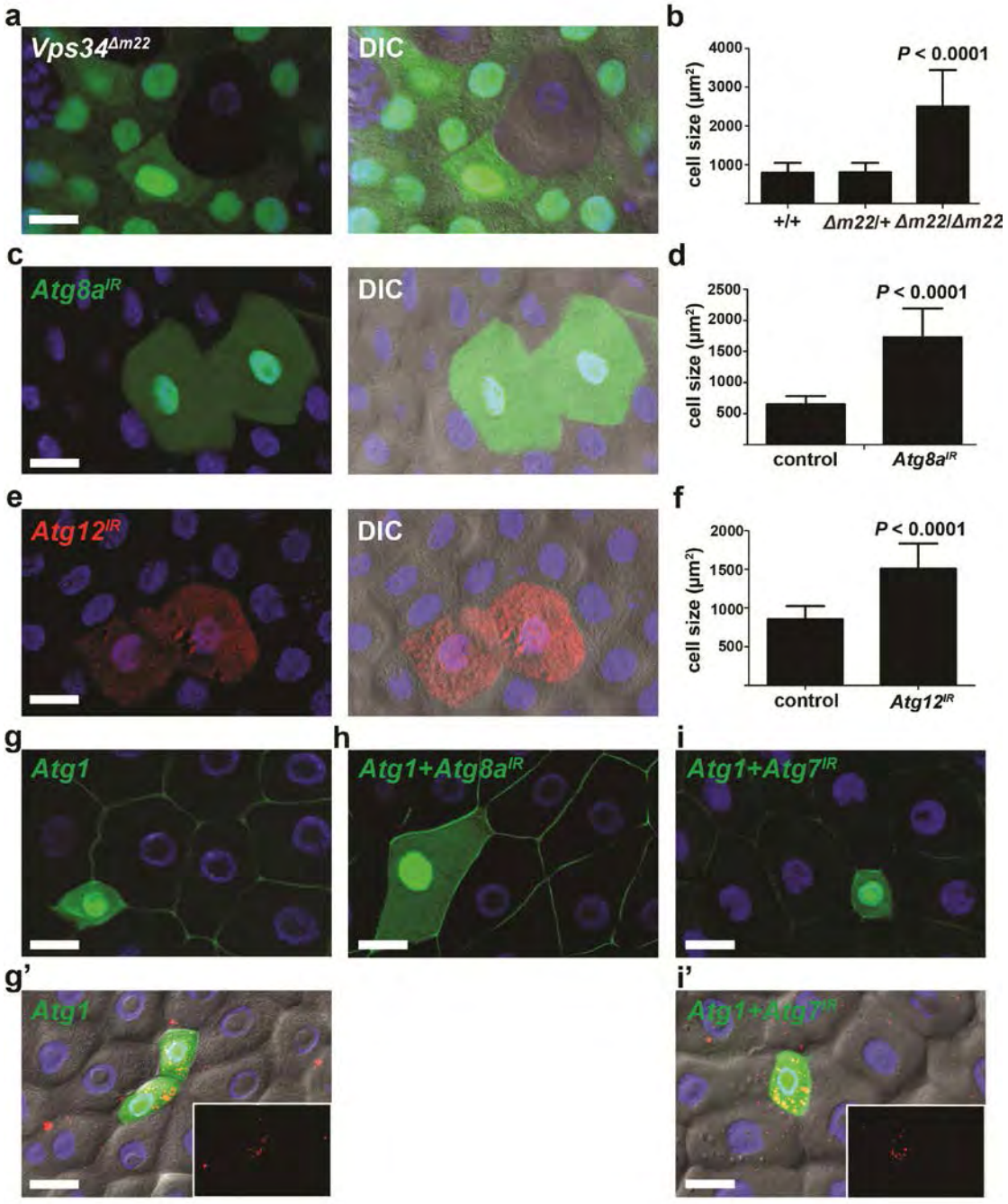

Figure 3-4 Autophagy is necessary and sufficient for cell size reduction. (**a**) Midguts dissected from animals at puparium formation that contain *Vps34*$^{\Delta m22}$ loss-of-function mutant cell clones (lacking GFP) and analyzed by fluorescence and DIC microscopy. Wild-type (+/+) control cells possess stronger GFP and heterozygous *Vps34*$^{\Delta m22}$/wild-type (*Δm22*/+) cells have weaker GFP. Representative images are shown. (**b**) Quantification (μm^2) from **a**, *n* = 14 animal

intestines/genotype with 1-5 cells measured/intestine. (**c**) Midguts dissected from animals expressing *Atg8a*^{IR} specifically in GFP-marked clones of cells at puparium formation and analyzed by fluorescence and DIC microscopy. Representative images are shown. (**d**) Cell size quantification (μm^2) from **c**, *n* = 10 animal intestines/genotype with 1-5 cells measured/intestine. (**e**) Midguts dissected from animals expressing *Atg12*^{IR} specifically in DsRed-marked clones of cells at puparium formation and analyzed by fluorescence and DIC microscopy. Representative images are shown. (**f**) Cell size quantification (μm^2) from **e**, *n* = 14 animal intestines/genotype with 1-5 cells measured/intestine. (**g**-**i**) Midguts dissected from early third instar larvae that mis-express *Atg1*^{GS10797} (*Atg1*) (**g**, GFP in nucleus and cytoplasm), both *Atg1* + *Atg8a*^{IR} (**h**), or both *Atg1* + *Atg7*^{IR} (**i**) and stained to detect Discs large (green) on the cortex of all cells. Representative images are shown. (**g'** and **i'**) DIC images of midguts expressing mCherry-Atg8a in all cells, *Atg1* (**g'**), and *Atg1* + *Atg7*^{IR} (**i'**) in GFP-marked clones of cells. mCherry-Atg8a puncta are shown in insets. Representative images are shown. Quantification is shown as mean ± s.d.. Scale bars represent 20 μm.

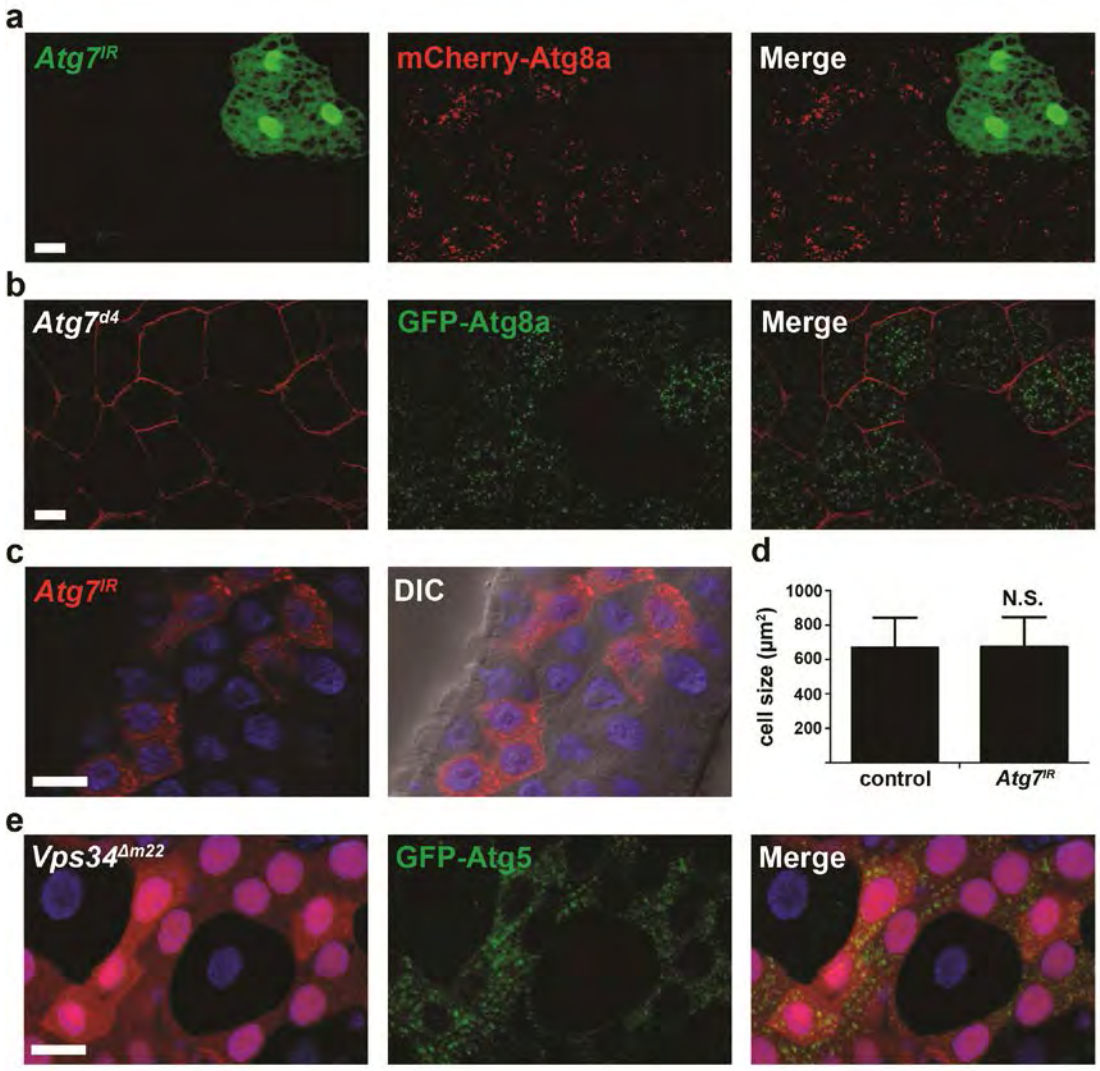

Figure 3-5 *Atg7* is required for nutrient deprivation-induced autophagy in starved larval fat body and *Vps34* is required for GFP-Atg5 puncta formation in the midgut at puparium formation. (**a**,**b**) Fat body dissected from early 3rd instar larvae and subjected to 4 h of starvation. Representative images are shown. (**a**) Fat body expressing mCherry-Atg8a in all cells, and $Atg7^{IR}$ in GFP-marked clones of cells analyzed by fluorescence microscopy. (**b**) $Atg7^{d4}$ loss-of-function mutant cells are shown lacking of myrRFP. Wild-type and heterozygous $Atg7^{d4}$/wild-type control cells possess myrRFP. All fat body cells express GFP-Atg8a. (**c**) Midguts dissected from animals expressing $Atg7^{IR}$ specifically in DsRed-marked clones of cells at puparium formation and analyzed by fluorescence and DIC microscopy. Representative images are shown. (**d**) Cell size quantification (μm^2) from **c**, *n* = 10 animal intestines/genotype with 1-5 cells measured/intestine.

(**e**) Midguts expressing GFP-Atg5 in enterocytes (larger nuclei) and with *Vps34*$^{\Delta m22}$ loss-of-function clone cells (lacking RFP) at puparium formation. Wild-type control cells possess stronger RFP and heterozygous cells have weaker RFP. Representative images are shown. Quantification is shown as mean ± s.d.. N.S.: no significance. Scale bars represent 20 μm.

Programmed cell size reduction, autophagy and clearance of mitochondria are Atg7-independent

Atg7 encodes an evolutionarily conserved E1 activating enzyme that is required for autophagy in all organisms and cell types that involve Atg8/LC3 that have been previously studied [113, 117]. Unlike several other genes that are required for autophagy in *Drosophila*, loss of *Atg7* fails to cause animal lethality, and previous studies indicate that *Atg7* mutations inhibit autophagy in the fly midgut [119]. This previous study analyzed autophagy in midguts of third instar larvae when autophagy is relatively low and variable. These results, combined with our observation that *Atg7* knockdown failed to suppress Atg1-induced decrease in cell size, prompted us to revisit the role of *Atg7* in midgut autophagy in greater detail. As reported previously [119], mutant clones of *Atg7*^{d4} cells failed to induce autophagy under nutrient deprivation in larval fat body cells (Fig. 3-5b). By contrast, *Atg7*^{d4} mutant clones of midgut cells, as well as *Atg7* knockdown midgut cells, possessed autophagy and underwent normal reductions in cell size (Fig. 3-5c,d and Fig. 3-6a-c). In addition, GFP-Atg8a puncta formation is similar in control and null loss of *Atg7* function mutant midgut cells (Fig. 3-6d,e). Furthermore, loss of *Atg7* did not influence the formation of GFP-Atg5 puncta (Fig. 3-6f) which depended on the function of *Vps34* (Fig. 3-5e). We used TEM to analyze control and *Atg7* null mutant midguts, and found that autophagosomes and autolysosomes were present even in the

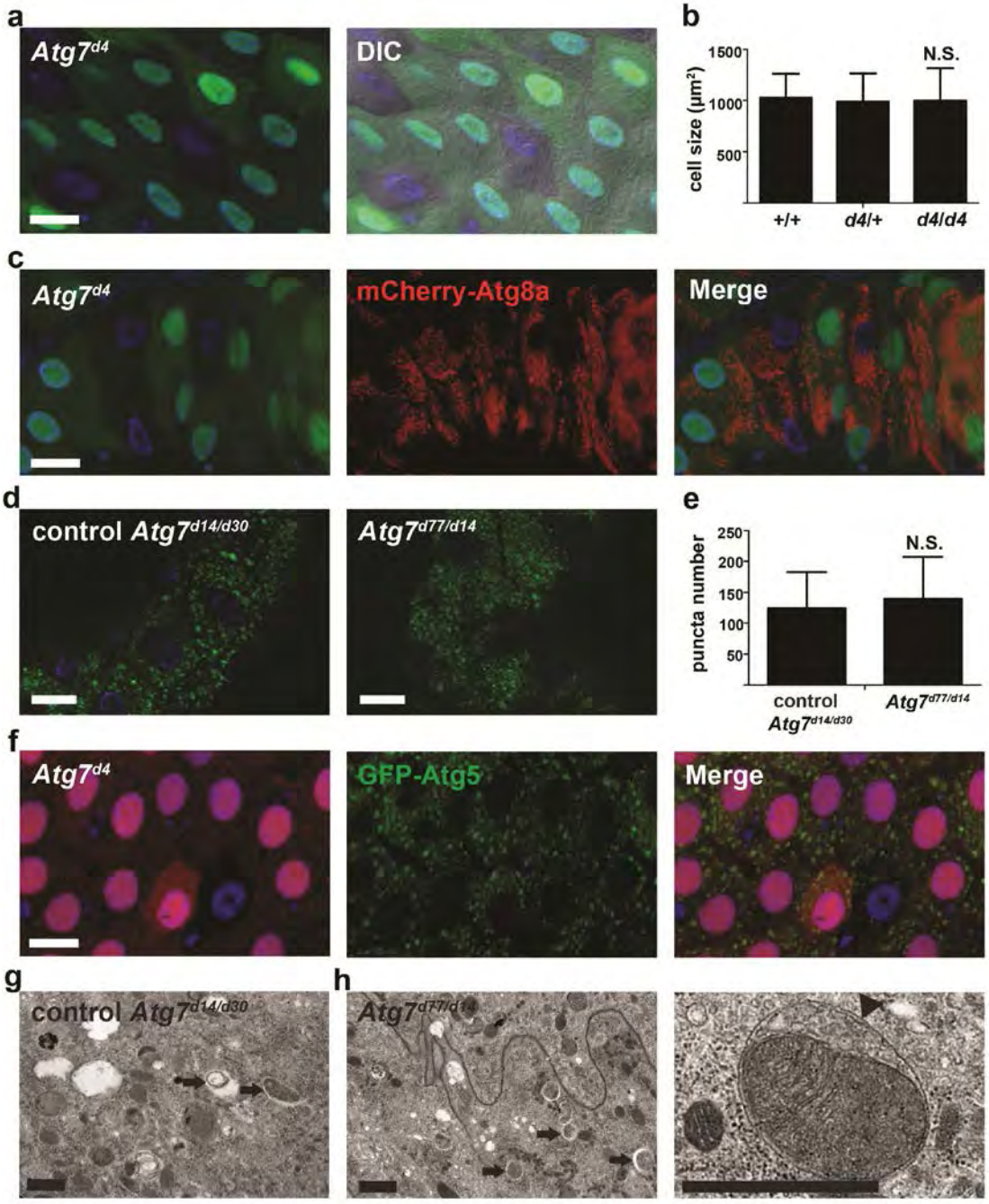

Figure 3-6 *Atg7* is not required for programmed cell size reduction and autophagy. (**a**) Midguts dissected from animals at puparium formation that contain $Atg7^{d4}$ loss-of-function mutant cell clones (lacking GFP) and analyzed by fluorescence and DIC microscopy. Wild-type (+/+) control cells possess stronger GFP and heterozygous $Atg7^{d4}$/wild-type (*d4*/+) cells have weaker GFP. Representative images are shown. (**b**) Cell size quantification (μm^2) from **a**, *n* = 8 animal

intestines/genotype with 1-5 cells measured/intestine. (**c**) Midguts expressing mCherry-Atg8a in all cells, and with *Atg7*^{d4} loss-of-function clone cells (lacking GFP) at 2h after puparium formation. Representative images are shown. (**d**) Gastric caeca expressing GFP-Atg8a in all cells from control (*Atg7*$^{d30/d14}$) and *Atg7* mutant (*Atg7*$^{d77/d14}$) animals. Representative images are shown. (**e**) Quantification of GFP-Atg8a puncta number from **d**, *n* = 31 animal intestines per genotype with puncta quantified in image field/intestine. (**f**) Midguts expressing GFP-Atg5 in in enterocytes (larger nuclei) with an *Atg7*^{d4} loss-of-function clone cell (lacking RFP) at puparium formation. Representative images are shown. (**g**,**h**) Representative TEM images of intestine cells 2 h after puparium formation. Arrows indicate autolysosomes. (**g**) Control (*Atg7*$^{d30/d14}$) and (**h**) *Atg7* mutant (*Atg7*$^{d77/d14}$) cells both contain autophagic structures. (**h**) Enlarged *Atg7* mutant cell image of a double membrane autophagosome (arrowhead) surrounding a mitochondrion. Quantification is shown as mean ± s.d.. N.S.: no significance. Scale bars represent 20 μm (**a**,**c**,**d**, and **f**) and 1 μm (**g**,**h**).

absence of *Atg7* function (Fig. 3-6g, h). Significantly, we observed cytoplasmic material, including mitochondria and ribosomes,in double membrane autophagosomes in *Atg7* mutant cells (enlarged image in Fig. 3-6h). These results indicate that *Atg7* is not required for autophagy and for cells to shrink in the midgut.

The presence of cytoplasmic material in the autophagosomes of *Atg7* null intestine cells prompted us to investigate if *Atg* genes are required for mitochondria clearance (mitophagy). We quantified the number of mitochondria in control, *Atg18* mutant, and *Atg7* mutant cells, and discovered that *Atg18* mutant cells, but not *Atg7* mutant cells, had more mitochondria than control midgut cells (Fig. 3-7a). Homozygous *Atg1* mutant clone and neighboring control cells possessed similar amounts GFP-labeled mitochondria before the onset of autophagy in the intestines of third instar

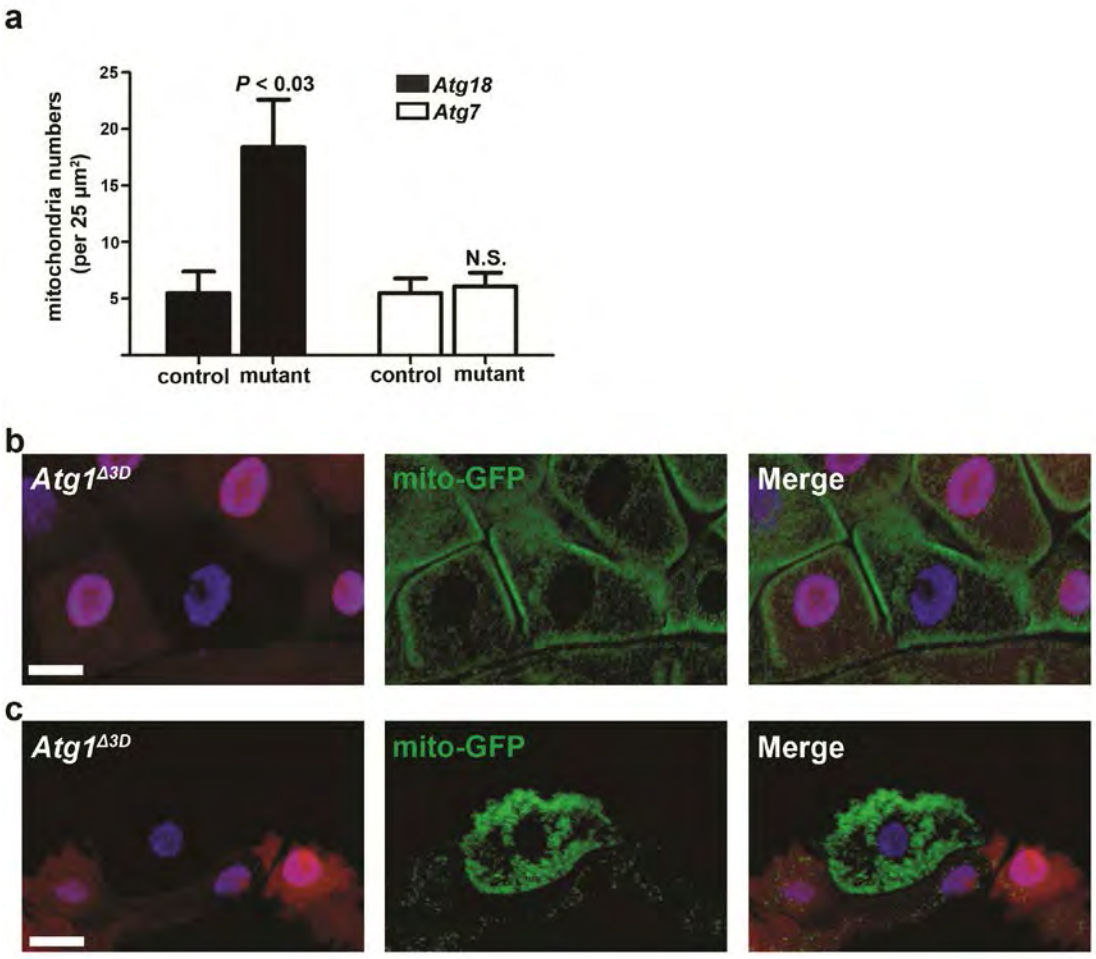

Figure 3-7 Autophagy is required for clearance of mitochondria. (**a**) Quantification of mitochondria numbers from *Atg18* control (*Atg18*^{KG03090}/wild-type) and mutant (*Atg18*^{KG03090}/*Df(3L)*^{6112}) or *Atg7* control (*Atg7*$^{d30/d14}$) and mutant (*Atg7*$^{d77/d14}$) TEM images. Mitochondria were quantified from 2 distinct 25 μm^2 regions per cell from 2 cells per animal from at least 3 different animals/genotype. (**b, c**) Midguts dissected from either early third instar larvae (**b**) or at puparium formation (**c**) that express GFP-labeled mitochondria in all cells and contain an *Atg1*$^{\Delta 3D}$ loss-of-function mutant cell clone (lacking RFP). Wild-type control cells possess stronger RFP and heterozygous cells have weaker RFP. Representative images are shown. Quantification is shown as mean ± s.d.. N.S.: no significance. Scale bars represent 20 μm.

larvae (Fig. 3-7b), indicating that loss of Atg1 does not dramatically alter mitochondria numbers during development. By contrast, we observed significant retention of GFP-labeled mitochondria in homozygous *Atg1* mutant intestine cells compared to their control neighbors following the onset of autophagy (Fig. 3-7c). Combined, these data indicate that most autophagy genes, but not *Atg7*, are required for cell size reduction, clearance of cytoplasmic material, and autophagy.

Uba1 is required for autophagy and cell size reduction

The lack of *Atg7* function in midgut cell autophagy and shrinking prompted us to screen for other Ubiquitin-like activating enzymes (Ubas) that are required for autophagy and midgut cells to decrease in size. Six predicted Ubas are encoded in the *Drosophila* genome, termed *Uba1* (CG1728), *Uba2* (CG7528), CG13343 (human *Uba3* homolog), CG13090 (*Uba4* homolog), CG1749 (*Uba5* homolog) and *Atg7*. We expressed RNAi knockdown transgenes against all of the Ubas, as well as *Aos1* (CG12276, *Uba2* binding partner) and *APP-BP1* (CG7828, CG13343 binding partner), in clones of midgut cells, and *Uba1* was the only gene that exhibited a defect in cell size reduction (Fig. 3-8a,b and Fig. 3-9). Both midgut cell size reduction and autophagy were inhibited when *Uba1* was knocked down (Fig. 3-8a,b and Fig. 3-10a). Consistent with this conclusion, *Uba1* knockdown did not alter cell growth during larval development (Fig. 3-10b,c). Similar defects in the reduction in midgut cell size were observed when *Uba1* function was reduced in clones of cells using the temperature sensitive mutant $Uba1^{H33}$ (Fig. 3-8c,d), thus demonstrating a cell-autonomous role for Uba1 in midgut cell size reduction. Clones of $Uba1^{H33}$cells also showed reduced Atg8a puncta, reduced Atg5 puncta, and accumulation of p62/Ref(2)P proteins (Fig. 3-8e-g),

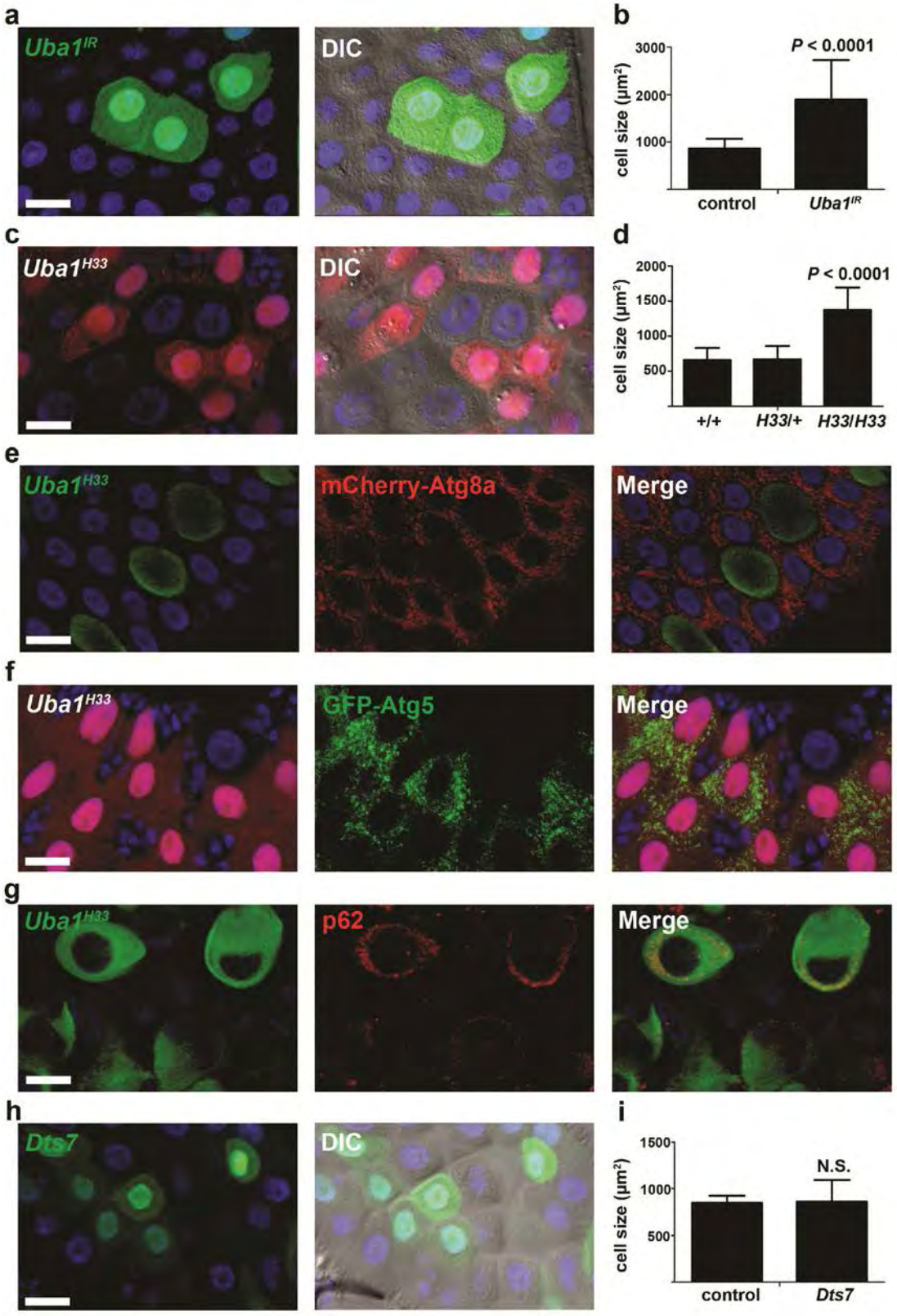

Figure 3-8 *Uba1* is required for midgut cell programmed size reduction and autophagy. (**a**)

Midguts dissected from animals expressing *Uba1*^{IR} specifically in GFP-marked clones of cells at puparium formation and analyzed by fluorescence and DIC microscopy. Representative images are shown. (**b**) Cell size quantification (μm^2) from **a**, *n* = 16 animal intestines/genotype with 1-5 cells measured/intestine. (**c**) Midguts dissected from animals at puparium formation that contain *Uba1*^{H33} loss-of-function mutant cell clones (lacking RFP) and analyzed by fluorescence and DIC microscopy. Wild-type (+/+) control cells possess stronger RFP and heterozygous *Uba1*^{H33}/wild-type (*H33*/+) cells have weaker RFP. Representative images are shown. (**d**) Quantification (μm^2) from **c**, *n* = 8 (+/+), *n* = 11 (*H33*/+), and *n* =11 (*H33*/*H33*) animal intestines/genotype with 1-5 cells measured/intestine. (**e**) Midguts dissected from animals at puparium formation that contain *Uba1*^{H33} loss-of-function MARCM mutant cell clones (GFP-positive) that also have mCherry-Atg8a expressed in all cells and analyzed by fluorescence microscopy. Control wild-type and heterozygous cells have no GFP. Representative images are shown. (**f**) Midguts expressing GFP-Atg5 in enterocytes (larger nuclei), and with an *Uba1*^{H33} loss-of-function clone cell (lacking RFP) at puparium formation analyzed by fluorescence microscopy. Representative images are shown. (**g**) Midguts dissected from animals at puparium formation that contain *Uba1*^{H33} loss-of-function MARCM mutant cell clones (GFP-positive) that are stained with p62 antibody and analyzed by fluorescence microscopy. Control wild-type and heterozygous cells have no GFP. Representative images are shown. (**h**) Midguts dissected from animals expressing *Dts7*, a dominant temperature sensitive mutant of the β2 subunit of the proteasome, specifically in GFP-marked cells at puparium formation and analyzed by fluorescence and DIC microscopy. Representative images are shown. (**i**) Cell size quantification (μm^2) from **h**, *n* = 6 animal intestines/genotype with 1-5 cells measured/intestine. Quantification is shown as mean ± s.d.. N.S.: no significance. Scale bars represent 20 μm.

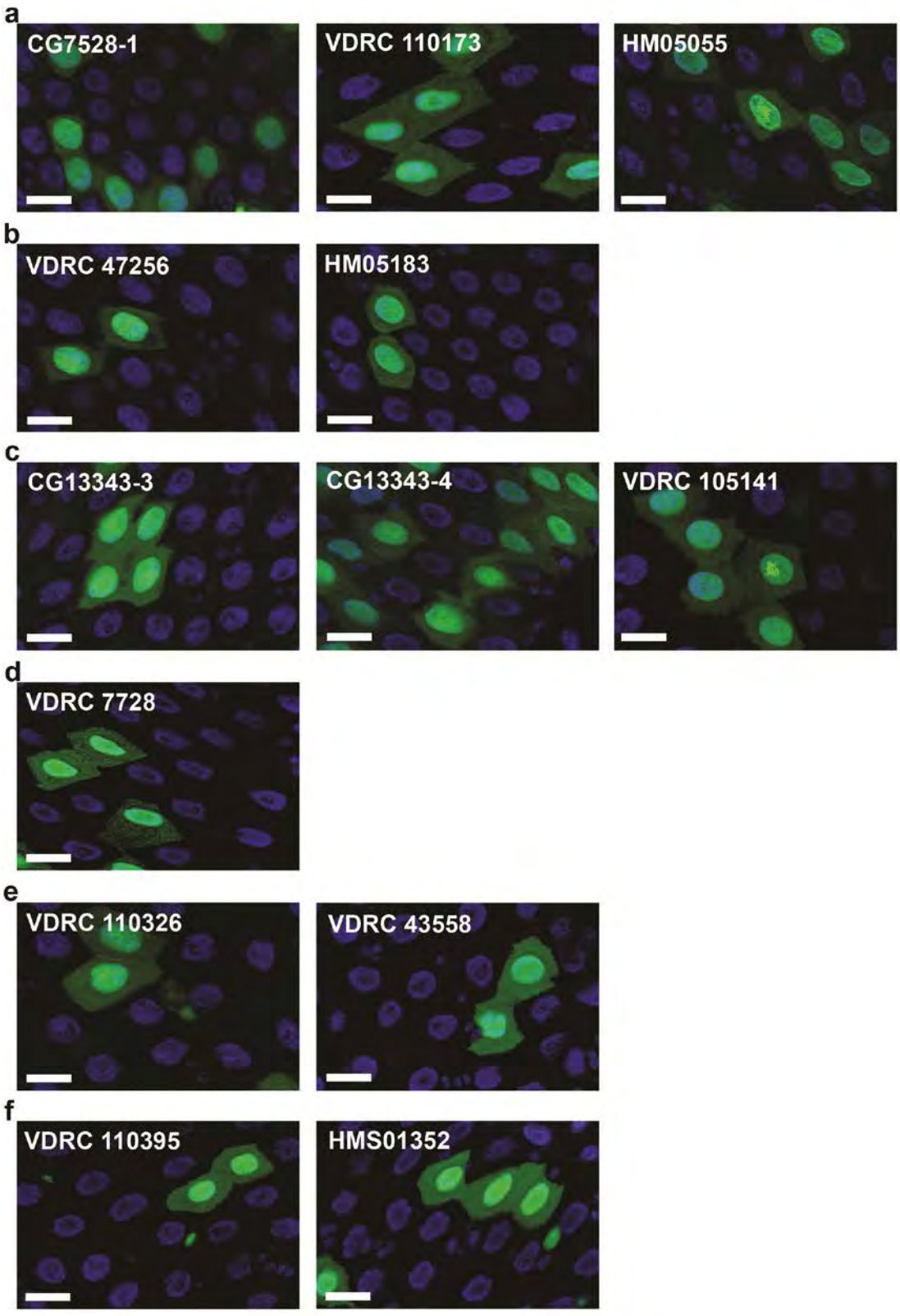
a
CG7528-1
VDRC 110173
HM05055
b
VDRC 47256
HM05183
c
CG13343-3
CG13343-4
VDRC 105141
d
VDRC 7728
e
VDRC 110326
VDRC 43558
f
VDRC 110395
HMS01352

Figure 3-9 Screen for Ubiquitin-like activating enzyme genes that function in midgut programmed cell reduction in size in *Drosophila*. Representative images of midgut cells from animals expressing RNAi in GFP-marked clones of cells against (**a**) *Uba2* (CG7528-1, *n* = 11, VDRC TID 110173, *n* = 14, and TRiP HM05055, *n* = 9), (**b**) Aos1 (TID 47256, *n* = 8, and HM05183, *n* = 9), (**c**) CG13343 (CG13343-3, *n* = 12, CG13343-4, *n* = 14, and TID 105141, *n* = 8), (**d**) APP-BP1 (TID 7728, *n* = 13), (**e**) CG13090 (TID 110326, *n* = 13, and TID 43558, *n* = 10), and (**f**) CG1749 (TID 110395, *n* = 14, and HMS01352, *n* = 12). *n* represents number of animal intestines analyzed/genotype. Scale bars represent 20 μm.

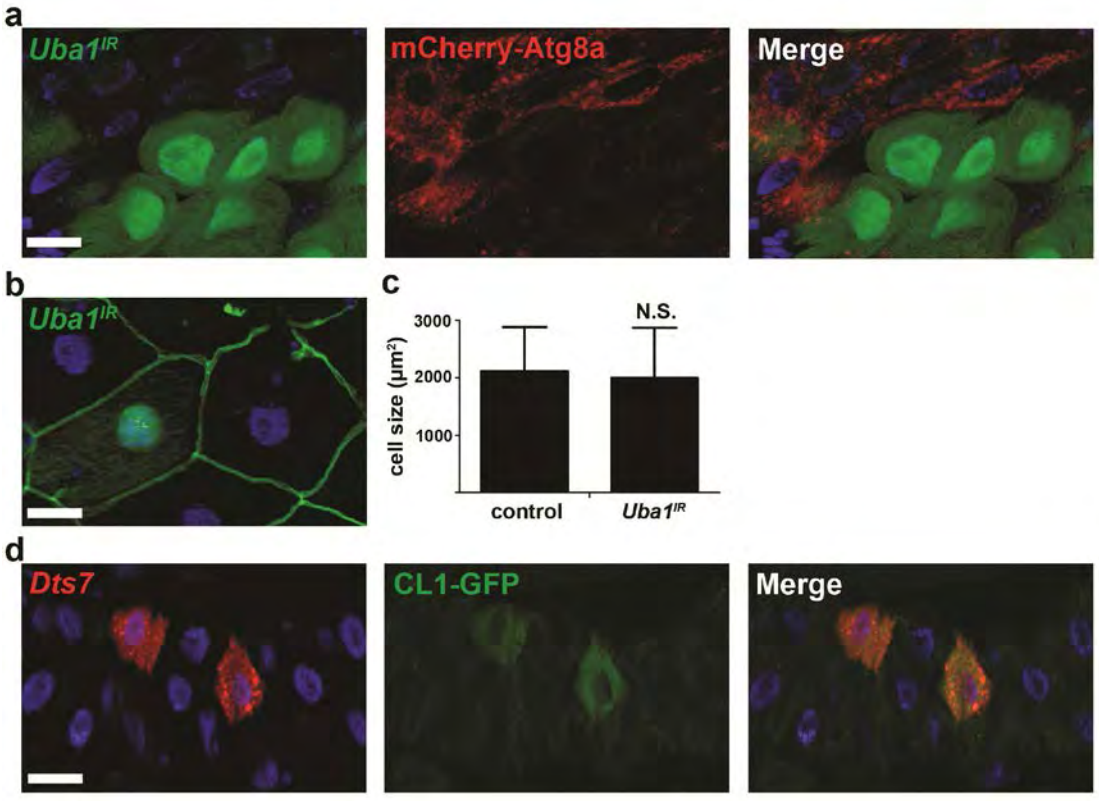

Figure 3-10 *Uba1* influences autophagy and programmed reduction of midgut cell size. (**a**) Midguts expressing mCherry-Atg8a in all cells, and expressing $Uba1^{IR}$ specifically in GFP-marked clones of cells at puparium formation. Representative images are shown. (**b**) Midguts dissected from early third instar larvae that mis-express $Uba1^{IR}$ (GFP in nucleus and cytoplasm) and were stained to detect Discs large (green) on the cortex of all cells. Representative images

are shown. (**c**) Cell size quantification (μm^2) from **b**, *n* = 10 animal intestines/genotype with 1-5 cells measured/intestine. (**d**) Midguts from animals expressing CL1-GFP in all cells and temperature sensitive *Dts7* specifically in DsRed-marked clones of cells at puparium formation. Representative images are shown. Quantification is shown as mean ± s.d.. N.S.: no significance. Scale bars represent 20 μm.

further demonstrating that Uba1 is required for midgut autophagy and programmed size reduction.

Uba1 activates ubiquitin and transfers it to a family of E2 conjugating enzymes, which then transfer ubiquitin to substrates via an E3 ubiquitin ligase. Protein carrying lysine-48 linked poly-ubiquitin chains are targeted to the proteasome for degradation. To determine if midgut cell shrinking was influenced by altered proteasome function, we expressed *Dts7*, a dominant temperature sensitive mutant of the β2 subunit of the proteasome [120], in clones of cells in the midgut. We also monitored the activity of the proteasome using CL1-GFP as a reporter [68]. When proteasome function was impaired by mis-expression of dominant proteasome subunit mutant *Dts7* in clones of cells, CL1-GFP was retained, and midgut cells underwent normal reductions in cell volume (Fig. 3-8h,i and Fig. 3-10d). These data indicate that the function of the proteasome is not required for programmed reduction of midgut cell size.

We tested if *Uba1* is required for autophagy that is induced by stress in different tissues. Decreased *Uba1* function did not influence starvation-induced autophagy in either the fat body or midgut (Fig. 3-11a-d). In addition, knockdown of *Uba1* did not alter hydrogen peroxide-triggered autophagy in the midgut (Fig. 3-11e,f).

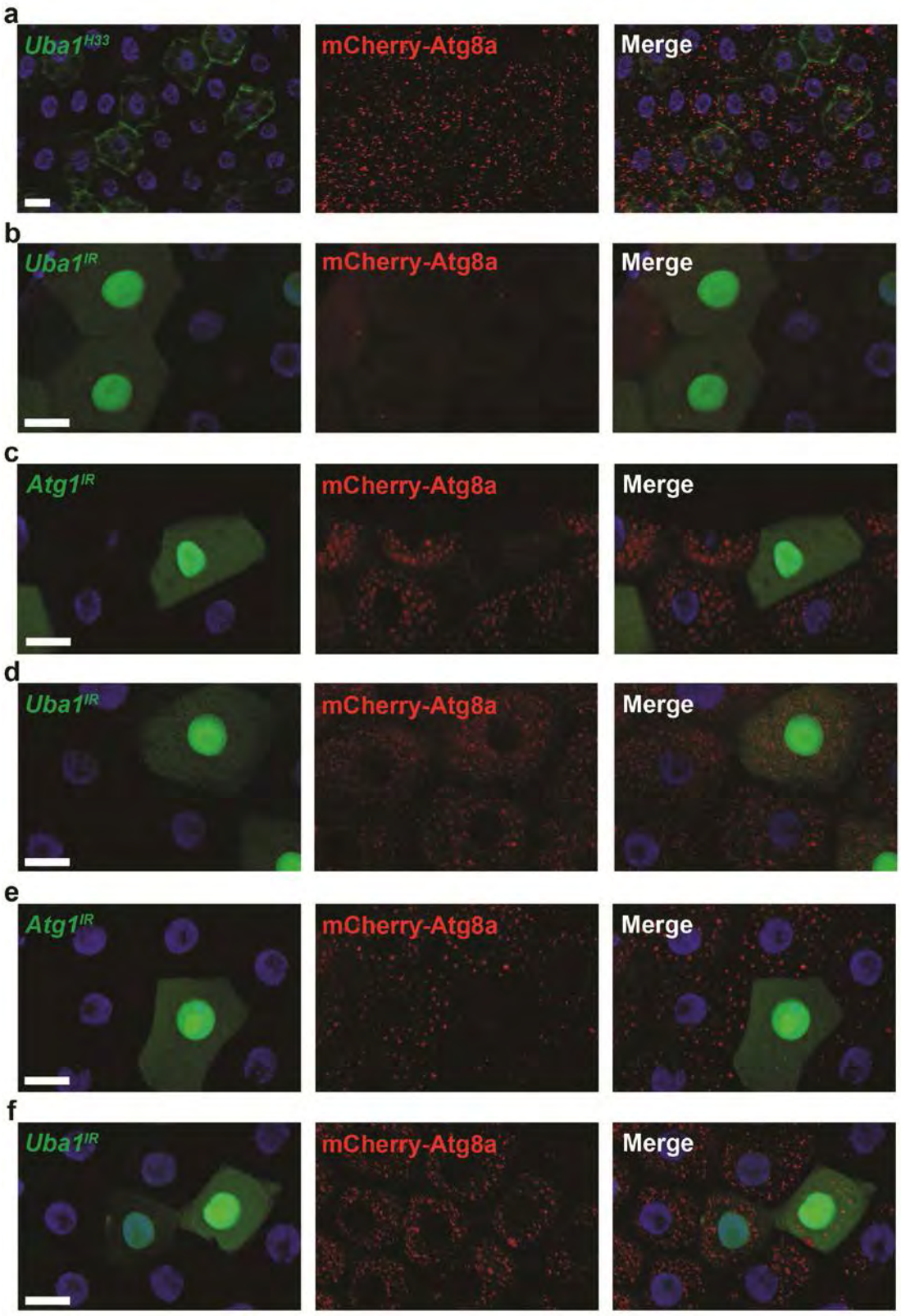
a
Uba1H33
mCherry-Atg8a
Merge
b
Uba1IR
mCherry-Atg8a
Merge
c
Atg1IR
mCherry-Atg8a
Merge
d
Uba1IR
mCherry-Atg8a
Merge
e
Atg1IR
mCherry-Atg8a
Merge
f
Uba1IR
mCherry-Atg8a
Merge

Figure 3-11 *Uba1* is not required for autophagy that is induced by stress in different tissues. (**a**) Fat body dissected from early third instar larvae and subjected to 4 h of starvation that contain $Uba1^{H33}$ loss-of-function MARCM mutant cell clones (GFP-positive) that also have mCherry-Atg8a expressed in all cells and analyzed by fluorescence microscopy. Control wild-type and heterozygous cells have no GFP. Representative images are shown. (**b**-**f**) Early third instar midguts expressing mCherry-Atg8a in all cells and expressing either $Uba1^{IR}$ (**b**,**d**,**f**) or $Atg1^{IR}$ (**c**,**e**) in GFP-marked clones of cells in control untreated animals (**b**), 4 h after starvation (**c**,**d**), or 7 h after 1.5 % H_2O_2 treatment (**e**,**f**). Representative images are shown. Scale bars represent 20 μm.

Uba1 could regulate autophagy by multiple possible mechanisms. One possibility is that Uba1 functions as the E1 enzyme in place of Atg7 to control the lipidation of Atg8. To test this possibility, we performed an *in vitro* E1 charging assay using Uba1 and Atg7 as E1s to be charged with either Atg8a or ubiquitin (Ub). As expected, Uba1 and Atg7 were charged with ubiquitin and Atg8a, respectively, and these thioester bonds were reversed by the addition of reducing agent (Fig. 3-12a,b and Fig. 3-13a,b). By contrast, Uba1 was unable to activate Atg8a and Atg7 was unable to activate ubiquitin (Fig. 3-7a,b). These data suggest that Uba1 does not substitute for Atg7 as the E1 for Atg8a conjugation.

Most autophagy genes that we tested are required for the formation of *Atg8a* puncta and programmed cell size reduction in the midgut cells of intestines (Fig. 3-1 to 3-4), but *Atg7* is not needed for these cellular changes (Fig. 3-6). Since Atg8a puncta formation is thought to always depend on conjugation of phosphatidyl-ethanolamine, we tested whether Atg8a lipidation occurs in *Atg7* mutant intestines. Protein extracts from midguts of wild-type control, *Atg7* mutant and *Atg8a* mutant animals at puparium formation were subjected to immunoblot analysis using Atg8a antibody. Small amounts of lipidated Atg8a (Atg8a-II) were detected in wild-type midgut

extracts, but not in either *Atg7* or *Atg8a* mutant midguts (Fig. 3-12c), indicating that *Atg7* is indeed essential for Atg8 lipidation.

Since *Atg7* mutant midgut cells exhibited normal autophagy (Fig. 3-4), we hypothesized that Atg8 lipidation is not required for midgut autophagy and programmed cell size reduction. This hypothesis would predict that *Atg3*, the E2 conjugating enzyme for Atg8 lipidation, is also not required for midgut autophagy. Although *Atg3* is required for starvation-induced autophagy in *Drosophila* fatbody [17], *Atg3* null mutant midgut cells exhibited normal size reduction and autophagy (Fig. 3-12d,e and Fig. 3-13c,d). Moreover, knockdown of *Atg3* showed similar phenotype as knockdown of *Atg7*; although Atg3 was required for autophagy in starved fatbody, knockdown of *Atg3* did not suppress Atg1-induced reduction in midgut cell size (Fig. 3-12f, Fig. 3-13e).

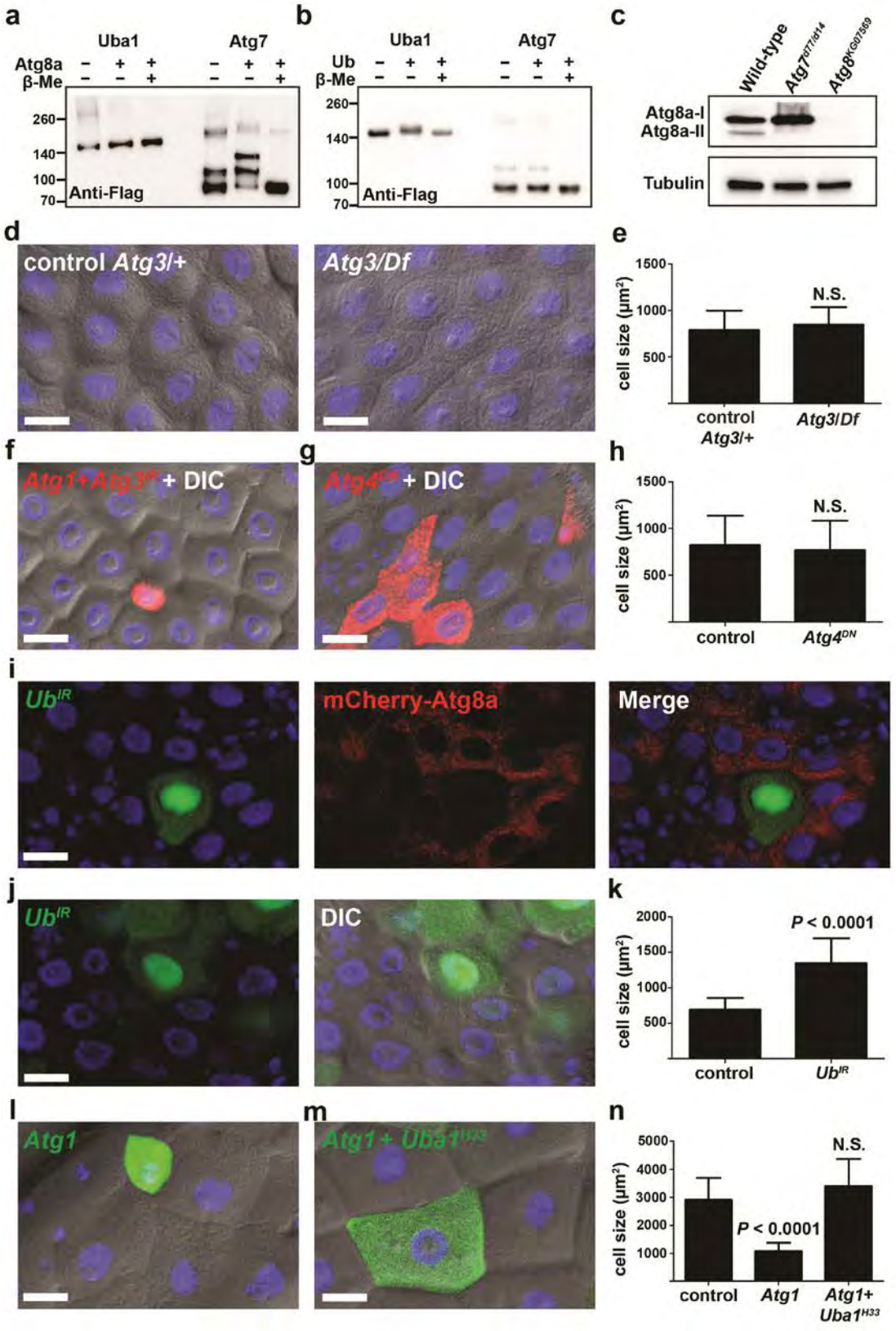

Figure 3-12 Role of *Uba1* in midgut autophagy. (**a** and **b**) E1 charging assay for Uba1 and Atg7

with either Atg8a (**a**) or Ub (**b**), *n* = 2 experiments with independently isolated proteins and analyses. Flag-tagged baculoviral expressed E1s were incubated with either His-tagged Atg8a or Ub in the presence or absence of β-mercaptoethanol, separated by electrophoresis and blotted. Band shift was detected with anti-Flag antibody. Molecular weight ladders are indicated. Representative images are shown. Molecular weights: Flag-Uba1 135 kDa, Flag-Atg7 81 kDa, His-Atg8a 29kDa, Ub 9 kDa. (**c**) Midgut protein extracts at puparium formation from wild-type, *Atg7* mutant ($Atg7^{d77/d14}$) and *Atg8* ($Atg8^{KG07569}$) mutant blotted with anti-Atg8 and anti-Tubulin, *n* = 3 independent biological experiments. Representative images are shown. (**d**) Midguts from control $Atg3^{10}$/wild-type (*Atg3*/+), and $Atg3^{10}$/*Df(3L)cat* mutant (*Atg3*/*Df*) animals at puparium formation analyzed by DIC microscopy. Representative images are shown. (**e**) Cell size quantification (μm^2) from **d**, *n* = 11 (*Atg3*/+) and *n* = 9 (*Atg3*/*Df*) animal intestines/genotype with 5 cells measured/intestine. (**f**) Midguts dissected from early 3rd instar larvae that mis-express $Atg1^{GS10797}$ (*Atg1*) and $Atg3^{IR}$ only in the DsRed-marked cell clone and analyzed by fluorescence and DIC microscopy. Representative images are shown. (**g**) Midguts dissected from animals expressing $Atg4^{DN}$ specifically in DsRed-marked clones of cells at puparium formation and analyzed by fluorescence and DIC microscopy. Representative images are shown. (**h**) Cell size quantification (μm^2) from **g**, *n* = 10 animal intestines/genotype with 1-5 cells measured/intestine. (**i**) Midguts dissected from animals expressing mCherry-Atg8a in all cells, and expressing Ub^{IR} specifically in GFP-marked clones of cells at puparium formation. Representative images are shown. (**j**) Midguts dissected from animals expressing Ub^{IR} specifically in GFP-marked clones of cells at puparium formation and analyzed by fluorescence and DIC microscopy. Representative images are shown. (**k**) Cell size quantification (μm^2) from **j**, *n* = 12 animal intestines/genotype with 1-5 cells measured/intestine. (**l**,**m**) Midguts dissected from early third instar larvae that contain $Atg1^{GS10797}$ (*Atg1*) mis-expression in either a wild-type GFP positive cell clone (**l**) or a $Uba1^{H33}$ loss-of-function MARCM mutant cell clone (GFP-positive) (**m**) and analyzed by fluorescence and DIC microscopy. Control wild-type and heterozygous $Uba1^{H33}$/wild-type cells have no GFP. Representative images are shown. (**n**) Quantification (μm^2) from **l** and **m**, *n* = 22 (control), *n* = 16 (*Atg1*), and *n* =6 (*Atg1* + $Uba1^{H33}$) animal intestines/genotype with 1-5 cells

measured/intestine. Quantification of control cells (**l**,**m**) were pooled since they are genetically identical. Quantification is shown as mean ± s.d.. N.S.: no significance. Scale bars represent 20 μm.

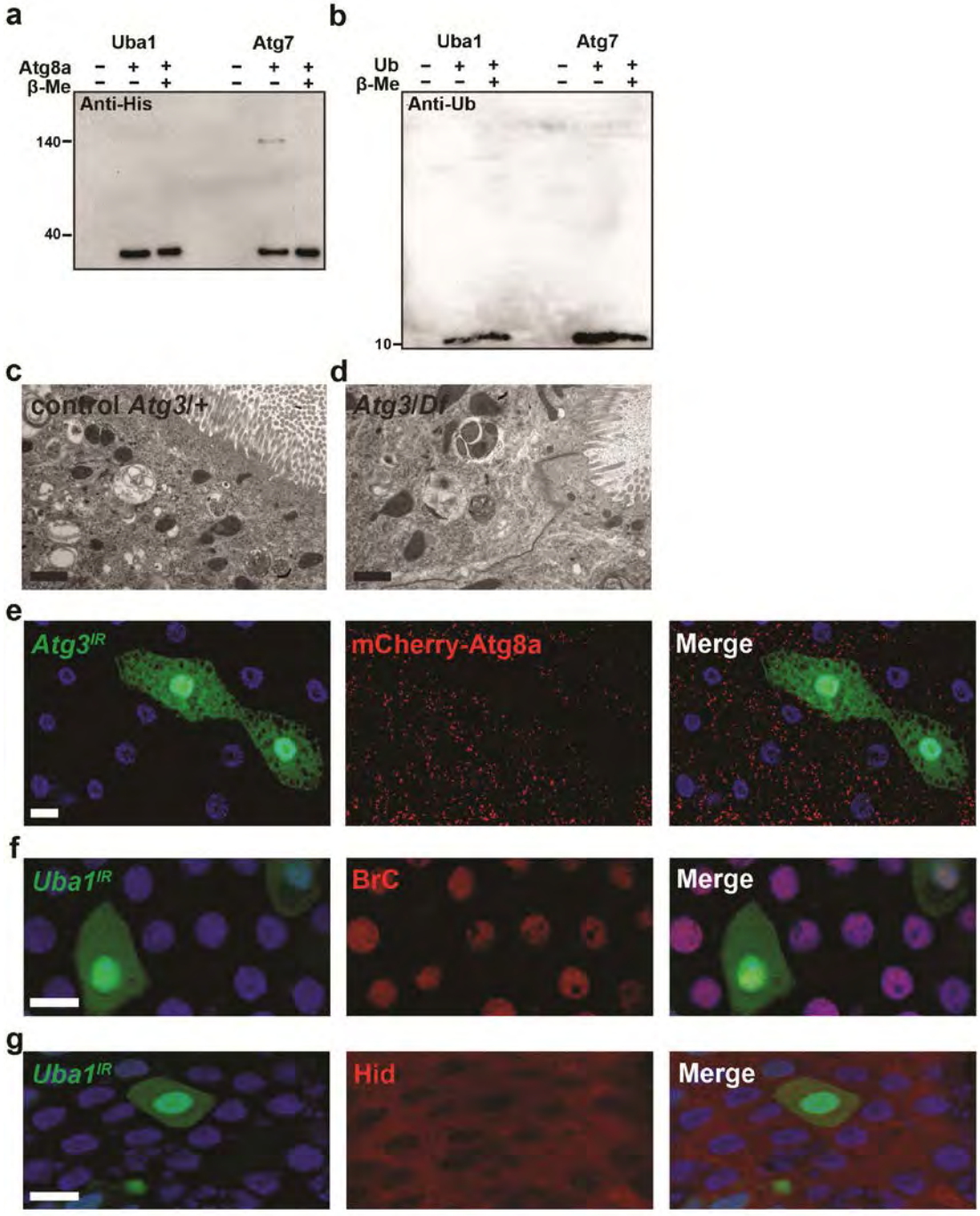

Figure 3-13 *Uba1*, but not loss of *Atg3*, influences autophagy and programmed reduction of midgut cell size. (**a**,**b**) Loading controls for the E1 charging assays, *n* =2. Representative images are shown. (**c**,**d**) Representative TEM images of intestine cells 2 h after puparium formation. (**c)** $Atg3^{10}$/wild-type control (*Atg3*/+) and (**d**) $Atg3^{10}$/*Df(3L)cat* mutant (*Atg3*/*Df*) cells both possess autophagic structures. (**e**) Starved third instar larval fat body expressing mCherry-Atg8a in all cells and $Atg3^{IR}$ in GFP-marked clones of cells and analyzed with fluorescence microscopy. Representative images are shown. (**f**,**g**) Midguts dissected from animals at puparium formation that mis-express $Uba1^{IR}$ (GFP in nucleus and cytoplasm) and stained to detect either BrC (**f**, red) or Hid (**g**, red). Representative images are shown. Scale bars represent 1 μm (**c**,**d**) and 20 μm (**e-g**).

The cysteine protease Atg4 is required for processing of Atg8/LC3 so that it can be conjugated to phosphatidyl-ethanolamine, as well as for de-lipidation of Atg8/LC3 at a later stage in autophagy. A dominant negative form of human Atg4B was shown to inhibit LC3 lipidation and autophagy [121], and a similar dominant negative form of Atg4a was shown to inhibit autophagy in *Drosophila* [122]. To further test the requirement for Atg8a lipidation in midgut cell size reduction, we expressed dominant negative Atg4 ($Atg4^{DN}$). Consistent with our other results, expression of $Atg4^{DN}$ in clones of cells did not alter their reduction in size (Fig. 3-12g,h). Combined, these data suggest that Atg8a lipidation, as well as the E1 and E2 enzymes Atg7 and Atg3, are not required for midgut autophagy.

Our data indicate that Uba1 does not substitute for Atg7. Therefore, we investigated alternative explanations for how Uba1 regulates autophagy and cell size reduction in the dying midgut of *Drosophila*. A rise in steroid hormone triggers the

induction of caspases and autophagy that precede midgut cell death [19, 81, 84], and it is possible that Uba1 influences all of these pathways. The steroid-regulated primary response protein BrC was present in *Uba1* knockdown cells even though cell size reduction was inhibited (Fig. 3-13f), indicating that Uba1 does not influence global aspects of steroid signaling. In addition, *Uba1* knockdown did not influence the expression of the steroid-regulated pro-apoptotic factor Hid (Fig. 3-13g). Combined, these data suggest the possibility that Uba1 may function directly in regulating autophagy. Although previous studies have suggested that receptors that bind to ubiquitinated cargo play an important role in early stages of autophagy [123, 124], no study has directly implicated ubiquitination as a key regulatory step in autophagosome formation. Therefore, such a model would predict that ubiquitin is required for autophagy and cell size reduction. We tested this model by knockdown of ubiquitin in clones of midgut cells, and saw that ubiquitin was required for Atg8a puncta formation (Fig. 3-12i) and programmed cell size reduction in the midgut (Fig. 3-12j,k). Significantly, the Atg1-induced small cell size phenotype (Fig. 3-7l) was suppressed when *Uba1* function was reduced (Fig. 3-12m,n). These data indicate that *Uba1* functions downstream of Atg1-regulated autophagy.

Midgut cells accumulate p62 and fail to form both Atg8a and Atg5 puncta when *Uba1* function is reduced (Fig. 3-8e-g). To determine if this E1 is required for removal of cytoplasmic material, we investigated the clearance of mitochondria from the cytoplasm of cells with decreased *Uba1* function. Homozygous *Uba1* mutant and neighboring control cells possessed similar amounts GFP-labeled mitochondria before the onset of

autophagy in the intestines of third instar larvae (Fig. 3-14a). These data indicate that reduced *Uba1* function does not dramatically alter mitochondria numbers during development. Significantly, we observed retention of both GFP-labeled mitochondria and mitochondrial ATP synthase complex V (ATPV) in intestine cells with reduced *Uba1*

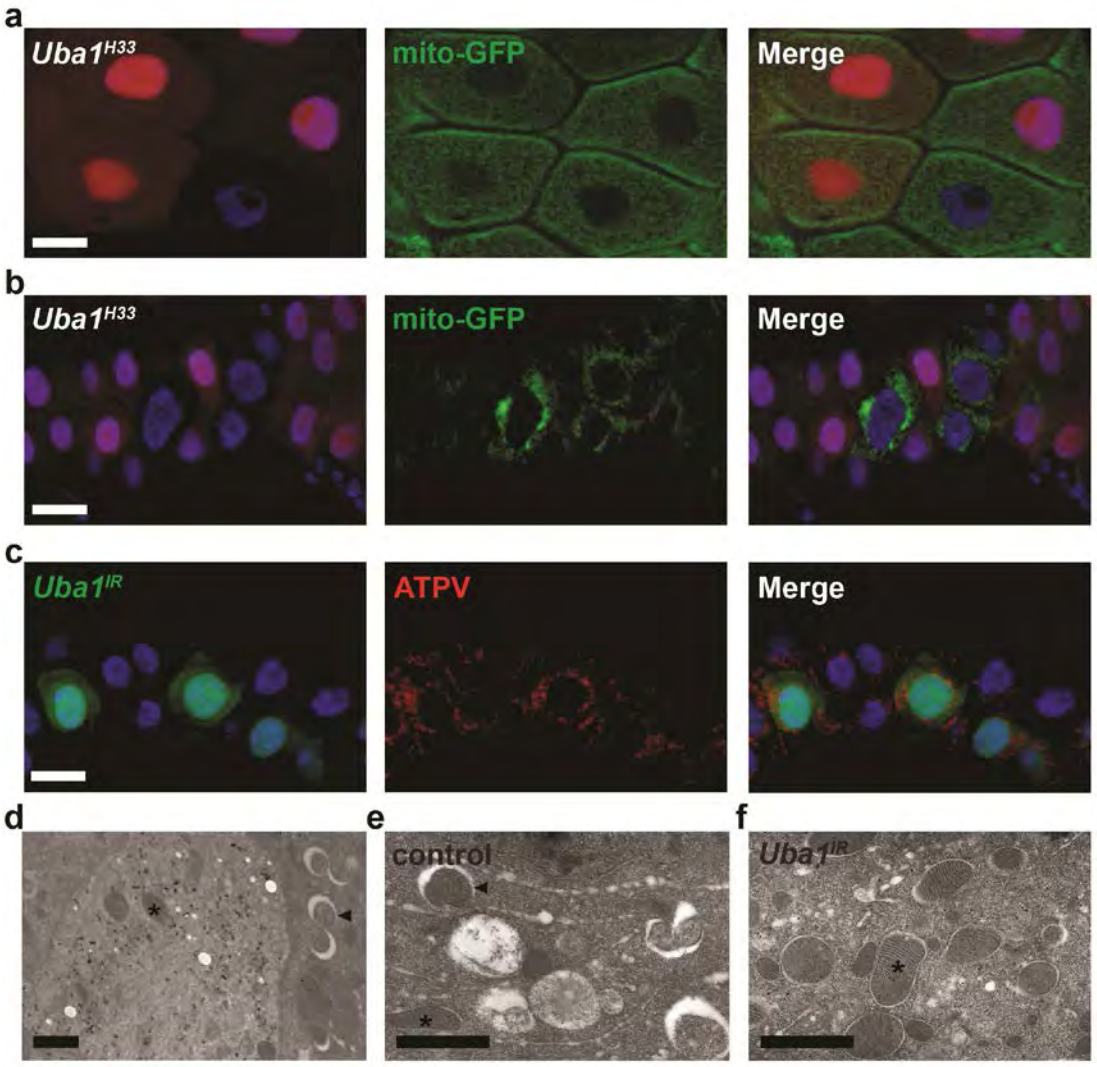

Figure 3-14 *Uba1* is required for clearance of mitochondria. (**a, b**) Midguts dissected from either early third instar larvae (**a**) or at puparium formation (**b**) that express GFP-labeled mitochondria in enterocytes (larger nuclei) and contain *Uba1*^{H33} loss-of-function mutant cell clones (lacking RFP). Wild-type control cells possess stronger RFP and heterozygous cells have weaker RFP. Representative images are shown. (**c**) Midguts dissected at puparium formation that express

Uba1^{IR} (GFP in nucleus and cytoplasm) and stained with ATP synthase complex V (ATPV) to detect mitochondria in all cells. Representative images are shown. (**d-f**) Representative immuno-TEM images of *Uba1*^{IR} clone cells at puparium formation. *Uba1*^{IR}-expressing cells possess gold particles, while control cells lack gold particles (**d**). Control cells possess numerous autolysosomes in the cytoplasm (arrowheads) and few mitochondria (asterisks), while *Uba1*^{IR}-expressing cells possess numerous mitochondria and few autophagic structures. Scale bars represent 20 μm (**a-c**) and 1 μm (**d-f**).

function compared to their control neighbors following the onset of autophagy (Fig. 14b,c). We then performed immuno-TEM to identify *Uba1* knockdown cells that express both *Uba1*^{IR} and GFP. Control cells lacking immuno-labeled gold particles possessed large numbers of autolysosomes (Fig. 3-14d,e). By contrast, cells with reduced *Uba1* function had more mitochondria and few autophagic structures (Fig. 3-14d,f). These data indicate that Uba1 plays an important role in the clearance of cytoplasmic material by regulating autophagy.

Discussion

Autophagy has been shown to influence cell size during growth factor and nutrient restriction in mammalian cells lines [125, 126], but this study indicates that autophagy controls cell size as part of a normal developmental program. Our discovery that *Atg7* and *Atg3* are not required for autophagy and cell size reduction in dying midgut cells in *Drosophila* is surprising. While an *Atg5*-, *Atg7*-, and *LC3*-independent autophagy pathway has been reported [55], we describe autophagy that requires *Atg8/LC3* and does not require *Atg7* and *Atg3*. It has been assumed that components of the core Atg8/LC3 and Atg12 conjugation pathways are used by all eukaryotic cells, but

this study provides evidence that alternative factors can function to regulate autophagy in a cell context-specific manner.

This study highlights that autophagy may have different regulatory mechanisms in distinct cell types within an animal. Different forms of autophagy could involve either unique regulatory pathways [127, 128], different amounts/rates of autophagy or alternative cargo selection mechanisms [129], and these are not mutually exclusive. Another possibility is that differences in cargo selection alone, perhaps based on specific cargo adaptor proteins, could mediate a distinct type of autophagy.

We report that an E1 enzyme other than *Atg7* is required for Atg8/LC3 and Atg5 puncta formation, and clearance of p62 and mitochondria. Our studies indicate that *Uba1* fails to function in place of *Atg7,* as expected based on the unique architecture and use of ubiquitin-like proteins and E2 binding domains in these highly divergent E1s [117]. Although we cannot exclude the possibility that Atg8a is activated by unknown factors, the simplest model to explain our data positions *Uba1* function at a different stage of the autophagy process that depends on ubiquitin conjugation. Previous work in a mammalian cell line indicated that *Uba1* is required for protein degradation by lysosomes, but this was not because of decreased autophagosome formation [130]. In addition, recent work in *Drosophila* implicated the de-ubiquitination enzyme USP36 in autophagy [131]. However, the inability of *Atg5* knockdown to suppress the *USP36* mutant phenotype, as well as the accumulation of both GFP-Atg8a and p62 in *USP36* mutant cells, suggests a defect in autophagic flux rather than a defect in the formation of

autophagosomes. p62 and other ubiquitin binding proteins are known to facilitate recruitment of ubiquitinated cargoes into autophagosomes [129]. In addition, p62 was recently shown to accumulate at sites of autophagosome formation even when autophagosome formation is blocked [123]. Thus, it is possible that Uba1 promotes cargo recruitment to the sites of autophagosome formation to facilitate autophagy. However, it is also possible that Uba1 could function at multiple stages in the regulation of autophagy.

It is critical to understand the mechanisms that regulate autophagy given the interest in this catabolic process as a therapeutic target for multiple age-associated disorders, including cancer and neurodegeneration. Significantly, our studies illuminate that autophagy has different regulatory mechanisms in distinct cell types within an animal, and highlight the importance of studying core autophagy genes in specific cell types under physiological conditions.

Acknowledgements

We thank A. Bergmann, M. Brodsky, S. Cherry, G. Juhasz, P. Meier, T.P. Neufeld, H. Stenmark, the Bloomington Stock Center, the VDRC, and the Developmental Studies Hybridoma Bank for flies and antibodies, G. Juhasz for advice about immuno-EM, and T. Fortier for technical support, M. Freeman, S. Doxsey and the Baehrecke lab for constructive comments. This work was supported by NIH grants GM079431 to EHB, GM095567 to JWH, and S10RR027897 to the UMass EM Core, and by Millennium

Pharamceuticals to JWH. EHB is an Ellison Medical Foundation Scholar and a member of the UMass DERC (DK32520).

Author contribitions

T.-K.C., B.V.S., S.D.H., J.W.H., and E.H.B. designed the experiments. All experiments were performed by T.-K.C., except Fig. 4d,e by B.V.S., TEM by T.-K.C., B.V.S., C. M. P., and R.T.S. and E1 charging assays by S.D.H.. T.-K.C., B.V.S. and E.H.B. wrote the manuscript and all authors commented on it.

Materials and methods

Drosophila strains

We used Canton-S as wild-type control. For loss-of-function mutations (obtained from the Bloomington stock center or otherwise specified), we used *Atg18*^{KG03090}, *Df(3L)*^{6112}, *Atg2*^{EP3697}, *Df(3L)*^{6091}, *Atg1*$^{\Delta 3D}$ [24], *Atg13*$^{\Delta 74}$ [25], *Atg6*^{1} [32], *Vps34*$^{\Delta m22}$ [30], *Atg7*^{d30}, *Atg7*^{d14}, *Atg7*^{d77}, *Atg7*^{d4} [119], *Atg3*^{10} [17], *Atg8a*^{KG07569}, *Df(3L)cat*, and *Uba1*^{H33} [132]. For RNAi knockdown assays, we used *CG7528-1*, *CG13343-3*, *CG13343-4* from P. Meier. We used RNAi lines from Vienna Drosophila RNAi Center (VDRC): UAS-*Atg18*^{IR} VDRC Transformant ID (TID) 22646, *UAS-Atg1*^{IR} TID 16133, *UAS-Atg8a*^{IR} TID 43097, UAS-*Atg7*^{IR} TID 45561, UAS-*Atg3*^{IR} TID 108666, *UAS-Uba2*^{IR} TID 110173, *UAS-Aos1*^{IR} TID 47256, *UAS-CG13343*^{IR} TID 105141, *UAS-APP-BP1*^{IR} TID 7728, *UAS-CG13090*^{IR} TID 110326, *UAS-CG13090*^{IR} TID 43558, *UAS-CG1749*^{IR} TID 110395. We also used the following TRiP lines from the Bloomington Stock Center: JF02703 (for *Atg5*) stock number BL27551, HMS01153 (for *Atg12*) BL34675, HMS01347 (for *Atg16*) BL34358, JF01977 (for *Uba1*) BL25957, HM05055 (for *Uba2*) BL28569, HM05183 (for *Aos1*) BL28972, HMS01352 (for *CG1749*) BL34363, and HMS00284 (for *Ub*) BL33405. For mis-expression studies, we used *UAS-p35*, *UAS-Atg1*^{GS10797} [17], *UAS-mito-GFP* (Bloomington, BL8442, 8443), *UAS-eGFP-Atg5* (BL8731), *UAS-Dts7*^{ts} [120], *UAS-CL1-GFP* [68], and *UAS-Atg4*^{DN} [122].

Induction of cell clones

To induce mis-expression in clones of cells, virgin females of *y w hsFlp*; +; *Act>CD2>GAL4* (> is FRT site), *UAS-DsRed* or *y w hsFlp*; *pmCherry-Atg8a*;

Act>CD2>GAL4, *UAS-nlsGFP*/*TM6B* [111] were crossed to indicated RNAi or transgenic lines. One day egg lays were heat shocked at 37°C except for *Uba1* RNAi clones that were heat shocked at first instar larval stage. To induce loss-of-function clones, we used *y w hsFlp*; +; *FRT80B Ubi-nlsGFP*, *y w hsFlp*; +; *FRT82B Ubi-GFP*, *y w hsFlp*; +; *FRT82B Ubi-nlsmRFP*, *y w hsFlp*; *NP1-GAL4*, *UAS-mito-GFP*; *FRT80B Ubi-nlsmRFP*, *y w hsFlp*; *FRT42D Ubi-nlsGFP, y w hsFlp*; *NP1-GAL4*, *FRT42D Ubi-nlsmRFP*; *UAS-eGFP-Atg5*, *y w hsFlp*; *NP1-GAL4*, *FRT42D Ubi-nlsmRFP*; *UAS-mito-GFP*, *y w hsFlp*; *CG-GAL4*, *UAS-GFP-Atg8a*, *FRT42D UAS-myrRFP* [119] and *y w hsFlp*, *UAS-CD8GFP*; *FRT42D Tub-GAL80^{ts}*; *Tub-GAL4*/*TM6B*. We heat shocked one day egg lays for 1 hr at 37°C.

Immuno-labeling and microscopy

We dissected midguts in PBS, fixed with 4% formaldehyde in PBS, blocked with 1% bovine serum albumin, and incubated with primary antibodies. We used mouse anti-Discs large (1:100, from Development Studies Hybridoma Bank, Cat#4F3), rat anti-p62 (1:1,000, H. Stenmark), mouse anti-BrC (1:100, Development Studies Hybridoma Bank, Cat#25E9), guinea pig anti-Hid (1:50, H. D. Ryoo), and mouse anti-ATP synthase complex V (1:1000, Abcam, Cat# ab14748). For secondary antibodies, we used anti-mouse Oregon Green 488, anti-mouse/guinea pig Alexa Fluor 546 antibody (1:250, Invitrogen, Cat#s O-6380, A-11030, and A-11074 respectively), and mounted in VectaShield containing DAPI (Vector Lab, USA) to detect DNA. We imaged samples with a Zeiss Axiophot II microscope. For GFP- or mCherry-Atg8 imaging, we briefly

fixed samples with 4% formaldehyde in PBS and stained DNA with Hoechst. DNA is blue in all Fig.s.

Electron microscopy (EM) and immuno-EM

Larval intestines were dissected from control and mutant animals at 2 hours after puparium formation in PBS. Intestines were fixed for 30 minutes at 25^{o}C in 2.5% glutaraldehyde in 0.1 M cacodylate buffer pH 7.4 (Electron Microscopy Sciences), washed 3 times for 5 minutes at 4^{o}C with 0.1M cacodylate buffer pH7.4, post-fixed in buffered 1% osmium tetroxide for 1 hour at room temperature, dehydrated, treated with propylene oxide and infiltrated for embedding in SPI-pon/Araldite.

For immuno-EM, intestines with GFP-positive *Uba1^{IR}* clone cells were dissected at puparium formation, fixed in 3.2% formaldehyde, 0.25% glutaraldehyde, 1% sucrose, 2mM calcium chloride in 0.1M cacodylate buffer pH7.4 at 4^{o}C overnight, buffer washed, dehydrated, infiltrated, and embedded in LR White resin with polymerization for 2 days at 45-50^{o}C. Ultrathin sections on gold grids were subjected to heat-induced antigen retrieval [133], blocked with buffered 1% BSA and 3% powdered milk, incubated with anti-GFP antibody (1:100, Novus Biologicals, Cat# NB 600-308), followed by 18nm colloidal gold donkey anti-rabbit (1:30, Jackson ImmunoResearch, Cat#111-215-144). All ultrathin sections were stained with uranyl acetate and lead citrate before examination using Philips CM10 and FEI Tecnai G2 Bio12 TEMs.

Quantification of cell size

All control and mutant midguts were processed in an identical fashion for image acquisition. Two-dimensional (2D) cell size was quantified using the measure outline function of Zeiss Axiovision Rel 4.7 software (Zeiss Inc, USA). Three-dimensional (3D) images were acquired using the Z-stack function of Zeiss Axiovision software, and quantified using Volocity software (Perkin Elmer, USA). We compared the 2D and 3D measurements of control and mutant midgut cells at both the third larval instar and white pre-pupal stages (Fig. 3-2), and determined that 2D measurements of cell size accurately reflect 3D measurements. Therefore, we used 2D measurements of cell size in all additional experiments. The number (n) analyzed in each experiment represents number of intestines analyzed, and 1-5 cells of each genotype were measured/intestine.

Starvation of larvae

Early third instar larvae were transferred from food to 20% sucrose in PBS for 4 h.

Quantification of mitochondria number

Mitochondria numbers were quantified from 2 distinct 25 μm^2 regions per cell from 2 cells per animal and at least 3 individual animals/genotype.

Immuno-blotting

Midguts were dissected in PBS at puparium formation. Proteins were extracted with RIPA buffer with complete protease inhibitor (Roche). Western blotting was performed using rabbit anti-Atg8 (1:500, S. Cherry), mouse anti-β-Tubulin (1:50, Development Studies Hybridoma Bank, Cat# E7), HRP-conjugated goat anti-rabbit and anti-mouse

IgG (1:2000, Invitrogen, Cat# G-21234 and G-21040 respectively) as previously described [100]. Three independent biological experiments were performed.

Protein production and E1 activating enzyme charging assay

Open reading frames for *Drosophila* Uba1, Atg7, and Atg8a were cloned into pDONR223 using the Gateway recombination system (Invitrogen). Expression constructs were also constructed using Gateway recombination. Recombinant FLAG-tagged Uba1 and Atg7 were produced in Sf9 cells using the Bac-N-Blue system (Invitrogen). Cells were lysed using 50 mM Tris-HCl pH 7.5, 150 mM NaCl, 0.5% NP40, 1 mM DTT, and EDTA-free protease inhibitor cocktail (Roche) and then ruptured using a dounce homogenizer. Lysates were precleared by spinning in a table-top centrifuge at 16,000 x g at 4°C for 20 minutes and the FLAG-tagged proteins were purified using anti-FLAG M2 affinity gel (Sigma). Proteins were eluted using 3X FLAG peptide (Sigma). The buffer was exchanged and the FLAG peptide removed by spinning the eluate in an Ultracel 10K Amicon Ultra centrifugal unit (Millipore) and finally stored in a buffer containing 50 mM Tris-HCl pH 7.5, 150 mM NaCl, 1mM DTT, and 10% glycerol. Recombinant His-Thioredoxin-tagged Atg8a was produced using the pET59-DEST vector (EMD Millipore) and expressed in Rosetta DE3 cells (EMD Millipore). Following induction with 0.4 mM IPTG for 4 hours at 37°C, Atg8a was purified using Ni-NTA agarose (Qiagen) and stored in 50 mM Tris-HCl pH 7.5, 150 mM NaCl, 1 mM DTT, and 10% glycerol. Recombinant human ubiquitin was purchased from Boston Biochem.

Charging reactions were set up on ice in a buffer containing 50 mM Tris-HCl pH 7.5, 5 mM KCl, 5 mM $MgCl_2$, and 1mM DTT made up to a total of 30 µL. For each reaction 10 nM E1, 500 nM ubiquitin, or 500 nM HIS-Atg8a were added where appropriate. Just before starting the reaction, ATP was added to 2 mM final concentration and the reactions were performed at 30°C for 15 minutes. Immediately following the reaction, samples were incubated with 2X Laemmli sample buffer with either 50 mM MES pH5.0 or 10% v/v β-Mercaptoethanol as indicated. Samples were incubated at room temperature and loaded onto two 4-12% NuPAGE Bis-Tris gels (Invitrogen), run in MES running buffer (Invitrogen). Gels were processed for immunoblotting with either rabbit anti-His H-15 (Santa Cruz, Cat#sc-803), mouse anti-Flag M2 (Sigma, Cat#F3165), or rabbit anti-Ubiquitin (Dako, Cat# Z0458) antibodies at 1:1000 in 5% milk in TBS plus 10% Tween-20 (Sigma). Two independent experiments were performed.

Statistics

Indicated *P* values were obtained using a two-tailed t-test, and all quantitative data are shown as mean ± standard deviation.

CHAPTER IV

Discussion and Conclusions

Regulation of larval midgut autophagy during metamorphosis

Ecdysone, the ecdysone receptor/Ultraspriracle complex, and the ecdysone receptor target early gene axis are important for insect development, and are thought to be the key signaling pathway that initiates metamorphosis in *Drosophila* [134]. Regulation of midgut autophagy and programmed cell size reduction requires functional EcR (Chang and Baehrecke, unpublished data). Surprisingly, I do not see a cell shrinking phenotype when the functions of the EcR target early genes are disrupted. Cells with loss-of-function mutations in E93 and E74, and RNAi knockdown of BrC and E75 exhibit normal cell size reduction (see appendix 9). Knockdown of the EcR binding partner Usp by two independent RNAi lines show no size difference, suggesting that either Usp is not required for midgut autophagy or that these RNAi lines do not adequately reduce *Usp* function. It is possible that multiple early genes function redundantly upstream of autophagy, and therefore a phenotype would only be observed when more than one of them is inhibited. Alternatively, *Atg* genes could be a direct EcR target that may not involve Usp, and could involve an alternative heterodimerization partner.

Midgut cell size reduction requires *Atg* genes, with the exception of *Atg7* (E1), *Atg3* (E2) and *Atg4* (see Chapter III). I do observe a defect in cell size reduction when *Atg4a* and *Atg4b* are both mis-expressed (data not shown). However, since Atg4s are cysteine proteases, mis-expression of *Atg4s* could lead to artificial effects due to non-specific enzymatic activity. Otherwise, all *Atg* genes tested show defects in cell size regulation. Although Atg12/5/16 complex has been proposed to function as the E3 ligase for Atg8 lipidation [51], a recent study shows that Atg8 was successfully lipidated with purified Atg7, Atg3 and synthetic liposomes, showing that *in vitro* Atg8 lipidation does not require Atg12/5/16 [71]. Interestingly, we also show that Atg12/5/16 are necessary for autophagy in the dying midgut, indicating that Atg12/5/16 may function in other aspects supporting formation of autophagic structures other than being the E3 ligase for Atg8. Moreover, the conjugation of Atg12 to Atg5 requires Atg7 [43], which raises a question whether Atg12-Atg5 conjugation is required in autophagy in the dying midgut. We have attempted to detect Atg5 and Atg12 conjugation by immunoblot against the green fluorescent protein (GFP) from Atg5-GFP fusion protein. The lack of antibodies against *Drosophila* Atg5 and Atg12 prevent us from resolving this issue without the production of either additional transgenic animals or antibodies. However, Atg5-GFP puncta form in *Atg7* mutant cells (see Chapter III), but fail to form when either *Vps34* or *Uba1* functions are impaired. Combined, these data indicate that components of the *Atg12*/*5*-*16* complex are required for autophagy in the midgut, but like *Atg8*, this is independent of *Atg7* function. Future studies should resolve how most *Atg* factors, but not *Atg7* control this unique form of autophagy.

Lots of *Atg* genes are conserved from yeast to humans. However, the human genome contains more genes that regulate autophagy that are not in the yeast genome. I have identified several of these genes in the fly genome, and tested for their functions in cell size reduction and autophagy in the midgut. These genes, including *Atg1* complex genes *CG1347* (mammalian *FIP200*), *CG7053* (mammalian *Atg101*), *Vps34* complex genes *CG11877 (*mammalian *Atg14*) and *Uvrag*, and *CG31033* (mammalian *Atg16*) are essential for autophagy and cell size reduction in the midgut. Some of these genes are required for salivary gland destruction and starvation-induced autophagy in the larval fat body (appendix 1). Moreover, I also identified genes that are required for other aspects of autophagy, such as isolation membrane formation, that are required for midgut cell size reduction including *Tango5* and the *VMP1* homolog *CG32675*. Together, these data indicate that the midgut can serve as a good system to screen for genes that regulate autophagy. Since caspases are not required for midgut destruction, midguts may be among the best *in vivo* models to perform experiments to understand the role of autophagy in cell death with minimal interference from factors that function in apoptosis.

Autophagy degrades materials via lysosomal enzymes and therefore, components in the lysosomal machinery are also important autophagy regulators. I tested if some lysosomal proteins are important in regulating autophagy in the midgut. Surprisingly, neither loss of *TRPML*, nor RNAi knockdowns of *CathD* or *Lysozyme E* affected cell size reduction and autophagy (data not shown), even though TRPML does regulate autophagy in *C. elegans* [135] and in *Drosophila* [136], and Lysozyme E has been

shown to be required for salivary gland destruction (see McPhee dissertation, 2010). Since a large number of potential proteases and transporters function in lysosomes, these results would suggest either other lysozymes play more important roles than those I tested or these enzymes can function redundantly. Therefore, a more systematic approach to studying the function of these factors is needed before making strong conclusions about degradation of autophagosomal cargo in the midgut.

An Atg8 lipidation-independent autophagy and the role of Uba1 in programmed cell size reduction

I showed that programmed cell size reduction and autophagy can function independently of Atg7 and lipidation of Atg8. This phenotype was confirmed with *Atg3* null mutant cells and mis-expression of dominant negative *Atg4*. Future experiments should be performed to further address this mechanism. These experiments include the following,

1. Rescue the *Atg8* mutant midgut cell size reduction with an Atg8 mutant transgene that cannot be lipidated.

The glycine residue G112 of fly Atg8 is evolutionarily conserved and is critical for covalent binding to the lysine residue of the E1 Atg7 and subsequent lipidation with PE [45]. Mutation of the G112 residue to an alanine should inhibit Atg8 lipidation such that no lipidated Atg8 (Atg8-II) should be detected by Western blot. *Atg8* is required for midgut autophagy and programmed cell size reduction. If the lipidation of Atg8 is not essential, then the expression of $Atg8^{G112A}$ in the Atg8 mutant background should lead to cell size

reduction in the midgut. I have constructed an expression plasmid containing a GFP-tagged *Atg8*^{G112A} under control of the endogenous *Atg8* promoter. Transgenic animals are made but the one I have tested did not show any rescued phenotype. This could be due to low expression level. Therefore, this needs to be retested with a transgene with stronger expression.

2. Enzymatically modifying Atg8 by bacterial protein RavZ.

Pathogen *Legionella pneumophila* uses its own enzyme Cysteine protease RavZ to modify host Atg8 protein so that host Atg7 and Atg3 can no longer recognize endogenous Atg8 Therefore, in this circumstances, Atg8 is not lipidated and autophagy is attenuated [71]. Although fly is not the natural host for *Legionella*, it would be interesting to see whether RavZ can also modify fly Atg8. If so, then mis-expression of RavZ would serve as a tool to study if lipidation of Atg8 plays a role in midgut autophagy.

Atg8-dependent, but lipidated *Atg8*-independent biology has been reported previously [137, 138]. In both cases, *Atg8* was required but loss of *Atg7* did not convey any phenotype. However, other *Atg* genes were also not required, suggesting these events were associated with *Atg8* in a non-autophagy fashion. To our knowledge, our study is the first one showing the requirement of many *Atg* genes, including *Atg8*, but does not require its lipidation activation.

Itakura and Mizushima reported that under nutrient deprivation, oligomerization of the autophagic cargo receptor protein p62 [or Ref(2)p in *Drosophila*] was required for

its targeting to the autophagosome formation site, and this did not require binding to LC3 [123]. They showed that p62 puncta formed when the formation and maturation of autophagosome were inhibited in *Atg3*, *Atg5* and *FIP200* knocked out cells. These data suggest that either p62 alone is sufficient to bring cargo to autophagosome formation site or p62-cargo can locally trigger formation of pre-autophagosomal structures. This concept can be used to explain how Atg8 may be recruited to the autophagy formation site in the *Drosophila* midgut; p62 induces autophagosome formation then recruits Atg8, whether it is lipidated or not. However, loss of either *Ref(2)p* (fly homolog of *p62* and *NBR1*, predicted by Psi-blast), *Kenny* (or *iκB kinase-γ*, fly homolog of *Optineurin* [139] by Psi-blast), or *Bruchpilot* (fly homolog of *NDP52* by Psi-blast) does not influence programmed cell size reduction. This indicates that these autophagic cargo receptors may play redundant role during autophagy in the midgut to induce autophagosome formation (see Fig. 4-1 and appendix 9).

Since p62-cargo complex might be able to induce the formation of autophagosome, it is intriguing to ask how the membrane is delivered. One explanation is that p62-cargo complex is recruited to the vicinity of ER and mitochondria which have been shown to provide membrane during autophagy. An alternative way is to deliver the membrane to p62-cargo directly via vesicle trafficking. Regulators of vesicle trafficking have been shown to participate in autophagy as well. These regulators may recruit vesicular membrane, for example, membrane from endosome, to PAS by interacting with p62 and the ubiquitinated cargos. ESCRT component *Tsg101*/*Vps23* possesses an ubiquitin binding domain and may manage membrane recruitment to the p62-cargo site.

Endosomes receive membrane from the plasma membrane via endocytosis and this mechanism will be discussed in the next section of discussion.

Uba1 is required for autophagy and programmed cell size reduction in the *Drosophila* midgut, but not in starvation-induced autophagy in the fat body. Uba1 does not likely substitute for Atg7 in the midgut. Uba1 functions as the E1 activating enzyme in ubiquitination and is genetically downstream of *Atg1*. Therefore, it is possible that *Uba1* regulates autophagy by ubiquitinating cargo proteins by sending them to the PAS to potentially promote isolation membrane formation (see Fig. 4-1). This may be difficult to test as Ref(2)p, Kenny and Bruchpilot may function redundantly. Alternatively, Uba1 might ubiquitinate some proteins that results in the induction of autophagy. To further investigate this possibility, I clonally knocked down all the known E2 enzymes in the *Drosophila* genome using RNAi (see appendix 5). Of the over 30 predicted E2s, half were previously characterized whereas the other half (listed as CG numbers) were speculated to have enzymatic activities and bind ub. In my experiments, only three showed defects in cell size reduction when their functions were attenuated: *UbcE2H*, *TSG101* (see below), and *CG4502*. I saw a defect in cell size reduction and autophagy with one of the *UbcE2H* RNAi lines, however the effect was weak. Unfortunately, due to lack of published mutants of *UbcE2H*, I cannot further investigate the role of *UbcE2H* as a potential regulator of autophagy in the midgut. Knockdown of *CG4502* gave a strong phenotype. However, this RNAi line could have off target effects as 96 potential genes predicted to be targeted by the RNAi sequence (http://stockcenter.vdrc.at/control/main). I also selectively reduced the functions of several E3 ligases based on their potential

roles in autophagy regulation. These E3s include *Nedd4* [140] and *TRAF6* [141], and they did not exhibit phenotypes in cell size reduction. Furthermore, which ubiquitination chain plays most important role in regulation of autophagy and cell size reduction remains unclear. Future genetic screening, for example a mutagenesis screen for factors that affect cell size reduction and autophagy, is required for the identification of these novel autophagy regulators to answer how Uba1, and which kind of ubiquitination contribute greatest to autophagy in the midgut.

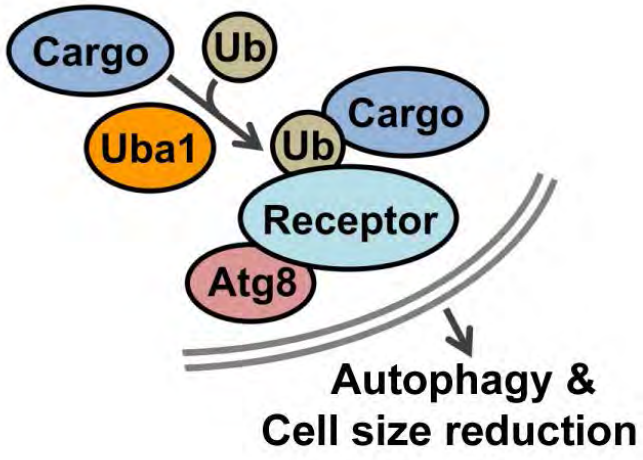

Fig. 4-1: Possible model of how Uba1 functions in regulating autophagy and programmed cell size reduction.

Role of cell membrane in midgut developmental autophagy

Autophagy is capable of reducing cell size by degrading materials in the cytoplasm. However, when the cell size is reduced, the surface area (plasma membrane) should reduce as well. It is not known whether plasma membrane can be degraded by autophagy, although membrane proteins can be withdrawn via Endosomal Sorting Complexes Required for Transport (ESCRT) and endocytosis into endosomes

[142]. In addition, the plasma membrane has been reported to be a potential source of membrane for autophagosome formation [11]. However, this is controversial, and the most accepted membrane source for autophagosomes is the ER [8]. In the midgut, we have shown that midgut cells reduce cell size during animal development, which makes the plasma membrane the best candidate as the membrane source. Therefore, we speculate that the plasma membrane can be the lipid source for autophagosomes.

Myristoylated RFP (myrRFP) was localized to the plasma membrane in early third instar larvae. Interestingly, myrRFP puncta became cytoplasmic and were colocalized with GFP-Atg5 and Lamp1-GFP when autophagy is augmented at the pre-pupal stage. This indicates that plasma membranes might be loaded into isolation membranes (marker: GFP-Atg5) and therefore co-existed on autolysosomes (marker: Lamp1-GFP). The same phenotype was also observed with colocalization of membrane bound CD8-GFP and mCherry-Atg8a, further confirms that the plasma membrane could be the membrane source for autophagosome. When the formation of autophagosome was inhibited by loss of *Atg1* function, myrRFP puncta were missing (Chang and Baehrecke, unpublished), further strengthening the argument that the plasma membrane is a source of membrane for the formation of autophagosomes.

The endocytic pathway, especially components of the ESCRTs, are required for sorting plasma membrane bound proteins, such as growth hormone receptor EGFR, back into the cytoplasm for degradation via lysosome. There are four ESCRT complexes, ESCRT-0, -I, -II, and –III. These factors sequentially bind to ubiquitinated

target proteins, and form early endocytic vesicles (early endosomes). These vesicles then gradually acidify, become late endosomes, multi-vesicular bodies, and later fuse with lysosomes [142]. Thus we hypothesize that ESCRT proteins not only sort membrane proteins, but also the membranes to the PAS. Loss of *Vps22* (also called *Larsen*, ESCRT-III) function inhibited the formation of myrRFP puncta and programmed cell size reduction. Similarly, cell size reduction defects were found in loss-of-function mutants of *TSG101* (also called *Vps23*, ESCRT-I), *Vps25* and *Vps36* (both are ESCRT-II), and *Vps2* (ESCRT-III), as well as RNAi knockdowns of *Hrs* (ESCRT-0), *Vps28* (ESCRT-I) and *Vps32* (ESCRT-III, Chang and Baehrecke, unpublished, see appendix 6). However, ESCRT proteins are also required for the fusion of autophagosomes and lysosomes to form autolysosomes [143]. Therefore, it is very challenging to dissect one mechanism (*i.e.* upstream membrane uptake) from another (*i.e.* downstream vesicle fusion), since these all could participate in regulating autophagy. Although it has been published that plasma membrane can be used as membrane source for autophagosome formation *in vitro* [11], future high resolution experiments should be performed to test whether the plasma membrane could serve as membrane source *in vivo*.

Difference between autophagic cell death in midgut and salivary gland

Degradation of larval organs during metamorphosis is important for animal development; incomplete degradation leads to developmental defects (Tracy and Baehrecke, unpublished data). The degradation of the midgut requires only autophagy [19]. By contrast, degradation of the salivary gland needs both autophagy and caspases. Moreover, the mechanisms of autophagy regulation are different in the midgut and the

salivary glands. For example, although growth arrest is essential for augmenting autophagy in both tissues, the cell growth Hippo regulatory pathway which negatively regulates autophagy in the salivary gland does not impact midgut degradation [100] (also see Chapter II). Moreover, members in the Baehrecke lab have screened for autophagy regulators in the dying salivary gland and have discovered numerous novel target genes. These targets include phagocytic receptor *Draper*, septate junction proteins, and micro RNA machinery. Genetic knockdowns of these molecules result in defects in salivary degradation [128] (also unpublished data from Chang, Nelson, Lin and Baehrecke). When these genes were clonally knocked down in the midgut, no phenotype was observed in either cell size reduction or autophagy levels (data not shown, and see the appendix 9). To screen for regulators for autophagy, RNAi knockdowns against potential Atg1 complex interactors and Atg8 (LC3s and GABARAPs) interactors [144] were performed in the midgut. These interactors were originally identified in normal HEK293 cells, which reflected molecule binding under basal autophagy condition. Unfortunately, none of these interactors appeared to influence autophagy in the midgut using RNAi techniques. I also cross referenced these interactors with microarray data from the larval salivary gland during the pupal stage. In the salivary gland, those interactors with upregulated RNA levels were knocked down by RNAi and analyzed by histology. Some of the interactors showed defects in gland destruction, for example *CG7337*, *CG6051*, *Coracle*, etc. (see appendixes 2, 3, 7). Together, this strengthens the argument that the salivary gland uses different ways to regulate autophagy and its destruction than the midgut. But why?

One possibility is the duration of organ destruction. Steroid hormone ecdysone signals for salivary gland destruction at 12 hours APF with complete gland destruction occurring 4 hours later. By contrast, larval midgut starts to decrease its size when the animal leaves food and starts wandering (see Chapter III). The midgut keeps on decreasing the size during the entire pupal stage and does not “disappear”. The larval gut remains visible even after adult ecloses (Chang and Baehrecke, unpublished observation). The larval gut remnant then is removed by bowel movement hours later. This suggests that, first, midgut destruction is a relatively slow process, and second, it is different from salivary gland destruction. Thus, midgut destruction could be simpler and use fewer pathways to accomplish its goal.

Drosophila midgut and salivary glands are degraded by autophagy during metamorphosis. One of the questions raised is why they degrade differently morphologically: the midgut shrinks, whereas the salivary gland disappears during metamorphosis. Since the larval midgut is no longer required for an adult animal, why not completely degrade it? There are several possible explanations for this. First, the dying, shrunken larval midgut could serve as the basis for the dispersing adult midgut epithelium. It is unclear if there are directional cues for the adult epithelium to grow and connect anteriorly to the mouth and posteriorly to the hindgut. Since the larval midgut was previously connected to these two organs, it would be convenient for the adult epithelium to use the larval midgut remnant as a scaffold. Second, the dying gut could also serve as a scale for measuring the circumference of the forming adult digestive

tube; the circumference is appropriate if the adult epithelium can cover the larval counterpart.

Last but not least, the *Drosophila* midgut, much like the mammalian small intestine, has microbes that reside in it. The midgut stops growing during late larval stage but the microbes probably continue to proliferate. The shrinking midgut thus confines where the microbes can be. If the larval midgut disappeared, the microbes could invade to the growing adult midgut and even to the whole animal, possibly affecting animal development or even causing lethality. By contrast, the cell/tissue shrinking mechanism would likely guarantee the proper development of the animal and prevent outbreak infections. These intestinal microbes will be expelled together with the larval midgut as the meconium.

I have described an Atg8 lipidation-independent autophagy that has not been reported previously. This form of autophagy does not need *Atg7* and *Atg3*, but requires *Uba1*, and is very different from other published autophagy studies. One of the differences is the membrane source; this midgut developmental autophagy could possibly use the cell membrane, ER membrane, and also the mitochondria membrane for autophagosome formation; whereas other autophagy, such as starvation-induced autophagy, may use the latter two only. ER and mitochondria are metabolic organelles that translate proteins and produce ATP to maintain cell viability. In the case of starvation, cells have low energy to sustain normal metabolism and likely need only limited amounts of ER and mitochondria. Thus, cells may use the ER and mitochondria

membrane as the source to form autophagosome. Starved cells might not utilize the plasma membrane because the cells still need the plasma membrane-bound growth factor receptors and the nutrient transporters to be intact. Depletion of the plasma membrane could disturb the integrity of the receptors and transporters, making the plasma membrane an undesirable source during starvation-induced autophagy. By contrast, midgut cells stop growing at the late larval to pre-pupal stage and would not need these receptors and transporters. These cells decrease their cell size and cell surface area, which would produce an excessive amount of membrane that could be used as the source for the forming autophagosomes. It is an intriguing question to ask whether this Atg8 lipidation-independent autophagy is conserved in evolution or if it is unique to the midgut of the *Drosophila*. Based on the above statements, I would think that induction of autophagy in non-proliferating and soon-to-be-eliminated cells would use the plasma membrane as one of the sources for the autophagosomes. Future experiments should emphasize how plasma membrane gets recruited to the cytoplasm for generating autophagosomes.

Conclusion

Autophagy is related to aging and many human disorders, and therefore, it is important to understand how autophagy is regulated. The function of autophagy as a cell survival mechanism is clear, but its role in cell death is less clear. I use the fruit fly *Drosophila melanogaster* as a model to study the role regulation of autophagy during animal development. Autophagy during cell death has been shown in the *Drosophila* larval salivary gland, but here in this thesis, I first demonstrate in the larval midgut of the

intestine, growth signaling and autophagy antagonize each other. Therefore, proper cell cycle arrest is required for augmenting autophagy in late larval stage. Molecules regulating autophagy are thought to be conserved from yeast to human, including the autophagy-related (*Atg*) genes *Atg8* (an ubiquitin-like molecule) and *Atg7* (E1 activating enzyme for *Atg8*). I show in this thesis that programmed cell size reduction in the dying midgut requires many *Atg* genes, including *Atg8*, but does not required *Atg7*. Instead, *Uba1*, the E1 for ubiquitination is essential for autophagy, cell size reduction and clearance of cytoplasmic materials. Atg8 lipidation needs Atg7, indicating lipidation is not required for autophagy in the midgut. Loss of *Ubiquitin* phenocopies *Uba1*, suggesting *Uba1* functions through ubiquitination of unknown molecule(s). Moreover, loss of *Uba1* function does not affect steroid hormone signaling and cell growth, and *Uba1* is acting genetically downstream of the autophagy initiator *Atg1*. Future genetic screenings would help understand how *Uba1* influences autophagy and may reveal possible therapeutic value of *Uba1* against cancer, neurodegeneration and infectious diseases.

Appendix: Screens for autophagy regulators

Filled box: phenotype detected, X: No phenotype, Empty Box: experiment not performed
MG: midgut, SG: salivary gland, FB: fat body

1. Atg and related genes

Gene name	CG#	VDRC#	TRiP#	Mutant	MG	SG	FB
Atg1	10967	16133			■	▒	▒
UAS-Atg1^{KD}	10967			KD	■	▒	
Atg1	10967			FRT80B Atg1$^{\Delta 3D}$	■		
Atg2	1241			Atg2^{EP3697}	■		
Atg3	6877		HMS01348		X		
Atg3	6877	101364			X		
Atg3	6877			EY08396	X		
Atg3	6877			Atg3^{10}	X	X	
Atg3	6877			gen-Nufip (5A); Atg3^{10}		X	
Atg4a+4b					■		
Atg4DN (II)							
Atg4DN (III)							
Atg5	1643		JF02703		■		
Atg6	5429	?			X		
Atg6	5429			FRT82B Atg6^{1}	■		
Atg7	5489	45561			X		▒
Atg8a	32672	43097			■		
Atg8b	12334	17079			X		
Atg10	12821		108980		X		X
Atg12-3	10861				■		▒
Atg12	10861		JF02704		■		
Atg12	10861		HMS01153		■		
Atg13	7331			FRT82B Atg13$^{\Delta 74}$	■		
Atg14	11877	49372			X		
Atg14	11877	108559			■		
Atg14	11877		?		X		
Atg16	31033		HMS01347		■		
FIP200/Atg17	1347	104864			■	▒	▒
Atg18	7986	22646			■		
Atg18	7986			Atg18^{KG03090}	■		
Atg101	7053		HMS01349		■	▒	▒
Atg101	7053	106176			■		
Vps34	5373			FRT42D Vps34$^{\Delta m22}$	■		
Vps34	5373	100296			■		
Rubicon	12772	109424			X		
UVRAG	6116		HMS1357		■		
UVRAG	6116			FRT40A Uvrag^{B21}	■		
UVRAG	6116			FRT40A Uvrag^{G13}	■		

Endophilin Beta/Bif	9834		JF02688		X		
Endophilin Beta/Bif	9834	104712			X		
Rab7/VMP1	5915	403377					
Tango5	32675	46668					

2. Atg1 complex interactors

Gene name	CG#	VDRC#	TRiP#	Mutant	MG	SG	FB
USP10	32479/12503/13903	37858			X		
Alicorn,Alc	8057		HMS00316		X		X
AMPK/SNF1A	3051		JF01951		X	X	
AMPK/SNF1A	3051	1827			X		
SNF4-PKG	5806/17299		JF02060		X		
cdc37	12019		JF03184		X		
	5446	108207			X	X	
Archipelago,Ago	15010		HM04005		X		
Slmb	3412	34274			X		
	7429	110316			X		
Neosin	8424	108950			X		X
ik2	2615		HMS01188		X		
ik2	2615	103748			X		
PRA2	9273		HMS01061		X		
	15220	101833			X		X
	32685	14635			X		
Polo	12306		HMS00530		X		
Polo	12306	20177			X		
Enolase,Eno	17654		JF02070		X		X
Coracle,Cora	11949	9788			X		X
Coracle,Cora	11949		HMS01447		X		
	12304	101667			X		X
Nep1	5894/5905	27537			X		X
copg	1528		HM05099		X		X
N-Cadherin	7100	1092			X		X
AP-47	9388		JF02685		X		X
Pds5	17509	36527			X		
	13902		HMS00579		X		X
	10133		HMS00578		X		X

3. Atg8/LC3/GABARAP interactors

Gene name	CG#	VDRC#	TRiP#	Mutant	MG	SG	FB
	6051	25500			X		
Hrs	2903		JF02860				X
Sara	15667		HMS01239		X	X	
CIP4	15015	108625				X	
Karyopherin beta 3	1059	105602				X	
Diablo	6224	105407					
Kelch	7210	105397				X	
	17754	104337				X	
	7337	110764			X		

NEDD4	42279/7555/32184		HMS01221		X		
NEDD4				EY00500	X		
NEDD4				DG05310	X		
NEDD4				EY/DG	X	X	
Blue cheese, Bchs	14001	110785			X		
TBC1D9/9B	7324		HMS00772		X		
TBC1D2B	12241		HMS00612		X		
TBC1D16	5337		HMS00324		X		
TBC1D17	11490		HMS00177		X		
TBC1D18/RABGAP1L	7112		HMS01132		X		

4. E1, E3 and DUB enzymes

Uba1	1728			FRT42D Uba1^{H42}			
Uba1	1728			FRT42D Uba1^{H33} (ts)		mix	X
Uba1	1728		JF01977				
Uba2 CG7528R-1	7528				X		
Uba2	7528	110173			X		
Uba2	7528		HM05056		X		
Aos1	12276	47256			X		
Aos1	12276		HM05183		X		
Aos1	12276	47257					
Uba3 CG13343-4	13343				X		
Uba3	13343	17139			X		
Uba3	13343	17137					
Uba3	13343	105141			X		
APP-BP1	7828	7728			X		
Uba4	13090	43558			X		
Uba4	13090	110326			X		
Uba5	1749	110395			X		
Uba5	1749		HMS01352		X		
Nedd4	42279/7555/32184		JF01860				
Nedd4	42279/7555/32184		HMS01221		X		
Nedd4	42279/7555/32184			EY00500	X		
Nedd4	42279/7555/32184			DG05310	X		
Nedd4	42279/7555/32184			EY/DG	X	X	
Cul-4	8711	44829			X		
Traf6	10961		HMS00880		X		
UAS-Ubp2	N/A				X		

5. E2 enzymes

Gene name	CG#	VDRC#	TRiP#	Mutant	MG	SG	FB
TAFII250	17603	41099					
TAFII250	17603	106119			X		
Effete, Eff	7425	26011			X		
Effete	7425	26012			X		
Effete	7425			mer1	X		
Effete	7425			8	X		
Lesswright, Lwr	3018		JF01386				

Lwr	3018	33685			X		
Lwr	3018			FRT40A lwr$^{4-3}$	X		
UbcD2	6720	31158			X		
UbcD4	8284	35873			X		
UbcD6	2013	23229			X		
UbcD10	5788	100570			X		
Ubc84D	12799	106363			X		
UbcE2H	2257	33509					X
UbcE2H	2257	33510					X
UbcE2H	2257	108386			X		
Vihar	10682	107720			X		
Bendless	18319	109638			X		
Bendless	18319			Bendless*	X		
Crossbronx	10536	16078			X		
Courtless	4443	104440			X		
Morgue	15437	11090			X		
TSG101/Erupted/Vps23	9712	23944					X
TSG101/Erupted/Vps23	9712			FRT80B Ept^{2}			
CG5823	5823	108292			X		
CG17030	17030	108804			X		
CG3473	3473	104207			X		
CG8188	8188	103362			X		
CG5440	5440	100099			X		
CG10254	10254	108657			X		
CG2574	2574	40173			X		
CG40045	40045	109167			X		
CG14739	14739	105594			X		
CG7656	7656	100791			X		
CG10862	10862	31372			X		
CG9602	9602	29499			X		
CG10723	10723	101360			X		
CG4502	4502	34855					
CG4502	4502		GL00418				
CG7375	7375	100761			X		
CG7220	7220	104478			X		
CG16894	16894	108983			X		
CG8386	8386	107382			X		
CG2924	2924	104482			X		
Bruce	6303			Bruce^{81}	X		

6. Shibire and ESCRT components

Gene name	CG#	VDRC#	TRiP#	Mutant	MG	SG	FB
Shibire	18102			ts	X		
Hrs	2903		JF02860				X
TSG101/Erupted/Vps23	9712	23944					X
TSG101/Erupted/Vps23	9712			FRT80B Ept^{2}			
Vps28	12770	31894					
Vps25	14750			FRT42D Vps25^{A3}			

Vps32	8055			FRT42D Vps32^{G5}			
Vps32	8055	106823					
Vps36	10711			FRT2A Vps36^{L5212}			
Vps36	10711	107417					
Vps2	14542			FRT82B Vps2^{PP6}			
Larsen/Lsn/Vps22	6637			FRT82B Lsn^{SS6}			

7. Septate junction components

Gene name	CG#	VDRC#	TRiP#	Mutant	MG	SG	FB
Coracle,Cora	11949	9788			X		
Coracle,Cora	11949		HMS01447		X		X
Lachesin	12369		HM05151		X		
Scrib	5462	27424				X	
Lethal giant larvae,Lgl	2671	51247				X	
Lgl	2671	51249				X	
Expanded,Ex	4144		HMS00874			X	
Merlin,Mer	14228		HMS00459			X	
Neurexin,Nrx IV	6827		JF03142				
Neuroglian, Nrg	1634		JF03151		X		
Contactin,Cont	1084		HM05134				
Gliotactin,Gli	3903		HMS05262				
Nervana,Nrv2	9261		JF03081				
polychaetoid,Pyd/ZO-1	43140		HMS00263				
Fasciclin,Fas 3	5803			FRT40A Fas3^{A142}	X		

8. FYVE domain containing

Gene name	CG#	VDRC#	TRiP#	Mutant	MG	SG	FB
Hrs	2903		JF02860				X
Sara	15667		HMS01239		X	X	
Sara	15667	19150			X		
	6051	25500			X		
Blue cheese, Bchs	14001	45028			X		
Rush hour	14782	12795			X		
	41099		HMS01228/TM3				
Rabenosyn5/Rbsn5	8506	24114			X		
	5168	22021			X		
	31064	103379			X		
	5270	27390			X		
dEEA1?	3632	26254			X		
Bitesize	7343/44012			FRT82B Btsz^{J5-2}	X		
	3530		JF01885		X		

9. Others

Gene name	CG#	VDRC#	TRiP#	Mutant	MG	SG	FB
	7177	106928			X		
Rab35	9575	101361			X		
Happyhour	7097	35166			X		
Jim	11352	12698			X		

p62/Ref(2)p	10360	108193			X		X
p62/Ref(2)p	10360			OD2			
p62/Ref(2)p	10360			OD3	X		
Kenny/IKKgamma	16910		GL00088				
Kenny	16910			Key^{1}	X		
Bruchpilot,Brp	42344/30337/34146		JF01932		X		
Blue cheese, Bchs	14001	45028			X		
Jaguar/Myosin VI	5695		JF02901		X		
Rictor	8002		JF01370				
Rictor	8002			Δ1	X		
Rictor	8002			Δ2	X		
PI3K68D	11621	16239			X		
PI3K68D	11621		HMS01296		X		
Stat92E	4257	43866				X	
Stat92E	4257			StatdNdC		X	
Stat92E	4257			$Stat^{06346}$	X		
EcRDN	1765						
ECR	1765						
Usp	4380		JF02546		X		
Usp	4380	16893			X		
E93	18389	45857			X		
E93	18389			$E93^{1}$/Df	X		
BrC	11491		JF02585		X		
BrC	11491	13705			X		
E74	32180			$E74^{neo}$/Df	X		
E75B	8127				X		
Basket/JNK	5680	104569			X		
Puckered	7850			WT	X		
	11665				X		
Dicer1	4792				X		
Draper	2086				X		
p53	33336		JF02513		X	X	
Torsin	3024				X		
CathD	1548		HM05189		X		
Lysozyme E	1180	109157			X		
TRPML	8743			$TRPML^{1}$	X		
TRPML	8743			FRT2A $TRPML^{PL00182}$			
Par1	8201		HMS00405		X		
Lkb1	9374		HMS01351		X		
Snail	3956		JF03094		X		
Twist	2956		JF02003		X		
Huntingtin	9995	107149			X		
Huntingtin	9995		JF01205		X		
Huntingtin	9995			Htt KO	X		
UAS-miR994					X		
UAS-E2F	6376						

Bibliography

1. Baehrecke, E.H. How death shapes life during development. *Nature Reviews Mol. Cell Biol.* **3**, 779-787 (2002).
2. Schweichel, J.-U. & Merker, H.-J. The morphology of various types of cell death in prenatal tissues. *Teratology* **7**, 253-266 (1973).
3. Kerr, J.F., Wyllie, A.H. & Currie, A.R. Apoptosis: a basic biological phenomenon with wide-ranging implications in tissue kinetics. *Br. J. Cancer* **26**, 239-257 (1972).
4. Elmore, S. Apoptosis: a review of programmed cell death. *Toxicologic pathology* **35**, 495-516 (2007).
5. Vandenabeele, P., Declercq, W., Van Herreweghe, F. & Vanden Berghe, T. The role of the kinases RIP1 and RIP3 in TNF-induced necrosis. *Science signaling* **3**, re4 (2010).
6. Mijaljica, D., Prescott, M. & Devenish, R.J. Microautophagy in mammalian cells: revisiting a 40-year-old conundrum. *Autophagy* **7**, 673-682 (2011).
7. Cuervo, A.M. Chaperone-mediated autophagy: selectivity pays off. *Trends in endocrinology and metabolism: TEM* **21**, 142-150 (2010).
8. Hayashi-Nishino, M. *et al.* A subdomain of the endoplasmic reticulum forms a cradle for autophagosome formation. *Nature cell biology* **11**, 1433-1437 (2009).
9. Yla-Anttila, P., Vihinen, H., Jokitalo, E. & Eskelinen, E.L. 3D tomography reveals connections between the phagophore and endoplasmic reticulum. *Autophagy* **5**, 1180-1185 (2009).
10. Hailey, D.W. *et al.* Mitochondria supply membranes for autophagosome biogenesis during starvation. *Cell* **141**, 656-667 (2010).
11. Ravikumar, B., Moreau, K., Jahreiss, L., Puri, C. & Rubinsztein, D.C. Plasma membrane contributes to the formation of pre-autophagosomal structures. *Nat. Cell Biol.* **12**, 747-757 (2010).
12. Kabeya, Y. *et al.* LC3, a mammalian homologue of yeast Apg8p, is localized in autophagosome membranes after

processing. *EMBO J.* **19**, 5720-5728 (2000).
13. Jin, S.M. & Youle, R.J. PINK1- and Parkin-mediated mitophagy at a glance. *Journal of cell science* **125**, 795-799 (2012).
14. Kim, J., Kundu, M., Viollet, B. & Guan, K.L. AMPK and mTOR regulate autophagy through direct phosphorylation of Ulk1. *Nat. Cell Biol.* **13**, 132-141 (2011).
15. Wang, R.C. *et al.* Akt-mediated regulation of autophagy and tumorigenesis through Beclin 1 phosphorylation. *Science* **338**, 956-959 (2012).
16. Egan, D.F. *et al.* Phosphorylation of ULK1 (hATG1) by AMP-activated protein kinase connects energy sensing to mitophagy. *Science* **331**, 456-461 (2011).
17. Scott, R.C., Juhász, G. & Neufeld, T.P. Direct induction of autophagy by Atg1 inhibits cell growth and induces apoptotic cell death. *Curr. Biol.* **17**, 1-11 (2007).
18. Berry, D.L. & Baehrecke, E.H. Growth arrest and autophagy are required for salivary gland cell degradation in *Drosophila*. *Cell* **131**, 1137-1148 (2007).
19. Denton, D. *et al.* Autophagy, not apoptosis, is essential for midgut cell death in Drosophila. *Curr. Biol.* **19**, 1741-1746 (2009).
20. Tsukada, M. & Ohsumi, Y. Isolation and characterization of autophagy-defective mutants of *Saccharomyces cerevisiae*. *FEBS Lett.* **333**, 169-174 (1993).
21. Harding, T.M., Morano, K.A., Scott, S.V. & Klionsky, D.J. Isolation and characterization of yeast mutants in the cytoplasm to vacuole protein targeting pathway. *J. Cell Bio.* **131**, 591-602 (1995).
22. Thumm, M. *et al.* Isolation of autophagocytosis mutants of *Saccharomyces cerevisiae*. *FEBS Lett.* **349**, 275-280 (1994).
23. Kamada, Y. *et al.* Tor-mediated induction of autophagy via an Apg1 protein kinase complex. *J. Cell Biol.* **150**, 1507-1513 (2000).
24. Scott, R.C., Schuldiner, O. & Neufeld, T.P. Role and regulation of starvation-induced autophagy in the Drosophila fat body. *Dev. Cell* **7**, 167-178 (2004).
25. Chang, Y.Y. & Neufeld, T.P. An Atg1/Atg13 complex with multiple roles in TOR-mediated autophagy regulation. *Mol. Biol. Cell* **20**, 2004-2014 (2009).

26. Hara, T. *et al.* FIP200, a ULK-interacting protein, is required for autophagosome formation in mammalian cells. *The Journal of cell biology* **181**, 497-510 (2008).
27. Kim, M. *et al.* Drosophila Fip200 is an essential regulator of autophagy that attenuates both growth and aging. *Autophagy* **9**, 1201-1213 (2013).
28. Hosokawa, N. *et al.* Atg101, a novel mammalian autophagy protein interacting with Atg13. *Autophagy* **5**, 973-979 (2009).
29. Kihara, A., Noda, T., Ishihara, N. & Ohsumi, Y. Two distinct Vps34 phosphatidylinositol 3-kinase complexes function in autophagy and carboxypeptidase Y sorting in Saccharomyces cerevisiae. *J. Cell Biol.* **152**, 519-530 (2001).
30. Juhász, G. *et al.* The class III PI(3)K Vps34 promotes autophagy and endocytosis but not TOR signaling in Drosophila. *J. Cell Biol.* **181**, 2347-2360 (2008).
31. Pattingre, S. *et al.* Bcl-2 antiapoptotic proteins inhibit Beclin 1-dependent autophagy. *Cell* **122**, 927-939 (2005).
32. Shravage, B.V., Hill, J.H., Powers, C.M., Wu, L. & Baehrecke, E.H. Atg6 is required for multiple vesicle trafficking pathways and hematopoiesis in Drosophila. *Development* **140**, 1321-1329 (2013).
33. Stack, J.H., DeWald, D.B., Takegawa, K. & Emr, S.D. Vesicle-mediated protein transport: regulatory interactions between the Vps15 protein kinase and the Vps34 PtdIns 3-kinase essential for protein sorting to the vacuole in yeast. *The Journal of cell biology* **129**, 321-334 (1995).
34. Lindmo, K. *et al.* The PI 3-kinase regulator Vps15 is required for autophagic clearance of protein aggregates. *Autophagy* **4**, 500-506 (2008).
35. Liang, C. *et al.* Beclin1-binding UVRAG targets the class C Vps complex to coordinate autophagosome maturation and endocytic trafficking. *Nat. Cell Biol.* **10**, 776-787 (2008).
36. Sun, Q. *et al.* Identification of Barkor as a mammalian autophagy-specific factor for Beclin 1 and class III phosphatidylinositol 3-kinase. *Proceedings of the National Academy of Sciences of the United States of America* **105**, 19211-19216 (2008).
37. Takahashi, Y. *et al.* Bif-1 interacts with Beclin 1 through UVRAG and regulates autophagy and tumorigenesis. *Nat. Cell Biol.* **9**, 1142-1151 (2007).
38. Yamamoto, H. *et al.* Atg9 vesicles are an important membrane source during early steps of autophagosome formation. *The Journal of cell biology* **198**, 219-233 (2012).
39. Reggiori, F., Tucker, K.A., Stromhaug, P.E. & Klionsky, D.J. The Atg1-Atg13 complex regulates Atg9 and Atg23 retrieval transport from the pre-autophagosomal structure. *Developmental cell* **6**, 79-90 (2004).
40. He, C. & Klionsky, D.J. Regulation mechanisms and signaling pathways of autophagy. *Annual review of genetics* **43**, 67-93 (2009).
41. Krick, R., Tolstrup, J., Appelles, A., Henke, S. & Thumm, M. The relevance of the phosphatidylinositolphosphat-binding motif FRRGT of Atg18 and Atg21 for the Cvt pathway and autophagy. *FEBS letters* **580**, 4632-4638 (2006).
42. Ichimura, Y. *et al.* A ubiquitin-like system mediates protein lipidation. *Nature* **408**, 488-492 (2000).
43. Mizushima, N. *et al.* A protein conjugation system essential for autophagy. *Nature* **395**, 395-398 (1998).
44. Ohsumi, Y. Molecular dissection of autophagy: two ubiquitin-like systems. *Nature Reviews Mol. Cell Biol.* **2**, 211-216 (2001).
45. Kirisako, T. *et al.* The reversible modification regulates the membrane-binding state of Apg8/Aut7 essential for autophagy and the cytoplasm to vacuole targeting pathway. *J. Cell Biol.* **151**, 263-276 (2000).
46. Tanida, I. *et al.* Apg7p/Cvt2p: A novel protein-activating enzyme essential for autophagy. *Mol. Biol. Cell* **10**, 1367-1379 (1999).
47. Kim, J., Dalton, V.M., Eggerton, K.P., Scott, S.V. & Klionsky, D.J. Apg7p/Cvt2p is required for the cytoplasm-to-vacuole targeting, macroautophagy, and peroxisome degradation pathways. *Mol. Biol. Cell* **10**, 1337-1351 (1999).
48. Shintani, T. *et al.* Apg10p, a novel protein-conjugating enzyme essential for autophagy in yeast. *EMBO J.* **18**, 5234-5241 (1999).
49. Ichimura, Y. *et al.* In vivo and in vitro reconstitution of Atg8 conjugation essential for autophagy. *The Journal of biological chemistry* **279**, 40584-40592 (2004).

50. Schlumpberger, M. *et al.* AUT1, a gene essential for autophagocytosis in the yeast Saccharomyces cerevisiae. *Journal of bacteriology* **179**, 1068-1076 (1997).
51. Hanada, T. *et al.* The Atg12-Atg5 conjugate has a novel E3-like activity for protein lipidation in autophagy. *The Journal of biological chemistry* **282**, 37298-37302 (2007).
52. Romanov, J. *et al.* Mechanism and functions of membrane binding by the Atg5-Atg12/Atg16 complex during autophagosome formation. *The EMBO journal* **31**, 4304-4317 (2012).
53. Kundu, M. & Thompson, C.B. Autophagy: basic principles and relevance to disease. *Annual review of pathology* **3**, 427-455 (2008).
54. Juenemann, K. & Reits, E.A. Alternative macroautophagic pathways. *International journal of cell biology* **2012**, 189794 (2012).
55. Nishida, Y. *et al.* Discovery of Atg5/Atg7-independent alternative macroautophagy *Nature* **461**, 654-658 (2009).
56. Scarlatti, F., Granata, R., Meijer, A.J. & Codogno, P. Does autophagy have a license to kill mammalian cells? *Cell death and differentiation* **16**, 12-20 (2009).
57. Grishchuk, Y., Ginet, V., Truttmann, A.C., Clarke, P.G. & Puyal, J. Beclin 1-independent autophagy contributes to apoptosis in cortical neurons. *Autophagy* **7**, 1115-1131 (2011).
58. Seo, G. *et al.* Hydrogen peroxide induces Beclin 1-independent autophagic cell death by suppressing the mTOR pathway via promoting the ubiquitination and degradation of Rheb in GSH-depleted RAW 264.7 cells. *Free radical research* **45**, 389-399 (2011).
59. Kondo, Y., Kanzawa, T., Sawaya, R. & Kondo, S. The role of autophagy in cancer development and response to therapy. *Nature reviews. Cancer* **5**, 726-734 (2005).
60. Mizushima, N., Levine, B., Cuervo, A.M. & Klionsky, D.J. Autophagy fights disease through cellular self-digestion. *Nature* **451**, 1069-1075 (2008).
61. Aita, V.M. *et al.* Cloning and genomic organization of beclin 1, a candidate tumor suppressor gene on chromosome 17q21. *Genomics* **59**, 59-65 (1999).
62. Qu, X. *et al.* Promotion of tumorigenesis by heterozygous disruption of the beclin 1 autophagy gene. *J. Clin. Invest.* **112**, 1809-1820 (2003).
63. Takamura, A. *et al.* Autophagy-deficient mice develop multiple liver tumors. *Genes Dev.* **25**, 795-800 (2011).
64. Kenzelmann Broz, D. *et al.* Global genomic profiling reveals an extensive p53-regulated autophagy program contributing to key p53 responses. *Genes & development* **27**, 1016-1031 (2013).
65. Shintani, T. & Klionsky, D.J. Autophagy in health and disease: a double-edged sword. *Science* **306**, 990-995 (2004).
66. Hara, T. *et al.* Suppression of basal autophagy in neural cells causes neurodegenerative disease in mice. *Nature* **441**, 885-889 (2006).
67. Komatsu, M. *et al.* Loss of autophagy in the central nervous system causes neurodegeneration in mice. *Nature* **441**, 880-884 (2006).
68. Pandey, U.B. *et al.* HDAC6 rescues neurodegeneration and provides an essential link between autophagy and the UPS. *Nature* **447**, 859-863 (2007).
69. Ravikumar, B. *et al.* Inhibition of mTOR induces autophagy and reduces toxicity of polyglutamine expansions in fly and mouse models of Huntington disease. *Nat. Genetics* **36**, 585-595 (2004).
70. Yoshikawa, Y. *et al.* Listeria monocytogenes ActA-mediated escape from autophagic recognition. *Nature cell biology* **11**, 1233-1240 (2009).
71. Choy, A. *et al.* The Legionella effector RavZ inhibits host autophagy through irreversible Atg8 deconjugation. *Science* **338**, 1072-1076 (2012).
72. Deretic, V. & Levine, B. Autophagy, immunity, and microbial adaptations. *Cell host & microbe* **5**, 527-549 (2009).
73. Abdulrahman, B.A. *et al.* Autophagy stimulation by rapamycin suppresses lung inflammation and infection by Burkholderia cenocepacia in a model of cystic fibrosis. *Autophagy* **7**, 1359-1370 (2011).
74. Mathur, D., Bost, A., Driver, I. & Ohlstein, B. A transient niche regulates the specification of Drosophila intestinal stem cells. *Science* **327**, 210-213 (2010).
75. Yao, T.-P., Segraves, W.A., Oro, A.E., McKeown, M. & Evans, R.M. *Drosophila ultraspiracle* modulates ecdysone receptor function via heterodimer formation. *Cell* **71**, 63-72 (1992).

76. Baehrecke, E.H. Steroid regulation of programmed cell death during *Drosophila* development. *Cell Death & Differ.* **7**, 1057-1062 (2000).
77. Lee, C.Y., Cooksey, B.A. & Baehrecke, E.H. Steroid regulation of midgut cell death during Drosophila development. *Developmental biology* **250**, 101-111 (2002).
78. Lee, C.-Y. *et al. E93* directs steroid-triggered programmed cell death in *Drosophila*. *Mol. Cell* **6**, 433-443 (2000).
79. Alva, A.S., Gultekin, S.H. & Baehrecke, E.H. Autophagy in human tumors: cell survival or death? *Cell Death Differ.* **11**, 1046-1048 (2004).
80. Lee, C.-Y. *et al.* Genome-wide analyses of steroid- and radiation-triggered programmed cell death in *Drosophila*. *Curr. Biol.* **13**, 350-357 (2003).
81. Jiang, C., Baehrecke, E.H. & Thummel, C.S. Steroid regulated programmed cell death during *Drosophila* metamorphosis. *Development* **124**, 4673-4683 (1997).
82. Galluzzi, L. *et al.* Molecular definitions of cell death subroutines: recommendations of the Nomenclature Committee on Cell Death 2012. *Cell death and differentiation* **19**, 107-120 (2012).
83. Denton, D., Nicolson, S. & Kumar, S. Cell death by autophagy: facts and apparent artefacts. *Cell death and differentiation* **19**, 87-95 (2012).
84. Lee, C.-Y., Cooksey, B.A.K. & Baehrecke, E.H. Steroid regulation of midgut cell death during *Drosophila* development. *Dev. Biol.* **250**, 101-111 (2002).
85. Cecconi, F. & Levine, B. The role of autophagy in mammalian development: cell makeover rather than cell death. *Developmental cell* **15**, 344-357 (2008).
86. Elgendy, M., Sheridan, C., Brumatti, G. & Martin, S.J. Oncogenic Ras-induced expression of Noxa and Beclin-1 promotes autophagic cell death and limits clonogenic survival. *Mol. Cell* **42**, 23-35 (2011).
87. Guo, J.Y. *et al.* Activated Ras requires autophagy to maintain oxidative metabolism and tumorigenesis. *Genes & development* **25**, 460-470 (2011).
88. Chang, Y.Y. & Neufeld, T.P. Autophagy takes flight in Drosophila. *FEBS Lett.* **584**, 1342-1349 (2010).
89. Arico, S. *et al.* The tumor suppressor PTEN positively regulates macroautophagy by inhibiting the phosphatidylinositol 3-kinase/protein kinase B pathway. *J. Biol. Chem.* **276**, 35243-35246 (2001).
90. Neufeld, T.P. TOR-dependent control of autophagy: biting the hand that feeds. *Current opinion in cell biology* **22**, 157-168 (2010).
91. Hou, Y.C., Chittaranjan, S., Barbosa, S.G., McCall, K. & Gorski, S.M. Effector caspase Dcp-1 and IAP protein Bruce regulate starvation-induced autophagy during Drosophila melanogaster oogenesis. *J. Cell Biol.* **182**, 1127-1139 (2008).
92. Nezis, I.P. *et al.* Cell death during Drosophila melanogaster early oogenesis is mediated through autophagy. *Autophagy* **5**, 298-302 (2009).
93. Mohseni, N., McMillan, S.C., Chaudhary, R., Mok, J. & Reed, B.H. Autophagy promotes caspase-dependent cell death during Drosophila development. *Autophagy* **5**, 329-338 (2009).
94. Gorski, S.M. *et al.* A SAGE Approach to Discovery of Genes Involved in Autophagic Cell Death. *Curr. Biol.* **13**, 358-363 (2003).
95. Daish, T.J., Mills, K. & Kumar, S. Drosophila Caspase DRONC Is Required for Specific Developmental Cell Death Pathways and Stress-Induced Apoptosis. *Dev. Cell* **7**, 909-915 (2004).
96. Mills, K. *et al.* The Drosophila melanogaster Apaf-1 homologue ARK is required for most, but not all, programmed cell death. *J. Cell Biol.* **172**, 809-815 (2006).
97. Martin, D.N. & Baehrecke, E.H. Caspases function in autophagic cell death in *Drosophila*. *Development* **131**, 275-284 (2004).
98. Lee, C.-Y. & Baehrecke, E.H. Steroid regulation of autophagic programmed cell death during development. *Development* **128**, 1443-1455 (2001).
99. Denton, D., Shravage, B., Simin, R., Baehrecke, E.H. & Kumar, S. Larval midgut destruction in Drosophila: not dependent on caspases but suppressed by the loss of autophagy. *Autophagy* **6**, 163-165 (2010).
100. Dutta, S. & Baehrecke, E.H. Warts is required for PI3K-regulated growth arrest, autophagy, and autophagic cell death in Drosophila. *Curr. Biol.* **18**, 1466-1475 (2008).
101. Britton, J.S., Lockwood, W.K., Li, L., Cohen, S.M. & Edgar, B.A. Drosophila's insulin/PI3-kinase pathway coordinates cellular metabolism with nutritional conditions. *Dev. Cell* **2**, 239-249 (2002).

102. Kozma, S.C. & Thomas, G. Regulation of cell size in growth, development and human disease: PI3K, PKB and S6K. *Bioessays* **24**, 65-71 (2002).
103. Kuranaga, E. Beyond apoptosis: caspase regulatory mechanisms and functions in vivo. *Genes to cells : devoted to molecular & cellular mechanisms* **17**, 83-97 (2012).
104. Harvey, K. & Tapon, N. The Salvador-Warts-Hippo pathway - an emerging tumour-suppressor network. *Nature reviews. Cancer* **7**, 182-191 (2007).
105. Rusten, T.E. *et al.* Programmed autophagy in the Drosophila fat body is induced by ecdysone through regulation of the PI3K pathway. *Dev. Cell* **7**, 179-192 (2004).
106. Sandilands, E. *et al.* Autophagic targeting of Src promotes cancer cell survival following reduced FAK signalling. *Nature cell biology* **14**, 51-60 (2012).
107. Kirisako, T. *et al.* Formation process of autophagosome is traced with Apg8/Aut7p in yeast. *J. Cell Biol.* **147**, 435-446 (1999).
108. Zinke, I., Schütz, C.S., Katzenberger, J.D., Bauer, M. & Pankratz, M.J. Nutrient control of gene expression in Drosophila: microarray analysis of starvation and sugar-dependent response. *EMBO J.* **21**, 6162-6173 (2002).
109. Juhasz, G. *et al.* Gene expression profiling identifies FKBP39 as an inhibitor of autophagy in larval Drosophila fat body. *Cell death and differentiation* **14**, 1181-1190 (2007).
110. Nezis, I.P. *et al.* Autophagic degradation of dBruce controls DNA fragmentation in nurse cells during late Drosophila melanogaster oogenesis. *J. Cell Biol.* **190**, 523-531 (2010).
111. Denton, D. *et al.* Relationship between growth arrest and autophagy in midgut programmed cell death in Drosophila. *Cell Death Differ.* **19**, 1299-1307 (2012).
112. Denton, D., Mills, K. & Kumar, S. Methods and protocols for studying cell death in Drosophila. *Methods in enzymology* **446**, 17-37 (2008).
113. Mizushima, N. & Komatsu, M. Autophagy: Renovation of Cells and Tissues *Cell* **147**, 728-741 (2011).
114. Levine, B. & Yuan, J. Autophagy in cell death: an innocent convict? *J. Clin. Invest.* **115**, 2679-2688 (2005).
115. Baehrecke, E.H. Autophagy: dual roles in life and death? *Nature Reviews Mol. Cell Biol.* **6**, 505-510 (2005).
116. Harding, T.M., Hefner-Gravink, A., Thumm, M. & Klionsky, D.J. Genetic and phenotypic overlap between autophagy and the cytoplasm to vacuole protein. *J. Biol. Chem.* **271**, 17621-17624 (1996).
117. Schulman, B.A. & Harper, J.W. Ubiquitin-like protein activation by E1 enzymes: the apex for downstream signalling pathways. *Nat. Rev. Mol. Cell Biol.* **10**, 319-331 (2009).
118. Micchelli, C.A., Sudmeier, L., Perrimon, N., Tang, S. & Beehler-Evans, R. Identification of adult midgut precursors in Drosophila. *Gene Expr. Patterns* **11**, 12-21 (2011).
119. Juhász, G., Erdi, B., Sass, M. & Neufeld, T.P. Atg7-dependent autophagy promotes neuronal health, stress tolerance, and longevity but is dispensable for metamorphosis in Drosophila. *Genes Dev.* **21**, 3061-3066 (2007).
120. Belote, J.M. & Fortier, E. Targeted expression of dominant negative proteasome mutants in Drosophila melanogaster. *Genesis* **34**, 80-82 (2002).
121. Fujita, N. *et al.* An Atg4B mutant hampers the lipidation of LC3 paralogues and causes defects in autophagosome closure. *Mol. Biol. Cell* **19**, 4651-4659 (2008).
122. Pircs, K. *et al.* Advantages and Limitations of Different p62-Based Assays for Estimating Autophagic Activity in Drosophila. *PLoS ONE* **7**, e44214 (2012).
123. Itakura, E. & Mizushima, N. p62 targeting to the autophagosome formation site requires self-oligomerization but not LC3 binding. *J. Cell Biol.* **192**, 17-27 (2011).
124. Fujita, K., Maeda, D., Xiao, Q. & Srinivasula, S.M. Nrf2-mediated induction of p62 controls Toll-like receptor-4-driven aggresome-like induced structure formation and autophagic degradation. *Proc. Natl. Acad. Sci. U S A* **108**, 1427-1432 (2011).
125. Lum, J.J. *et al.* Growth factor regulation of autophagy and cell survival in the absence of apoptosis. *Cell* **120**, 237-248 (2005).
126. Hosokawa, N., Hara, Y. & Mizushima, N. Generation of cell lines with tetracycline-regulated autophagy and a role for autophagy in controlling cell size. *FEBS Lett.* **580**, 2623-2629 (2006).
127. Tian, Y. *et al.* C. elegans screen identifies autophagy genes specific to multicellular organisms. *Cell* **141**, 1042-1055 (2010).

128. McPhee, C.K., Logan, M.A., Freeman, M.R. & E.H., B. Activation of autophagy during cell death requires the engulfment receptor Draper. *Nature* **465**, 1093-1096 (2010).
129. Johansen, T. & Lamark, T. Selective autophagy mediated by autophagic adapter proteins. *Autophagy* **7**, 279-296 (2011).
130. Lenk, S.E., Dunn, W.A.J., Trausch, J.S., Ciechanover, A. & Schwartz, A.L. Ubiquitin-activating enzyme, E1, is associated with maturation of autophagic vacuoles. *J. Cell Biol.* **118**, 301-308 (1992).
131. Taillebourg, E. *et al.* The deubiquitinating enzyme USP36 controls selective autophagy activation by ubiquitinated proteins. *Autophagy* **8**, 767-779 (2012).
132. Lee, T.V. *et al.* The E1 ubiquitin-activating enzyme Uba1 in Drosophila controls apoptosis autonomously and tissue growth non-autonomously *Development* **135**, 43-52 (2008).
133. Yamashita, S. The post-embedding method for immunoelectron microscopy of mammalian tissues: a standardized procedure based on heat-induced antigen retrieval. *Methods Mol. Biol.* **657**, 237-248 (2010).
134. King-Jones, K. & Thummel, C.S. Nuclear receptors--a perspective from Drosophila. *Nature reviews. Genetics* **6**, 311-323 (2005).
135. Sun, T., Wang, X., Lu, Q., Ren, H. & Zhang, H. CUP-5, the C. elegans ortholog of the mammalian lysosomal channel protein MLN1/TRPML1, is required for proteolytic degradation in autolysosomes. *Autophagy* **7**, 1308-1315 (2011).
136. Wong, C.O., Li, R., Montell, C. & Venkatachalam, K. Drosophila TRPML is required for TORC1 activation. *Current biology : CB* **22**, 1616-1621 (2012).
137. Reggiori, F. *et al.* Coronaviruses Hijack the LC3-I-positive EDEMosomes, ER-derived vesicles exporting short-lived ERAD regulators, for replication. *Cell host & microbe* **7**, 500-508 (2010).
138. Tamura, N., Oku, M. & Sakai, Y. Atg8 regulates vacuolar membrane dynamics in a lipidation-independent manner in Pichia pastoris. *J. Cell Sci.* **123**, 4107-4116 (2010).
139. Wild, P. *et al.* Phosphorylation of the autophagy receptor optineurin restricts Salmonella growth. *Science* **333**, 228-233 (2011).
140. Platta, H.W., Abrahamsen, H., Thoresen, S.B. & Stenmark, H. Nedd4-dependent lysine-11-linked polyubiquitination of the tumour suppressor Beclin 1. *The Biochemical journal* **441**, 399-406 (2012).
141. Nazio, F. *et al.* mTOR inhibits autophagy by controlling ULK1 ubiquitylation, self-association and function through AMBRA1 and TRAF6. *Nature cell biology* **15**, 406-416 (2013).
142. Raiborg, C. & Stenmark, H. The ESCRT machinery in endosomal sorting of ubiquitylated membrane proteins. *Nature* **458**, 445-452 (2009).
143. Rusten, T.E. *et al.* ESCRTs and Fab1 regulate distinct steps of autophagy. *Curr. Biol.* **17**, 1817-1825 (2007).
144. Behrends, C., Sowa, M.E., Gygi, S.P. & Harper, J.W. Network organization of the human autophagy system. *Nature* **466**, 68-76 (2010).